



2017

Biochemical And Functional Studies Of Histone Deacetylase 3 In Metabolic Tissues

Jarrett Renn Remsberg

University of Pennsylvania, jremberg@gmail.com

Follow this and additional works at: <https://repository.upenn.edu/edissertations>

 Part of the [Biochemistry Commons](#), and the [Molecular Biology Commons](#)

Recommended Citation

Remsberg, Jarrett Renn, "Biochemical And Functional Studies Of Histone Deacetylase 3 In Metabolic Tissues" (2017). *Publicly Accessible Penn Dissertations*. 2546.

<https://repository.upenn.edu/edissertations/2546>

This paper is posted at ScholarlyCommons. <https://repository.upenn.edu/edissertations/2546>

For more information, please contact repository@pobox.upenn.edu.

Biochemical And Functional Studies Of Histone Deacetylase 3 In Metabolic Tissues

Abstract

Organismal physiology is built upon the foundation of molecular processes. A central axis to maintaining homeostasis *in vivo* is at the level of gene regulation. Tissue specific gene expression is created at the level of epigenetics, where proteins guided by tissue specific DNA binding proteins create a chromatin landscape for precise gene programs. Understanding these molecular processes is of vital importance to understand the underpinning pathologies, such as metabolic syndrome, which are a growing medical concern and require greater research efforts in order to tackle its challenges. A major epigenetic regulator is histone deacetylase 3 (HDAC3), which is a core member of the nuclear receptor corepressor (NCoR) complex. This ubiquitously expressed chromatin associated protein complex functions to repress target gene transcription. Here we address the functional role of HDAC3 in β -cells of adult mice. An HDAC3 β -cell specific knockout was generated using the *MIP-CreERT* transgenic mouse model and while HDAC3 β -cell specific deletion did not increase total pancreatic insulin content, the mice demonstrated markedly improved glucose tolerance and increased glucose-stimulated insulin secretion. Cistromic and transcriptomic analyses of pancreatic islets revealed that HDAC3 regulated multiple genes that contribute to glucose-stimulated insulin secretion. Furthermore, using mass spectrometry in conjunction of cistromic analyses of interactors we have characterized the interactome of HDAC3 and detailed its function in mammalian liver. We identified PROX1 as an abundant interactor which is corecruited with HDAC3 by HNF4a in liver to corepress gene transcription important for maintenance of lipid homeostasis. Lastly, as we continue to explore the protein-protein interaction networks of these critical factors, novel tools are proving to be invaluable to their investigation. The advent of CRISPR-Cas9 genome editing has allowed for reliable and simple design and generation of mouse models. Therefore we have employed this technology to generate a variety of epitope tagged mouse models with the goal of comparing their tissue specific interactomes. This body of work includes a wide breadth of biological techniques that have succeeded in advancing knowledge of HDAC3 function *in vivo*, vital to our understanding of molecular pathology in diabetes and obesity.

Degree Type

Dissertation

Degree Name

Doctor of Philosophy (PhD)

Graduate Group

Biochemistry & Molecular Biophysics

First Advisor

Mitchell A. Lazar

Keywords

CRISPR-Cas9, histone deacetylation, lipid metabolism, mass spectrometry, nuclear receptor corepressor

Subject Categories

Biochemistry | Molecular Biology

BIOCHEMICAL AND FUNCTIONAL STUDIES OF HISTONE DEACETYLASE 3 IN

METABOLIC TISSUES

Jarrett Renn Remsberg

A DISSERTATION

in

Biochemistry and Molecular Biophysics

Presented to the Faculties of the University of Pennsylvania

in

Partial Fulfillment of the Requirements for the

Degree of Doctor of Philosophy

2017

Supervisor of Dissertation

Mitchell A. Lazar, M.D., Ph.D.

Willard and Rhoda Ware Professor in Diabetes and Metabolic Diseases

Graduate Group Chairperson

Kim A. Sharp, Ph.D., Associate Professor of Biochemistry and Biophysics, Chair Graduate Group
in Biochemistry and Molecular Biophysics

Dissertation Committee

Rahul M. Kohli, M.D., Ph.D., Assistant Professor of Medicine,
Benjamin A. Garcia, Ph.D., Presidential Professor of Biochemistry and Biophysics,
Doris A. Stoffers, M.D., Ph.D., Sylvan H. Eisman Professor of Medicine,
Morris J. Birnbaum, M.D., Ph.D., Emeritus Professor of Medicine, Senior Vice President and
Chief Scientific Officer, Cardiovascular and Metabolic Disease Research Unit, Pfizer

BIOCHEMICAL AND FUNCTIONAL STUDIES OF HISTONE DEACETYLASE 3 IN METABOLIC
TISSUES

COPYRIGHT

2017

Jarrett Renn Remsberg

Dedication Page

To Erica, without her I would be lost.

She is my inspiration.

To my family - mom, dad, and brother.

Thank you for your constant support and for building my foundation as a person. From the farm to science fairs, you've showered me with love and support.

ACKNOWLEDGMENT

First and foremost, I need to thank Dr. Mitch Lazar for granting me the opportunity to perform my doctoral studies in his laboratory. I'm especially thankful for his vigilance and perseverance to mold me into a better scientist. In my experience, no one matches his passion and love for science, and I wish to emulate these traits in my career.

I would also like to thank Dr. Ben Garcia, and the entire Garcia lab, especially Dr. Simone Sidoli. Their amazing generosity allowed me to learn and gain hands on experience with proteomic mass spectrometry techniques. During my time at National Cancer Institute, I was told there are two goals to achieve during your dissertation; to become an expert in a field, and to master a technique. Given the amazing environment provided to me by the Lazar lab, and the freedom to explore my technical passions in the Garcia lab, I believe I've accomplished both of these goals.

I'd like to thank everyone who has helped in my scientific journey, especially Dr. Dave Steger, Dr. Daniel Cohen, and Dr. Pamela Marino for scientific, career, and life advice. Dr. Jorge Henao-Mejia for teaching me CRISPR-Cas9 genome editing techniques, Dr. Jean Richa from the transgenic core, Dr. Nicolai Doliba and the islet core, and everyone in the Lazar laboratory.

I need to thank the entire Biochemistry and Molecular Biophysics graduate group, especially Ruth Keris and Dr. Kate Ferguson, for granting me the opportunity to conduct graduate studies at the University of Pennsylvania and for their support over the years. I'd also like to thank Dr. Franz Matschinesky for thoughtful discussions and advice and all the members of my committee. Dr. Rahul Kohli as my chair, Dr. Doris Stoffers, and Dr. Ben Garcia have all been instrumental in my growth, and I thank them for their advice and time over these past few years. They are model scientists, and I hope to continue to learn and lead by their example.

Finally, I need to acknowledge my family. My wife for giving me never ending support and love over the course of my graduate education. My parents for encouraging me to strive and accomplish whatever goals I set before myself. And of course, I need to thank Dr. Nadya Tarasova and Dr. Sergey Tarasov, I would not be where I am today without their guidance and support.

ABSTRACT

BIOCHEMICAL AND FUNCTIONAL STUDIES OF HISTONE DEACETYLASE 3 IN

METABOLIC TISSUES

Jarrett Renn Remsberg

Dr. Mitchell A. Lazar

Organismal physiology is built upon the foundation of molecular processes. A central axis to maintaining homeostasis *in vivo* is at the level of gene regulation. Tissue specific gene expression is created at the level of epigenetics, where proteins guided by tissue specific DNA binding proteins create a chromatin landscape for precise gene programs. Understanding these molecular processes is of vital importance to understand the underpinning pathologies, such as metabolic syndrome, which are a growing medical concern and require greater research efforts in order to tackle its challenges. A major epigenetic regulator is histone deacetylase 3 (HDAC3), which is a core member of the nuclear receptor corepressor (NCoR) complex. This ubiquitously expressed chromatin associated protein complex functions to repress target gene transcription. Here we address the functional role of HDAC3 in β -cells of adult mice. An HDAC3 β -cell specific knockout was generated using the *MIP-CreERT* transgenic mouse model and while HDAC3 β -cell specific deletion did not increase total pancreatic insulin content, the mice demonstrated markedly improved glucose tolerance and increased glucose-stimulated insulin secretion. Cistromic and transcriptomic analyses of pancreatic islets revealed that HDAC3 regulated multiple genes that contribute to glucose-stimulated insulin secretion. Furthermore, using mass spectrometry in conjunction of cistromic analyses of interactors we have characterized the interactome of HDAC3 and detailed its function in mammalian liver. We identified PROX1 as an abundant interactor which is corecruited with HDAC3 by HNF4 α in liver to corepress gene transcription important for maintenance of lipid homeostasis. Lastly, as we continue to explore the protein-protein interaction networks of these critical factors, novel tools are proving to be invaluable to their investigation. The advent of

CRISPR-Cas9 genome editing has allowed for reliable and simple design and generation of mouse models. Therefore we have employed this technology to generate a variety of epitope tagged mouse models with the goal of comparing their tissue specific interactomes. This body of work includes a wide breadth of biological techniques that have succeeded in advancing knowledge of HDAC3 function *in vivo*, vital to our understanding of molecular pathology in diabetes and obesity.

TABLE OF CONTENTS

ACKNOWLEDGMENT	IV
ABSTRACT	V
LIST OF TABLES	X
LIST OF ILLUSTRATIONS	XI
CHAPTER 1: GENERAL INTRODUCTION	1
1.1 Enzymatic Deacetylation and gene expression	2
1.1a Coordination of residues for catalysis	3
1.2 HDAC3 requires the deacetylase activating domain	4
1.2a HDAC3 enzymatic activity requires DAD	5
1.3 The Nuclear Receptor Corepressor Complex	5
1.3a Architecture and organization of the complex	6
1.3b Binding of NCOR1/SMRT to nuclear receptors	6
1.4 NCoR Complex is critical for homeostatic gene regulation	7
1.4a Tissue specific functions of the NCoR complex	7
1.5 Hypotheses and Objectives	8
CHAPTER 2: DELETION OF HISTONE DEACETYLASE 3 IN ADULT β-CELLS IMPROVES GLUCOSE TOLERANCE VIA INCREASED INSULIN SECRETION	14
2.1 Abstract	15
2.2 INTRODUCTION	15
2.2a Glucose homeostasis and diabetes mellitus	15
2.2b Role of HDAC3 in pancreatic β -cells	16
2.3 METHODS	17
2.3a Animal studies	17
2.3b Immunohistochemistry and immunofluorescence	17
2.3c Islet isolation and static incubations	18
2.3d RNA analysis	18
2.3e ChIP-seq	18
2.4. RESULTS	19
2.4a Deletion of HDAC3 in β -cells does not significantly alter insulin content or islet mass	19
2.4b HDAC3 ablation in β -cells of adult mice markedly improves glucose tolerance	20
2.4c Deletion of HDAC3 in β -cells of obese mice markedly improves glucose tolerance	21

2.4d Improved glucose tolerance is a due to increased insulin secretion	21
2.4e HDAC3 cistrome in isolated islets	22
2.4f Transcriptome of HDAC3 β -cell KO reveals potential pathways contributing to increased insulin secretion	22
2.4g Integrating transcriptomic and cistromic analyses of HDAC3 role in β -cells	23
2.5 DISCUSSION	23
CHAPTER 3: AN HDAC3-PROX1 COREPRESSOR MODULE ACTS ON HNF4α TO CONTROL HEPATIC TRIGLYCERIDES.....	34
3.1 ABSTRACT	35
3.2 Introduction	35
3.3 Methods	37
3.3a Animal studies	37
3.3b Constructs and viral vectors	38
3.3c Liver triglyceride measurement and Oil Red O staining	38
3.3d Cell culture and Luciferase Assay	38
3.3e Immunoprecipitation and western blotting	39
3.3f Mass spectrometry	40
3.3g RT-qPCR and RNA-seq	41
3.3h ChIP-qPCR, ChIP-reChIP, and ChIP-seq	42
3.3i Data availability	43
3.3j Statistical Methods	44
3.4 Results	44
3.4a In vivo screen for HDAC3 interactors	44
3.4b PROX1 and HDAC3 co-localize extensively at the genome	47
3.4c HNF4 α is required for the recruitment of the HDAC3-PROX1 module	48
3.4d Liver depletion of PROX1 causes increased hepatic triglycerides	49
3.4e HDAC3 and PROX1 coregulate a lipid gene expression program	49
3.5 DISCUSSION	51
CHAPTER 4: GENERATING EPITOPE TAGGED MOUSE MODELS USING CRISPR-CAS9	80
4.1 Abstract.....	81
4.2 Introduction	81
4.2a Targeting proteins of interest	82
4.3 Methods	84
4.3a Design guidelines	84
4.3b Cas9 mRNA and sgRNA production	84
4.3c Microinjection of zygotes	84
4.3d PCR genotyping and sequencing	85
4.3e Immunoprecipitation and western blotting	85
4.3f ChIP-qPCR.....	85

4.3g Mass spectrometry	86
4.4 Results	86
4.4a Designing targeting sequence for CRISPR/Cas9 targeted knockin	86
4.4b Confirming genome editing by PCR and Sanger sequencing	87
4.4c Validating epitope tagged proteins <i>in vivo</i>	88
4.5 Discussion	89
CHAPTER 5: SUMMARY AND FUTURE DIRECTIONS	101
5.1 Summary	102
5.2 Future Directions	104
5.3a Tissue specific interactomes	104
5.3b Cross-linking mass spectrometry	104
BIBLIOGRAPHY	108

LIST OF TABLES

Table 2.1 List of primers for quantitative RT-PCR gene expression.	33
Table 3.1 nLC-MS/MS analysis of HDAC3 high-confidence interacting proteins. Proteins listed met 10-fold enrichment versus EGFP and $p < 0.01$.	76
Table 3.2 List of primers used for quantitative RT-PCR, ChIP-reChIP-qPCR, and luciferase experiments.	79
Table 4.1 List of primers used for quantitative RT-PCR, ChIP-qPCR, and genotyping.	100

LIST OF ILLUSTRATIONS

Figure 1.1 Crystal structure of HDAC3-DAD interaction and mechanism of catalysis.	10
Figure 1.2 HDAC3 activation by DAD.	12
Figure 1.3 NCoR mediated repression of target genes.	13
Figure 2.1 HDAC3 β -cell KO does not increase insulin content or islet mass.	26
Figure 2.2 Deletion of HDAC3 in β -cells of adult mice markedly improves glucose tolerance.	27
Figure 2.3 HDAC3 β -cell KO improves glucose tolerance in the setting of diet-induced obesity.	28
Figure 2.4 HDAC3 β -cell KO mice have increased insulin secretion.	29
Figure 2.5 HDAC3 cistrome in isolated islets.	30
Figure 2.6 RNA-seq analysis of HDAC3 β KO compared to HDAC3 ^{fl/fl} ;Cre;Veh and HDAC3 ^{fl/fl} ;Tam mice.	31
Figure 2.7 HDAC3 cistromic analysis suggests multiple β -cell lineage factors utilize the NCoR complex.	32
Figure 3.1 NEAT ChIP-MS workflow to interrogate the HDAC3 liver nuclear interactome.	55
Figure 3.2 HDAC3 liver interactome by NEAT ChIP-MS reveals PROX1 as an abundant interactor.	56
Figure 3.3 Interrogation of PROX1 interaction with HDAC3-NCoR.	58
Figure 3.4 HDAC3 interactome network.	59
Figure 3.5 HDAC3 interactome topology analysis.	60
Figure 3.6 HDAC3 and PROX1 exhibit extensive co-binding and reveal a metabolic signature.	61
Figure 3.7 HDAC3 and PROX1 specific cistromic analysis.	62
Figure 3.8 Interrogation of cistrome data suggests distinct HDAC3 containing chromatin complexes.	63
Figure 3.9 The HDAC3-PROX1 module is recruited by HNF4 α in liver.	64
Figure 3.10 HDAC3, PROX1, and HNF4 α genomic binding in control and Hnf4 α knockout liver.	66
Figure 3.11 The HDAC3-PROX1 module requires HNF4 α for a majority of binding sites in liver.	67
Figure 3.12 PROX1 knockdown causes an increase in hepatic triglyceride content.	69

Figure 3.13 Transcriptomic analysis reveals the HDAC3-PROX1 module suppresses steatosis by controlling a hepatic lipid metabolism gene program.	70
Figure 3.14 RNA-seq and ChIP-seq correlation analysis of HDAC3-PROX1 module recruited by HNF4 α .	71
Figure 3.15 Genomic binding and nascent transcription near lipid-related genes coregulated by HDAC3-PROX1.	72
Figure 3.16 HDAC3-PROX1 repress putative G0s2 enhancers.	73
Figure 3.17 HNF4 α -induced enhancer function is dependent on an intact HNF4 α DNA binding motif.	74
Figure 3.18 Schematic model of HNF4 α recruitment of PROX1 and the NCoR complex to regulate a lipid-related metabolic gene program.	75
Figure 4.1 CRISPR-Cas9 genome editing.	92
Figure 4.2 Sanger sequencing confirmation of targeted genome editing.	93
Figure 4.3 Validation and immunoprecipitation western blot of 6His-HA-TR β 1.	95
Figure 4.4 Validation of 6His-HA-NCOR1 by immunoprecipitation western blot and mass spectrometry.	96
Figure 4.5 Circadian expression of 3xHA-Rev-erb α .	97
Figure 4.6 ChIP-qPCR confirming genomic binding of 3xHA-Rev-erb α .	98
Figure 4.7 Comparison of 3xHA-Rev-erb α protein abundance across tissues.	99
Figure 5.1 Future directions to interrogate interactomes <i>in vivo</i> .	106
Figure 5.2 CID cleavable cross-linker to identify peptide-peptide cross-links in complex mixtures.	107

CHAPTER 1: General Introduction

1.1 ENZYMATIC DEACETYLATION AND GENE EXPRESSION

A growing clinical concern in the developed world is the rampant increase in metabolic syndrome and diet induced obesity (Cohen et al., 2011). These new medical obstacles are challenging in part due to dysfunction of multiple tissues (Tilg et al., 2016). Therefore it is critical to understand the molecular underpinnings of these pathologic states for the development of therapeutic interventions. A central foundation to maintaining homeostasis *in vivo* and integrating changes in the environment is at the level of gene regulation. In fact, a major class of proteins exist at this axis, allowing cells to respond accordingly, termed nuclear receptors (Gronemeyer et al., 2004; Huang et al., 2010). Indeed, as with many molecular mechanisms, these proteins do not work alone and recruit multi-protein complexes to exert their function (Perissi et al., 2010). Nuclear receptors are especially interesting because they can shift between recruiting corepressors or coactivators as a function of ligand binding, a means to integrate metabolic signals from the environment.

A major mechanism by which nuclear receptor complexes regulate gene expression is in manipulating the acetylation state of nucleosomes. Briefly, a nucleosome is the basic unit of chromatin and how all eukaryotic genomic information is organized. This building block includes an octomer of histone proteins wrapped in DNA, analogous to string on a bead. These beads then are organized and regulated on a more macroscopic level (Luger et al., 2012). The amino (N-) terminal 'tail' of histones that are hyperacetylated no longer electrostatically attract the negatively charged phosphate backbone of the DNA and therefore allow increased transcription, whereas deacetylated histones will condense and prevent transcriptional machinery from progressing. The amino terminus of histones is unstructured and the site of a huge variety of potential post translational modifications (Zhao and Garcia, 2015). Differential modifications across the genome is one mechanism by which organisms gain tissue specific gene expression profiles. While acetylation has been known for many decades, only with the explosion of molecular biology advances have we begun to understand its importance (Inoue and Fujimoto, 1969; Phillips, 1963). The identification of the first histone deacetylases (HDACs) and subsequent structural studies provided

deeper insight into their function and importance in biology (Finnin et al., 1999; Taunton et al., 1996). This diverse protein family has a wide breadth of functions across tissues, but at its core has the same guiding principles for enzymatic deacetylation and repression of target genes through chromatin compaction (Haberland et al., 2009; Lombardi et al., 2011; Struhl, 1998). However, it is noteworthy that deacetylation can also occur on non-histone proteins (Yang and Seto, 2008). Here we will focus on the histone deacetylase 3 (HDAC3) in the context of the nuclear receptor corepressor complex function in gene regulation.

1.1a Coordination of residues for catalysis

At the core of all enzymes is the principle that they lower activation energy to facilitate a specific reaction. The class I histone deacetylases are members of the metalloenzymes, meaning they require the coordination of a metal ion to perform catalysis. We got our first glimpse to the structure of a histone deacetylase from a homolog, histone deacetylase like protein (HDLP) from *A. aeolicus* bound to an inhibitor (Finnin et al., 1999). This protein shares roughly 35% homology to HDAC1 and details the first HDAC catalytic core solved, but to the surprise of structural biologists the fold was observed previously in arginase (Kanyo et al., 1996; Lombardi et al., 2011). The metal ion, zinc is coordinated by histidine and aspartic acid residues (**Figure 1.1A**). This allows H135 to first act as a general base, promoting nucleophilic attack of a coordinated water molecule to the carbonyl of the acetylated lysine substrate (**Figure 1.1B**). During the formation of the tetrahedral intermediate, Y298 and G143 are critical for stabilization. Indeed, mutating tyrosine 298 to phenylalanine, which maintains a majority of the structural properties but lacks the hydroxyl to perform hydrogen bonding, cripples the enzyme's ability to perform catalysis (Dowling et al., 2008; Sun et al., 2013; Vannini et al., 2007). Since the catalytic pocket and proposed mechanism are conserved across HDACs, substrate specificity may come in the form of the surface residues surrounding the catalytic pocket, or from protein-protein interactions. HDAC3 is unique among the class I HDACs as it found stoichiometrically bound to the nuclear receptor corepressor (NCOR1)

(Hörlein et al., 1995) or the silencing mediator for retinoic acid and thyroid hormone receptors (SMRT or NCOR2) (Chen and Evans, 1995).

1.2 HDAC3 REQUIRES THE DEACETYLASE ACTIVATING DOMAIN

Histone deacetylases function in the context of large multiple-protein complexes to exert their function (Joshi et al., 2013). HDAC3 in particular was identified as a core member of the SMRT corepressor complex (Guenther et al., 2000). Both SMRT and NCOR1 are large proteins, approximately 270 kilodaltons in mass, share a large degree of homology, and interestingly are predicted to be mostly disordered with islands of structure (Watson et al., 2012a). This may allow for the multiple distinct protein domains, mediating interaction and recruitment of complex members and may be important for chromatin association or repression. One such structurally ordered region interacts with HDAC3 and is termed the deacetylase activating domain (DAD) (Guenther et al., 2001). Identified through truncation mutants, this region of SMRT shares a high degree of conservation with NCOR1, which was also shown to bind HDAC3. Furthermore, HDAC3 synthesized in the absence of NCOR1 or SMRT will bind the TCP-1 ring complex (TRiC), an ATP dependent chaperonin complex, suggesting HDAC3 may have difficulty folding and the DAD has a chaperone like function stabilizing HDAC3 (Guenther et al., 2002). This interaction has been extensively studied structurally (Abdelkarim et al., 2013; Millard et al., 2013a; Watson et al., 2012b, 2016), and recent *in vivo* studies have confirmed it is critical for proper gene regulation (Alenghat et al., 2008; You et al., 2013). Also, HDAC3 relies on this interaction for recruitment to chromatin (Sun et al., 2013). Moreover, the HDAC3-DAD interaction may be critical for the overall structural integrity of the nuclear receptor corepressor (NCoR) complex (Ishizuka and Lazar, 2005). One of the most important characteristics to this interaction, is that HDAC3 requires binding to DAD for enzymatic activity.

1.2a HDAC3 enzymatic activity requires DAD

Thanks to the recent solving of the HDAC3-DAD crystal structure we can begin to understand the extent of this interaction and activation with atomic resolution (Watson et al., 2012b). In addition to discovering a structural rearrangement of the DAD upon binding to HDAC3, the DAD makes extensive intermolecular contacts along HDAC3's surface. Surprisingly, electron density between HDAC3 and DAD identified inositol tetrakisphosphate (IP4) present in the crystal (**Figure 1.2A**). Indeed, without the 'intermolecular glue' of IP4, the HDAC3-DAD interaction would be challenged electrostatically due to the cleft of basic residues on HDAC3 and DAD. Furthermore, the discovery of IP4 regulation is not limited to HDAC3, and it is present for other class I HDACs (Millard et al., 2013a). IP4 makes various contacts with critical residues between HDAC3 and the DAD, including Y470 of SMRT. Mutagenesis demonstrated that this residue is critical for the binding and activation of HDAC3 (Ishizuka and Lazar, 2005). Extending these studies *in vivo* have highlighted the importance of HDAC3 activation by the DAD, and its contribution to gene expression (Alenghat et al., 2008; You et al., 2013). However catalytic mutants such as Y298F which do not stabilize the tetrahedral intermediate during deacetylation, can maintain a degree of proper gene expression (Sun et al., 2013). Hinting at a possible structural role for repression of target gene expression.

1.3 THE NUCLEAR RECEPTOR COREPRESSOR COMPLEX

While studies predominantly focus on HDAC3 as the workhorse of the NCoR complex, there has been significant gains in understanding the role of other members. Initially identified with HDAC3, transducing β -like 1 (TBL1) and its homolog receptor 1 (TBL1R1) coimmunoprecipitated with SMRT from HeLa cell extracts (Guenther et al., 2000; Yoon et al., 2003). The TBL1 proteins contain WD40 repeats and are highly conserved across species. As a core member of the NCoR complex, they are essential for repression. This may be in part due to their interaction with hypoacetylated histone, which may enhance the binding of the NCoR complex to target sites. However, some work suggests the TBL1's may have a more diverse function and are important for coregulatory exchange (Perissi et al., 2004, 2008). As techniques for coimmunoprecipitation and mass

spectrometry improved, the G-protein pathway suppressor 2 (GPS2) was also identified as a stoichiometric interactor (Zhang et al., 2002).

1.3a Architecture and organization of the complex

Indeed, biochemical techniques have addressed and narrowed the interaction domains of NCoR complex members in an attempt to better understand its organization and mechanism of repression. Interaction among the complex members TBL1X/R1 and GPS2 are localized to the N-terminus of NCOR1 and SMRT (Oberoi et al., 2011; Watson et al., 2012a). The ratio of complex members on chromatin is not well understood, nor is the utilization of NCOR1 versus SMRT *in vivo*. However, given structural insights into the individual components and interaction domains, we can postulate. The TBL1 proteins are similar to TUP1 in their WD40 repeat domains, and both have been shown to form tetramers. Perhaps this tetramerization is the basis for greater oligomerization on chromatin to mediate repression, analogous to the proposed TUP1 mechanism (Matsumura et al., 2012; Millard et al., 2013b). This suggests a conserved mechanism for higher order assembly of corepressors on chromatin, and is in agreement with the original finding that the NCoR complex is 1-2 megadaltons when isolated on gel filtration chromatography.

1.3b Binding of NCOR1/SMRT to nuclear receptors

Finally, to effectively repress target genes, the NCoR complex must be recruited to chromatin. While it is suggested that TBL1's interaction with histones can assist in this process through interactions with histones, the complex achieves site specificity through sequence specific DNA binding nuclear receptors. These interactions are mediated toward the C-terminus of NCOR1 and SMRT and are termed receptor-interacting domains. Interestingly this conserved motif, the coRNR box (IXXII) closely resembles the hydrophobic helix of the nuclear receptor (NR) box (LXXLL) used by coactivators (Heery et al., 1997; Hu and Lazar, 1999; McInerney et al., 1998). These subtle but distinct features contribute to the specificity of coregulators exchange on nuclear receptors as a function of ligand binding, but the precise distribution and kinetics are not well understood (Millard

et al., 2013b; Nagy et al., 1999; Perissi et al., 1999). Due to the fact both corepressors and coactivators interact with the same region on NRs in the ligand binding domain, these recruitment events are mutually exclusive (Darimont et al., 1998; Feng, 1998; Nolte et al., 1998; Wang et al., 2006; Xu et al., 2002).

1.4 NCOR COMPLEX IS CRITICAL FOR HOMEOSTATIC GENE REGULATION

The NCoR complex and its members has proven vital in maintaining proper gene expression. Use of mouse genetics allows for interrogation of individual component roles *in vivo* and in different tissues. As a ubiquitously expressed complex, tissue dependent binding and gene regulation would come from the tissue specific expression of DNA binding proteins relying on the complex (**Figure 1.3A**). The HDAC3 containing NCoR complex can metaphorically be symbolized as an umbrella, where its phenotypic effects encompass and are the sum of all of the DNA binding factors that utilize the NCoR complex to repress their individual target gene programs. This becomes clear when comparing the consequence of ablating HDAC3, NCOR1, or the nuclear receptor Rev-erb α from mouse liver as they all increase hepatic triglyceride content, but HDAC3 to the greatest extent (Feng et al., 2011; Sun et al., 2012, 2013).

1.4a Tissue specific functions of the NCoR complex

Mutant and phenotypic studies of NCOR1 and SMTR has been extensively reviewed (Astapova, 2016) and highlight the diversity of functions attributed to the NCoR complex. Deletion of individual components of the NCoR complex results in an increase in liver triglycerides (Kulozik et al., 2011; Li et al., 2015; Shimizu et al., 2015; Sun et al., 2012), highlighting the importance of these proteins acting together as a functional complex to regulate liver metabolic gene transcription.

Multiple tissue specific deletions of HDAC3 showcase the importance of this epigenomic modifying enzyme (Alenghat et al., 2013; Hong et al., 2016; McGee-Lawrence et al., 2013; Mullican et al., 2011; Singh et al., 2011; Sun et al., 2012). Liver, heart, and skeletal muscle ablations point HDAC3

to focusing on metabolic gene expression, whereas studies in macrophages and preliminary β -cell culture point toward inflammatory gene regulation (Chou et al., 2012; Lundh et al., 2012; Plaisance et al., 2014).

1.5 HYPOTHESES AND OBJECTIVES

HDAC3 plays a clear and significant role of regulating gene expression within mammalian metabolic organs. Preliminary studies suggest HDAC3 may play a pivotal role in the pancreatic β -cell, but this has not been addressed *in vivo* with proper genetic manipulation. Moreover, where the consequence of ablating HDAC3 in liver is well documented, fundamental questions remain. The vast number of transcriptionally relevant complexes highlights the important roles protein-protein interactions play in the control of gene expression and with regard to HDAC3, there are important questions about which transcription factors recruit it to the genome, and which HDAC3-associated proteins act as downstream effectors to impact lipid gene regulation and hepatic steatosis.

We hypothesize that HDAC3 regulates glucose homeostasis *in vivo* and ablation may improve insulin response in diet induced obesity. This is supported by a recent finding where treatment with an HDAC3 selective inhibitor improved glycaemia and insulin secretion in a diabetic rat model (Lundh et al., 2015). In Chapter 2, we apply mouse genetics to characterize and determine the contribution of HDAC3 in pancreatic β -cell gene expression. We measure classic physiologic parameters related to glucose homeostasis in mice lacking HDAC3 in their β -cells, in addition to applying advanced genomic approaches to determine the altered transcriptional landscape and HDAC3's genomic occupancy.

Furthermore, we hypothesize that multiple nuclear receptors utilize the NCoR complex in mammalian liver. To identify these interactors, in Chapter 3 we adopt a cross-linking mass spectrometry approaches in Chapter 3. Traditional chromatographic separation and

immunoprecipitations have only identified core NCoR complex members. Therefore, we applied a cross-linking set analogous to chromatin immunoprecipitation (ChIP) in order to capture lower affinity or transit interactors of HDAC3 and the NCoR complex. Indeed, interrogation of cistromic and ensemble mass spectrometry interaction data allow us to conclude there are multiple and distinct factors utilizing the NCoR complex and HDAC3 to repress their target gene program in mammalian liver. Also we identified PROX1 as a critical interactor, functioning to corepress gene transcription important for maintenance of lipid homeostasis.

Finally, we extend these technical achievements to other proteins of interest and into tissues beyond liver. In Chapter 4 we apply CRISPR-Cas9 genome editing to generate multiple epitope tagged mouse models to address previously unattainable questions, including tissue specific interactomes, interactomes across circadian time points, and overcoming technical limitations of poor antibodies.

In summary, this body of work aims to further our understanding of HDAC3 in regulating tissue specific gene expression and deepen our knowledge of its molecular mechanisms. Also, we utilize recent advances in genome editing to expand on the foundations built and continue investigating these proteins using mass spectrometry in tissues where current techniques and reagents previously count not.

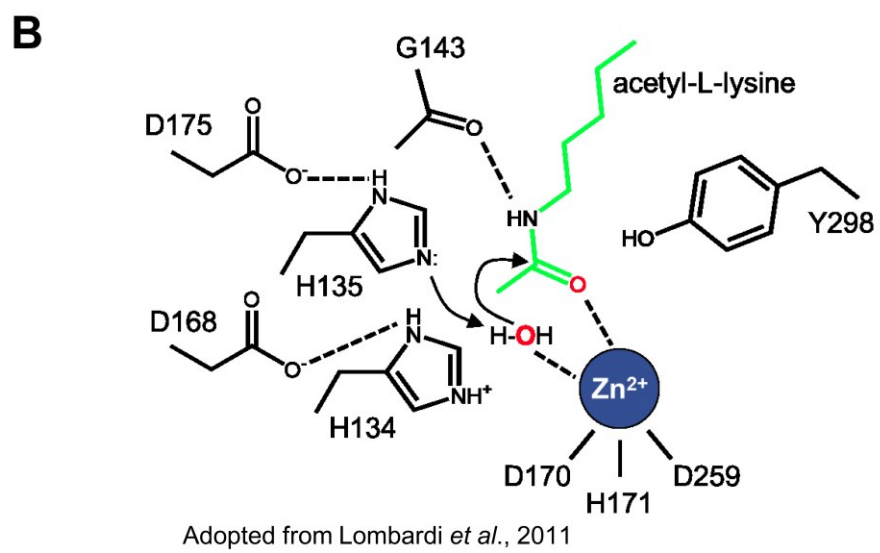
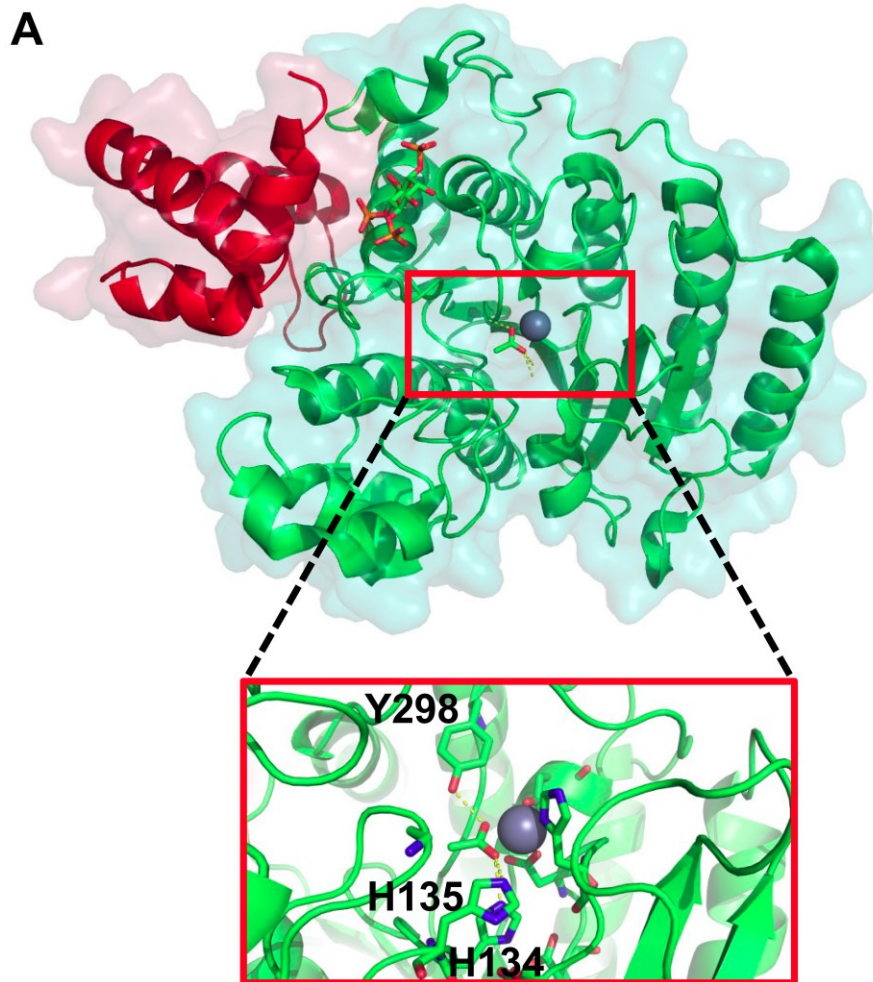


Figure 1.1 Crystal structure of HDAC3-DAD interaction and mechanism of catalysis. (A) Overview of the HDAC3-DAD crystal structure (PDB 4A69), HDAC3 in green and the DAD of SMRT in red. The zoomed insert is centered on the Zn²⁺ ion and residues involved in catalysis are shown as stick models. (B) Proposed mechanism for deacetylation by HDACs, adopted from Lombardi *et al.* to reflect HDAC3 residues. The general base promoted nucleophilic attack of the coordinated water molecule on the carbonyl is shown.

A

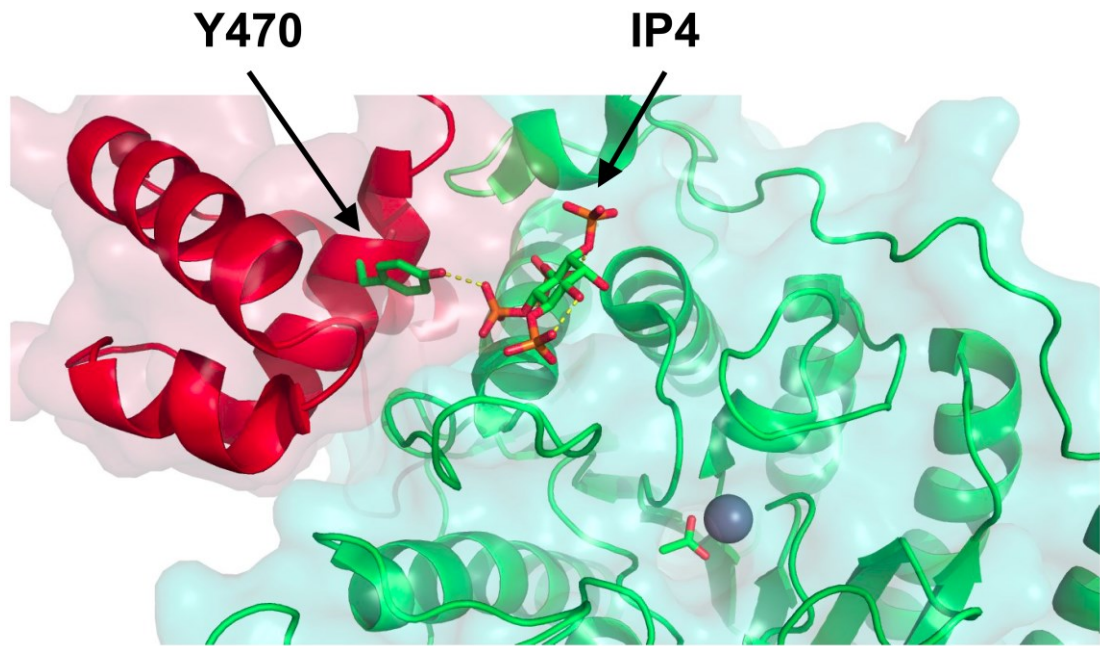


Figure 1.2 HDAC3 activation by DAD. (A) Crystal structure of HDAC3-DAD, highlighting the Y470 residue in the DAD critical for activation of HDAC3 *in vivo* and IP4 at the critical junction between HDAC3 and the DAD of SMRT.

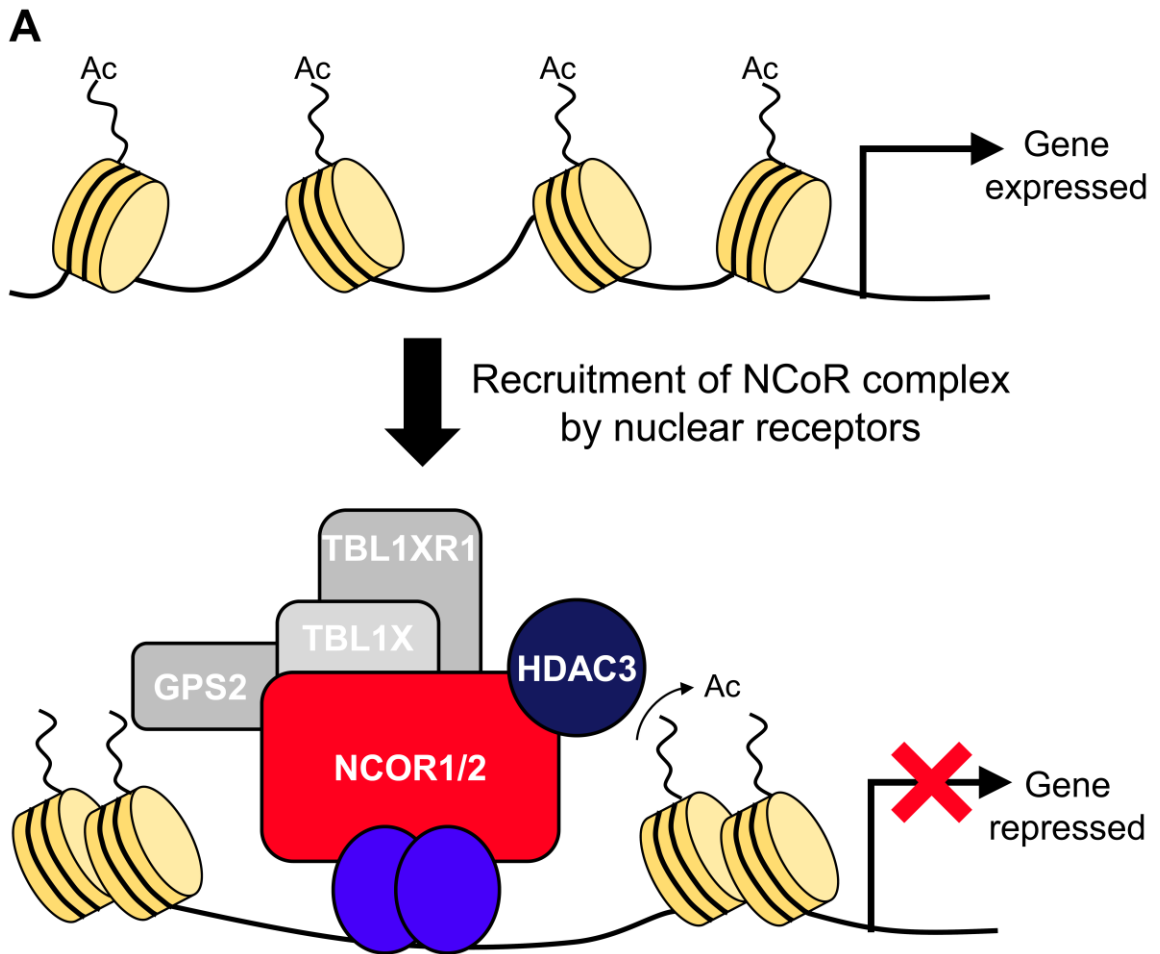


Figure 1.3 NCoR mediated repression of target genes. (A) Schematic of NCoR complex recruitment to chromatin by nuclear receptors (blue), deacetylation, and repression of gene transcription.

CHAPTER 2: Deletion of Histone Deacetylase 3 in Adult β -cells Improves Glucose Tolerance via Increased Insulin Secretion

Published in part in *Molecular Metabolism*, 2017; 6(1), 30-37.

The text, figures, and legends in this chapter were the work of Jarrett Renn Remsberg with the following exceptions. The CVI Histology core performed the immunofluorescent staining and the CHOP Pathology Core scanned insulin IHC. The Islet Core performed islet isolations and *ex vivo* batch incubations. Manashree Damle and Zhenghui Li performed ChIP-seq and RNA-seq bioinformatics analyses respectively. Ben Ediger, Wesley Ho, Christopher Teng, and Cristina Lanzillotta provided technical assistance.

2.1 ABSTRACT

Histone deacetylases are epigenetic regulators known to control gene transcription in a variety of tissues. A member of this family, histone deacetylase 3 (HDAC3), has been shown to regulate metabolic gene signatures in particular. Cell culture studies with HDAC-specific inhibitors and siRNA suggest HDAC3 plays an important role in pancreatic β -cell function, but a recent genetic study in mice has been contradictory. Here we address the functional role of HDAC3 in β -cells of adult mice. An HDAC3 β -cell specific knockout was generated using the *MIP-CreERT* transgenic mouse model. While HDAC3 β -cell specific deletion did not increase total pancreatic insulin content, the mice demonstrated markedly improved glucose tolerance and increased glucose-stimulated insulin secretion. Cistromic and transcriptomic analyses of pancreatic islets revealed that HDAC3 regulated multiple genes that contribute to glucose-stimulated insulin secretion.

2.2 INTRODUCTION

2.2a Glucose homeostasis and diabetes mellitus

Glucose homeostasis is a tightly controlled process that is critical for maintaining normal physiology. To achieve this balance, pancreatic endocrine cells secrete peptide hormones that act on peripheral tissue to properly respond. Specifically, the role of the β -cells in the pancreas is to secrete insulin in response to increase in plasma glucose levels.

This is first orchestrated by facilitated diffusion of glucose into pancreatic β -cells, mediated by the glucose transporter, GLUT2 in mice. Inside the cell, this imported glucose is rapidly converted to glucose-6-phosphate by glucokinase and proceeds through the glycolysis pathway. The glucokinase enzyme (GCK) kinetics are remarkably well tuned to be sensitive at physiologic increases in blood glucose concentration (Matschinsky, 2005). As a result of increased flux through the glycolysis pathway and subsequent TCA cycle, cellular ATP/ADP ratio increases, causing K_{ATP} channels close and depolarization. This in turn opens Ca^{2+} channels, causing an influx of Ca^{2+}

and leading to insulin granules fusing with the plasma membrane and being released into circulation. This is the canonical pathway for glucose-stimulated insulin secretion, however modulating or potentiating this response is of particular interest for therapeutic intervention.

Dysfunction of this glucose-stimulated insulin response can lead to diabetes mellitus. Type 1 diabetes mellitus is of growing clinical significance in the population and is hallmarked by autoimmune recognition of the pancreatic β -cells (Patterson et al., 2009). This proinflammatory environment created by the immune system leads to impaired function and death of the insulin producing β -cells of the pancreas, whereas type 2 diabetes mellitus is characterized by insulin resistance and failure of the insulin secreting β -cells, classically associated with obesity and low-grade inflammation (Donath and Shoelson, 2011; Weir and Bonner-Weir, 2004). Growing evidence suggests that changes in transcription, regulated by epigenetic changes may play a larger role in the pathogenesis of both these diseases than previously appreciated (Bramswig and Kaestner, 2014).

2.2b Role of HDAC3 in pancreatic β -cells

Histone deacetylase 3 (HDAC3) is a member of the class I HDACs. It functions as part of multi-protein complexes that deacetylate histone tails, thereby modifying chromatin structure and resulting in gene repression. HDAC3 has been shown to form stable complexes *in vivo* with, and be activated by, the nuclear receptor corepressor (NCoR1) and the silencing mediator for retinoic acid and thyroid hormone receptors (SMRT) (Guenther et al., 2001; Li et al., 2000). Class I HDACs are ubiquitously expressed and have been implicated in regulation of metabolic gene signatures (Sun et al., 2012). In the past several years, multiple studies of siRNA knockdown and pharmacological inhibition of HDAC3 have suggested a role for HDAC3 in β -cells, with loss of HDAC3 function protecting β -cells from cytokine-induced apoptosis and helping to maintain proper glucose-stimulated insulin secretion (Chou et al., 2012; Lundh et al., 2012, 2015; Plaisance et al., 2014; Wagner et al., 2016). Furthermore, an HDAC3-specific inhibitor was reported to improve

glucose homeostasis and insulin secretion in a diabetic rat model (Lundh et al., 2015). These studies presented an important question regarding HDAC3's role in the pancreatic β -cell, precisely the full extent of HDAC3's function. To determine this physiologic role of HDAC3 in β -cells, we applied mouse genetics to conditionally ablate HDAC3 *in vivo*. Here we demonstrate that the deletion of HDAC3 in β -cells of adult male mice improves glucose tolerance by increasing insulin secretion.

2.3 METHODS

2.3a Animal studies

The *MIP-CreERT* and HDAC3^{fl/fl} lines have previously been described (Mullican et al., 2011; Tamarina et al., 2014). Mice were maintained on a C57BL/6 background and normal chow unless otherwise noted. Analyses were restricted to male mice. Tamoxifen (Sigma T5648) was dissolved in corn oil at 20mg/mL and administered at 2mg/day via gavage for five days. Animals were assayed 2 weeks after tamoxifen induction. Intraperitoneal glucose tolerance tests (IPGTTs) were performed as previously described (Ediger et al., 2014). Glucose-stimulated insulin secretion (GSIS) assays were performed by administering mice a bolus of glucose (3g/kg) following a 16 hour fast. Plasma was separated using heparinized tubes, and insulin and C-peptide were measured using ELISA kits (Crystal Chem #90080 and #90050, respectively). Total pancreatic insulin and glucagon content were determined by radioimmunoassay (RIA) in which acid-ethanol extractions were performed on whole pancreata (EMD Millipore). All the animal care and use procedures followed the guidelines of the Institutional Animal Care and Use Committee of the University of Pennsylvania in accordance with the guidelines of the US National Institutes of Health.

2.3b Immunohistochemistry and immunofluorescence

Pancreata were dissected, weighed, fixed in 10% formalin for 16 hours at 4°C, washed with PBS, and embedded in paraffin. Tissue sections were stained as previously described using HDAC3 (H-

99 sc-11417), Insulin (ab7842), and Glucagon (N-17 sc-7780) antibodies (Ediger et al., 2014). Insulin immunohistochemistry (IHC) was performed as previously described (Ediger et al., 2014). Insulin signal was detected with Vectastain Elite ABC kit (standard; Vector, PK6100) and DAB Peroxidase Substrate Kit (Vector, SK4100). To quantify islet mass, sections were digitally scanned using an Aperio ScanScope CS2 and analyzed using ImageScope as previously described (Oropeza et al., 2015).

2.3c Islet isolation and static incubations

Islets were isolated using the standard collagenase (EC 3.4.24.3 Serva, 17449) digestion protocol as previously described (Doliba et al., 2015). For static incubations, islets were cultured for 3 days and then transferred to KREBS buffer. An equal number of islets were glucose starved for 30 minutes and then glucose-stimulated for 40 minutes. Supernatants were collected and insulin measurements performed by RIA.

2.3d RNA analysis

RNA was immediately extracted from isolated mouse islets two weeks after tamoxifen induction, and quantitative reverse transcription-PCR (RT-PCR) was performed as described (Soccio et al., 2015), using primers as indicated and normalized to *Actb* (**Table 2.1**). RNA-seq libraries were generated using the Tru-seq kit (Illumina). Raw reads were aligned to mm9 reference genome using Tophat version 2.1.0 and the parameters recommended by the original author (Trapnell et al., 2012a); gene level quantification was performed by HTSeq using default parameters (Anders et al., 2015), and differential expression analysis was performed using DESeq2 according to original authors' instructions (Love et al., 2014). RNA-seq datasets have been deposited at GEO.

2.3e ChIP-seq

Isolated mouse islets were washed with PBS, fixed with 1% formaldehyde at room temperature for 15 minutes, quenched with 125mM glycine for 5 minutes, and washed with PBS. Fixed islets were

probe sonicated at 10W and 15W for 10 seconds on and 10 seconds off, twice. Sonicated islets were lysed in RIPA buffer containing protease inhibitors and PSMF. ChIP was performed using 10 μ g HDAC3 antibody (ab7030) and protein A agarose. Cross links were reversed at 65°C overnight and proteinase K digested, followed by phenol/chloroform isolation. Libraries were prepared and sequenced as previously described (Zhang et al., 2015). Briefly, sequencing reads of biological replicates were aligned to the mm9 genome using Bowtie v0.12.7 (Langmead et al., 2009a). Duplicate reads were removed, and replicates were pooled using HOMER v4.7 (Heinz et al., 2010). Genome browser tracks were generated, and peaks were called using HOMER with default parameters and genomic DNA as input. Peaks from HDAC3^{fl/fl};Cre;Veh and HDAC3 β KO experiments were pooled, and an average profile was generated using HOMER. Additional analysis was limited to peaks in HDAC3^{fl/fl};Cre;Veh greater than 1 read per million (RPM) and more than 4-fold over HDAC3 β KO. Distribution of peaks in the genome was found using HOMER. BEDTools v2.26 was used to find peaks within 100kb of gene transcriptional start site (TSS) (Quinlan and Hall, 2010a), and gene ontology analysis was performed on said peaks using GREAT v3.0 (McLean et al., 2010). STRING analysis (Szklarczyk et al., 2015) was performed on transcription factors identified in *de novo* motif analysis of HDAC3 peaks and expressed in RNA-seq with greater than 1 normalized read count. Transcription factors with known interactions with HDAC3 are presented using Cytoscape v3.3.0. ChIP-seq datasets have been deposited at GEO.

2.4. RESULTS

2.4a Deletion of HDAC3 in β -cells does not significantly alter insulin content or islet mass

To generate β -cell specific deletion of HDAC3 in C57BL/6 mice, HDAC3^{fl/fl} mice were crossed with mice expressing tamoxifen-inducible Cre recombinase under control of the mouse insulin 1 gene promoter (*MIP-CreERT*) (Mullican et al., 2011; Tamarina et al., 2014). This Cre line has previously been shown to be β -cell specific without recombination detected in the brain, unlike other putatively

β -cell specific deletion models such as *RIP-Cre* (Magnuson and Osipovich, 2013). The HDAC3 β -cell knockout (HDAC3 β KO) was induced by 5 days of tamoxifen administration (2 mg/day) to 8 week old mice, and immunofluorescence studies confirmed the knockout of HDAC3 in insulin-positive islet cells when compared to HDAC3^{fl/fl} mice expressing the *MIP-CreERT* transgene administered corn oil vehicle (HDAC3^{fl/fl};Cre;Veh) two weeks after induction (**Figure 2.1A**). The remaining islet HDAC3 signal was likely due to non-beta cells in the islet in addition to any β -cells in which the knockout was incomplete. The β -cell deletion of HDAC3 was supported by quantitative RT-PCR for *Hdac3* transcript in freshly isolated islets (**Figure 2.1B**). There were no significant differences in the total pancreatic insulin (**Figure 2.1C**) or glucagon content (**Figure 2.1D**) in the HDAC3 β KO mice. Islet architecture, assessed by insulin immunohistochemistry staining (**Figure 2.1E**), and islet mass (**Figure 2.1F**) were not appreciably altered in the HDAC3 β KO mice.

2.4b HDAC3 ablation in β -cells of adult mice markedly improves glucose tolerance

To characterize the physiological consequences of the HDAC3 β KO on β -cell function, we determined their glucose tolerance. Notably, there was a marked improvement in glucose tolerance in HDAC3 β KO mice during glucose challenge, as well as a modest fasting hypoglycemia. (**Figure 2.2A**). The improvement in glucose tolerance was observed when comparing HDAC3 β KO animals to HDAC3^{fl/fl} mice administered tamoxifen (HDAC3^{fl/fl};Tam) or to HDAC3^{fl/fl} mice expressing the *MIP-CreERT* administered corn oil vehicle (HDAC3^{fl/fl};Cre;Veh). This result is consistent with a recent finding that the *MIP-CreERT* transgene does not impair or enhance glucose homeostasis despite expressing human growth hormone (Oropeza et al., 2015). The HDAC3 β KO did not significantly alter body weight relative to control 6 weeks after induction of the knockout (**Figure 2.2B**). In addition, the improved glucose phenotype remains present over time, as mice assayed 6 weeks after knockout induction have significantly increased glucose tolerance (**Figure 2.2C**).

2.4c Deletion of HDAC3 in β -cells of obese mice markedly improves glucose tolerance

To determine if the loss of β -cell HDAC3 improves glucose tolerance in a model of obesity with associated insulin resistance, mice were placed on high fat diet starting at 6 weeks of age. Tamoxifen was administered at 18 weeks of age, and glucose tolerance was assessed at 20 weeks of age. The knockout of HDAC3 in β -cells of obese mice did not alter body weight (**Figure 2.3A**) but did result in significant improvement in glucose tolerance (**Figure 2.3B**). These data show that acute deletion of HDAC3 has beneficial effects on glucose metabolism in the setting of diet-induced obesity.

2.4d Improved glucose tolerance is a due to increased insulin secretion

To investigate the physiological basis of improved glucose tolerance in HDAC3 β KO mice, we next explored the effect of HDAC3 β -cell specific knockout on insulin secretion. It has been shown previously that pharmacological HDAC3 inhibition or knockdown in cell culture can maintain glucose-stimulated insulin secretion in the presence of cytokines (Chou et al., 2012; Lundh et al., 2012; Wagner et al., 2016). Of note, HDAC3 β KO mice on normal chow displayed significantly increased circulating insulin after a 16 hour fast, as well as 3 minutes after a glucose challenge (**Figure 2.4A**). This finding was corroborated by increased plasma C-peptide in the fasted and glucose-stimulated conditions (**Figure 2.4B**). Further, in the setting of diet induced obesity, glucose-stimulated insulin secretion was increased in HDAC3 β KO mice (**Figure 2.4C**). These data suggest that the loss of HDAC3 in β -cells led to increased insulin secretion and was responsible for the improved glucose tolerance. To determine if the increased insulin secretion was a cell-autonomous effect of β -cell depletion of HDAC3, glucose-stimulated insulin secretion was examined *ex vivo* in isolated islets from mice on normal chow. Indeed, HDAC3 β KO islets secreted more insulin at lower glucose concentrations than control islets, whether normalized to the number of islets (**Figure 2.4D**) or to total insulin content (**Figure 2.4E**), which was not significantly altered by the loss of HDAC3 (**Figure 2.4F**). The enhanced insulin secretion at low glucose concentrations

ex vivo is consistent with the increased basal insulin secretion observed during fasting of HDAC3 β KO mice, whereas the plateau of insulin secretion at high glucose for 40 minutes may not be directly comparable to the *in vivo* GSIS measured 3 minutes after glucose challenge.

2.4e HDAC3 cistrome in isolated islets

To further investigate the means by which HDAC3 influences insulin secretion *in vivo*, we sought to determine the HDAC3 cistrome in isolated islets. To achieve this goal, islets from HDAC3^{fl/fl};Cre;Veh and HDAC3 β KO were isolated and pooled for chromatin immunoprecipitation with massively parallel DNA sequencing (ChIP-seq). There was robust enrichment for HDAC3 in the HDAC3^{fl/fl};Cre;Veh control islets compared to HDAC3 β KO (**Figure 2.5A**). We identified 9972 peaks in the HDAC3^{fl/fl};Cre;Veh control with greater than 1 read per million (RPM) and 4 fold over input library; 8975 of these peaks had greater than 4 fold enrichment over the HDAC3 β KO cistrome. Consistent with HDAC3 cistromes from other tissues, the majority of genomic binding was intronic or intergenic, with only a minority of binding sites at promoters or transcriptional start sites (TSS) (**Figure 2.5B**) (Feng et al., 2011). Using the genomic regions enrichment of annotations tool (GREAT), HDAC3 binding was found to be enriched at a variety of biological processes critical for β -cell function, including endocrine development and regulation of insulin secretion (**Figure 2.5C**). These data suggest that HDAC3 could be a critical transcriptional regulator of genes involved in β -cell function and maintaining glucose homeostasis.

2.4f Transcriptome of HDAC3 β -cell KO reveals potential pathways contributing to increased insulin secretion

To better understand the functional role of HDAC3 in the β -cell, we performed RNA-seq on islets from HDAC3 β KO mice in two separate cohorts of mice, one relative to HDAC3^{fl/fl};Tam controls that lack the *MIP-CreERT* transgene, and the other compared to the HDAC3^{fl/fl};Cre;Veh mice. Since the two control models displayed indistinguishable glucose homeostasis, we reasoned that genes significantly regulated in both experiments would shed light on the mechanisms by which HDAC3

influences insulin secretion. This was particularly relevant given the recent report that *Tph1* is dramatically induced in the *MIP-CreERT* transgenic mouse, leading to increased islet serotonin levels (Oropeza et al., 2015), which have been correlated with increased β -cell mass in pregnancy (Kim et al., 2010). Using both control groups, transcriptomic analysis revealed 264 and 222 significantly up- and down-regulated genes in the HDAC3 β KO islets (**Figure 2.6A**). Gene ontology analysis of the up-regulated genes revealed amino acid activation, vesicle transport, anion transport, and carbohydrate metabolism as significantly enriched processes (**Figure 2.6B**). Quantitative RT-PCR confirmed RNA-seq results for many of the up-regulated transcripts in the HDAC3 β KO (**Figure 2.6C**).

2.4g Integrating transcriptomic and cistromic analyses of HDAC3 role in β -cells

Intersection of the islet transcriptomes and HDAC3 cistrome revealed that HDAC3 bound more prevalently near genes that are subsequently up-regulated in the β -cell KO (**Figure 2.7A**). The concordance of HDAC3 genomic binding with derepressed transcription in the HDAC3 β KO islet is exemplified at the *Tmem40* locus (**Figure 2.7B**). Genome-wide *de novo* analysis of DNA sequences enriched under HDAC3 binding peaks revealed Forkhead, RFX5, PDX1, E-box, MADS-box, bZIP, nuclear receptor, SP1, and STAT motifs (**Figure 2.7C**). Intersection of these motifs with of transcription factors expressed in the islet transcriptome revealed several signal-responsive factors with the potential to function with HDAC3, including circadian proteins Rev-erb α , ROR, and CLOCK (**Figure 2.7D**), which may reflect the known role of HDAC3 in the circadian clock in other tissues (Feng et al., 2011).

2.5 DISCUSSION

Our work demonstrates that HDAC3 in β -cells regulates insulin secretion and glucose metabolism. HDAC3 is a critical epigenetic modifying enzyme and regulator of metabolic gene signatures. Previous studies suggested a role for HDAC3 in mediating cytokine-induced apoptosis in cultured

β -cell models and in a diabetic rat model, but the present study is the first to demonstrate that adult mice lacking HDAC3 in their β -cells display markedly increased glucose clearance and tolerance.

The present studies, determining the physiological consequence of acute HDAC3 ablation in adult mouse β -cells, suggest that HDAC3 plays an important role in modulating insulin secretion in normal conditions as well as in the setting of diet-induced obesity. While these conclusions are consistent with the beneficial result of HDAC3 specific inhibition in a diabetic rat model (Lundh et al., 2015), they are contrary to those of a recent report where HDAC3 ablation was generated using *RIP-Cre* (Chen et al., 2016). A major concern about the *RIP-Cre* model is that it has been shown to produce off-target tissue recombination, particularly in the brain, where HDAC3 has been shown to have important effects on behavior (McQuown et al., 2011; Nott et al., 2016; Rogge et al., 2013). Also, the *RIP-Cre* model is not inducible; therefore, the effects in β -cells may emphasize the role of HDAC3 in development rather than in the mature adult pancreas. Indeed, our cistromic results suggest that HDAC3 genomic binding is enriched near genes involved in endocrine development, and two genes upregulated in the HDAC3 β KO, *Rgs8* and *Rgs16*, have been shown to be dynamically regulated in the developing pancreas (Villasenor et al., 2010). Nevertheless, the *MIP-CreERT* model that we have used to delete HDAC3 avoids the problem of brain expression and clearly demonstrates an inhibitory role of HDAC3 on insulin secretion from adult β -cells *ex vivo* and *in vivo*.

We have identified a number of genes controlled by HDAC3 in β -cells with known or plausible roles in glucose-stimulated insulin secretion. Among these are the organic anion transporters *Slco1a5* and *Slco1a6*. Intriguingly, the *Slco1a6* gene locus has been identified as an important quantitative trait locus (QTL) in β -cells, regulating gene transcription by altering transport of bile acids in islets (Tian et al., 2015). Notably, bile acids have been shown to potentiate glucose-stimulated insulin secretion (Düfer et al., 2012). In addition to these transporters, *Rgs16* was shown to be regulated, which has been shown to increase glucose-stimulated insulin secretion (Vivot et al., 2016).

Furthermore, *S100a4* and its paralog *S100a6* are identified as up-regulated in the HDAC3 β KO RNA-seq analysis. These genes are defined to be calcium binding proteins, and *S100a6*, also known as Calcyclin, has been shown to potentiate Ca²⁺ stimulated insulin release (Okazaki et al., 1994).

In silico analysis of the HDAC3 binding sites in islets suggested a potential role of several signal responsive transcription factors including STAT and bZip family members, as well as components of the circadian clock. Although highly speculative, the latter is intriguing given the known role of the molecular clock in controlling β -cell functions (Lee et al., 2015; Perelis et al., 2015). Interestingly, we did not detect an increase in insulin gene transcription in HDAC3 β KO islets (data not shown). Although this is consistent with the physiologic data presented here, it is worth noting that a previous study using the pan-HDAC inhibitor Trichostain A (TSA) increased insulin gene transcription (Mosley and Özcan, 2003). However, this drug inhibits all class 1 HDACs and thus the present results suggest that other HDACs and/or other targets are responsible for the effects of TSA in β -cells.

In summary, we have described the physiological role of HDAC3 in adult mouse β -cells and identified several target genes that may in combination act to increase glucose-stimulated insulin secretion *in vivo*. Thus, HDAC3 is a critical regulator of gene transcription in β -cells and, as a druggable enzyme that modulates the epigenome, a potential therapeutic target to improve glucose homeostasis, especially in the setting of diet-induced obesity and metabolic stress.

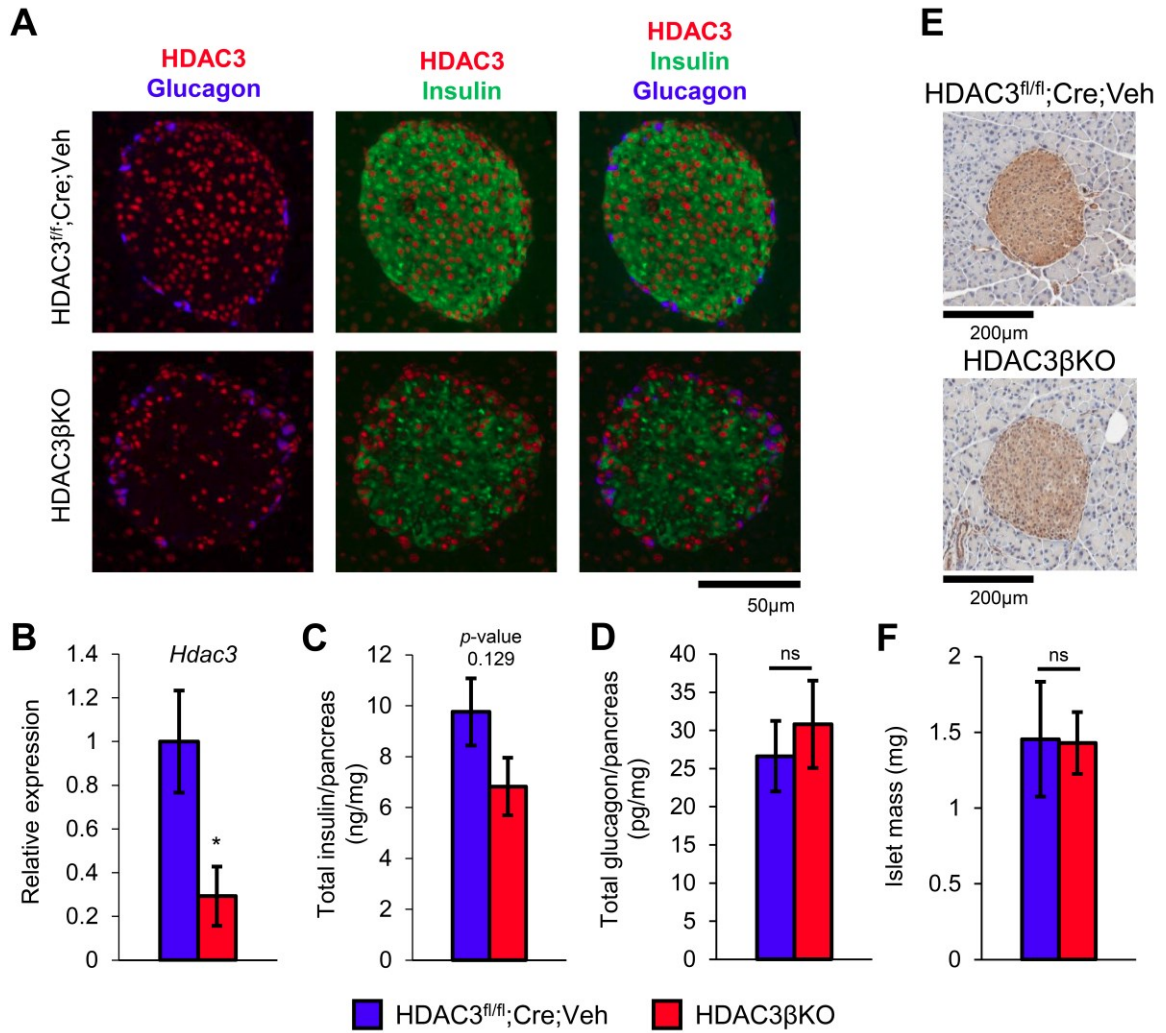


Figure 2.1 HDAC3 β -cell KO does not increase insulin content or islet mass. (A) Co-immunofluorescence for HDAC3, Insulin, and Glucagon (20X). (B) Quantitative RT-PCR of freshly isolated islets (n=5). (C, D) Total pancreatic insulin and glucagon content normalized to pancreatic weight (n=4-6). (E) Insulin immunohistochemistry (IHC) staining (20X). (F) β -cell mass quantified from insulin IHC staining (n=4). All error bars, s.e.m. (t-test, * p <0.001).

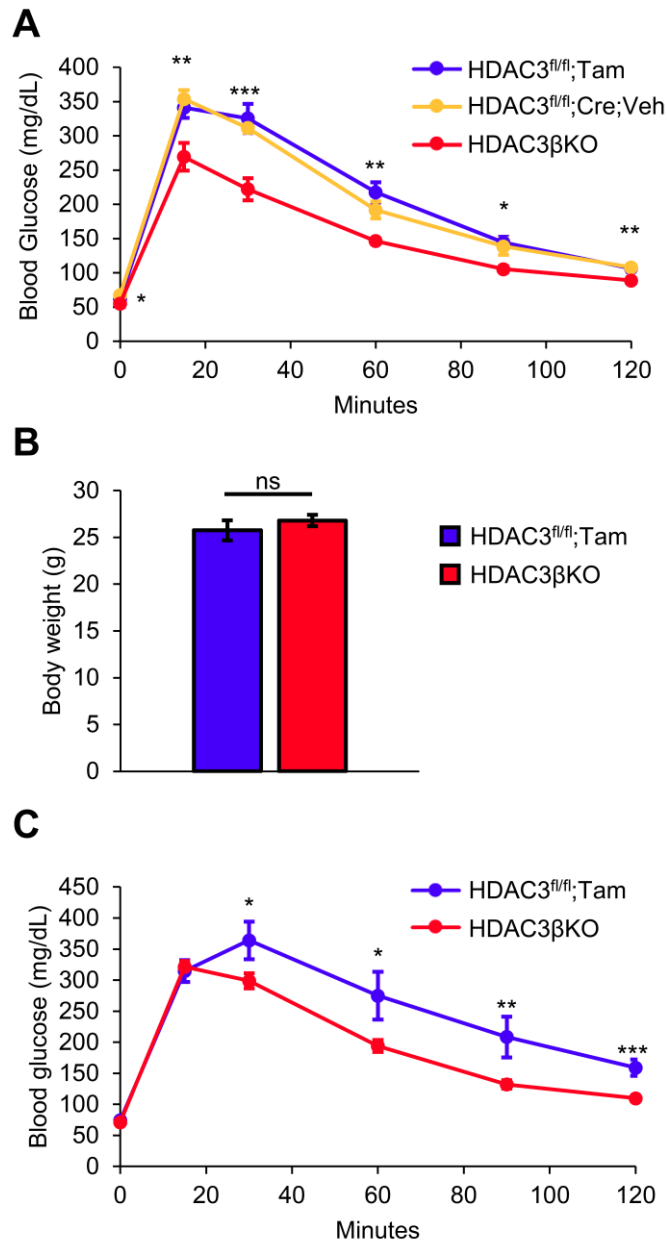


Figure 2.2 Deletion of HDAC3 in β -cells of adult mice markedly improves glucose tolerance.

(A) Intraperitoneal glucose tolerance test (IPGTT) of mice on normal chow (NC) at 10 weeks of age, 2 weeks after tamoxifen administration, 2g/kg glucose (n=5, t-test compares HDAC3^{fl/fl};Cre;Veh and HDAC3 β KO). **(B)** Weight of mice on NC 6 weeks after tamoxifen induction of KO. **(C)** IPGTT 6 weeks after KO induction (n=6-11). All error bars, s.e.m. (t-test, * p <0.05, ** p <0.01, *** p <0.001).

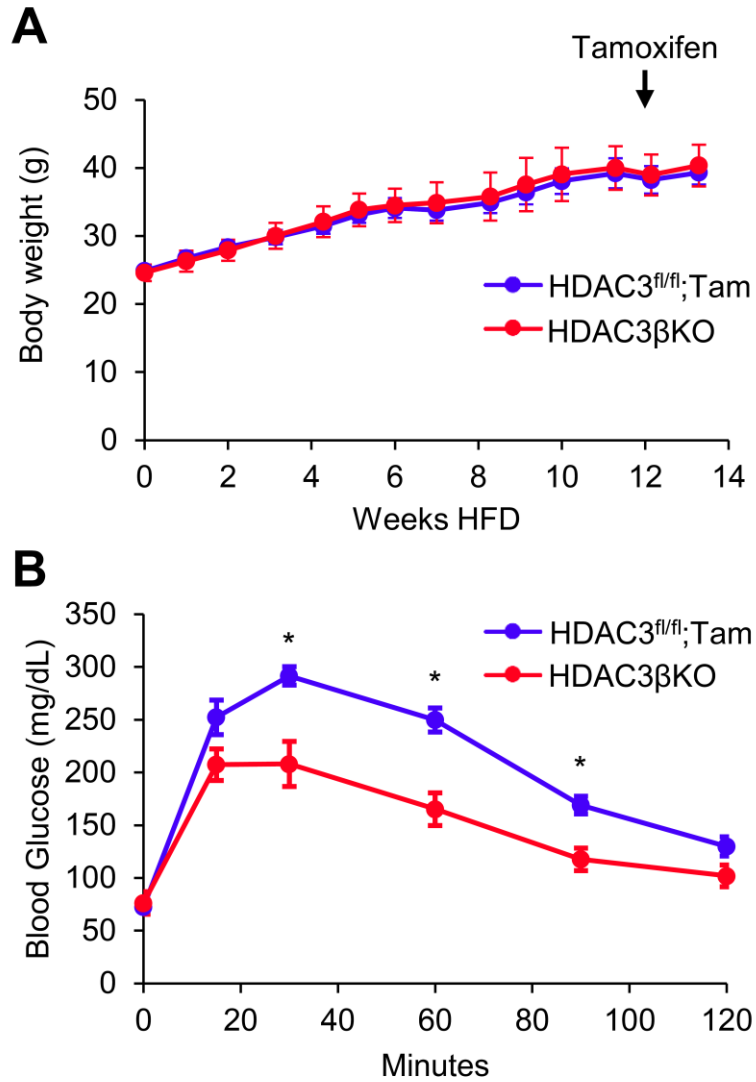


Figure 2.3 HDAC3 β -cell KO improves glucose tolerance in the setting of diet-induced obesity. (A) Body weights of mice on high fat diet (HFD). (B) IPGTT in mice after 14 weeks high fat diet and 2 weeks after tamoxifen administration, 1g/kg glucose (n=5). All error bars, s.e.m. (t-test, * p <0.01).

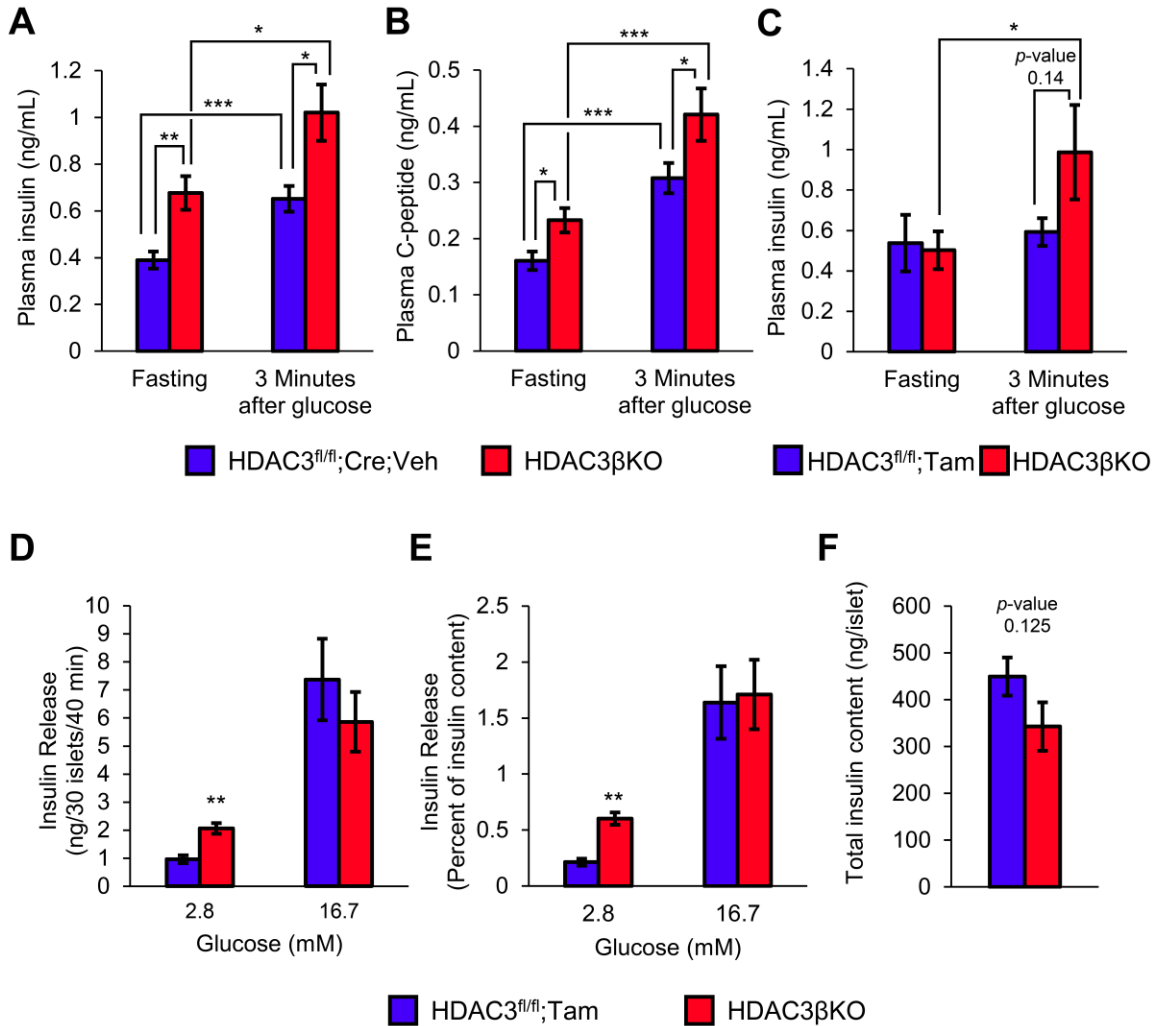


Figure 2.4 HDAC3 β -cell KO mice have increased insulin secretion. (A, B) Plasma insulin and C-peptide of mice on normal chow after a 16 hour fast, and 3 minutes after intraperitoneal glucose injection (3g/kg) (n=14). (C) Plasma insulin in mice on HFD for 15 weeks after a 16 hour fast, and 3 minutes after intraperitoneal glucose injection (3g/kg) (n=5). (D, E, F) Glucose-stimulated insulin secretion (GSIS) *ex vivo* from isolated islets and corresponding total insulin content (n=5-9). All error bars, s.e.m. (t-test, * p <0.05, ** p <0.01, *** p <0.001).

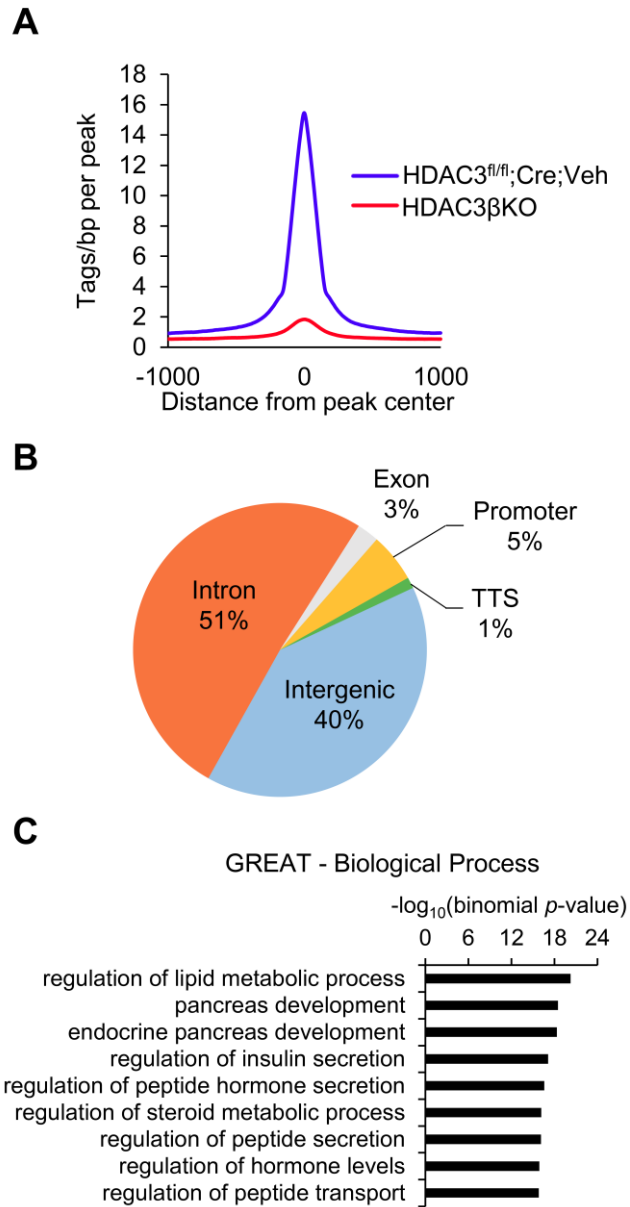


Figure 2.5 HDAC3 cistrome in isolated islets. (A) Average profile of HDAC3 binding in HDAC3^{fl/fl};Cre;Veh and HDAC3 β KO. (B) Distribution of HDAC3 genomic binding relative to known genes. (C) GREAT analysis of HDAC3^{fl/fl};Cre;Veh specific peaks filtered against HDAC3 β KO.

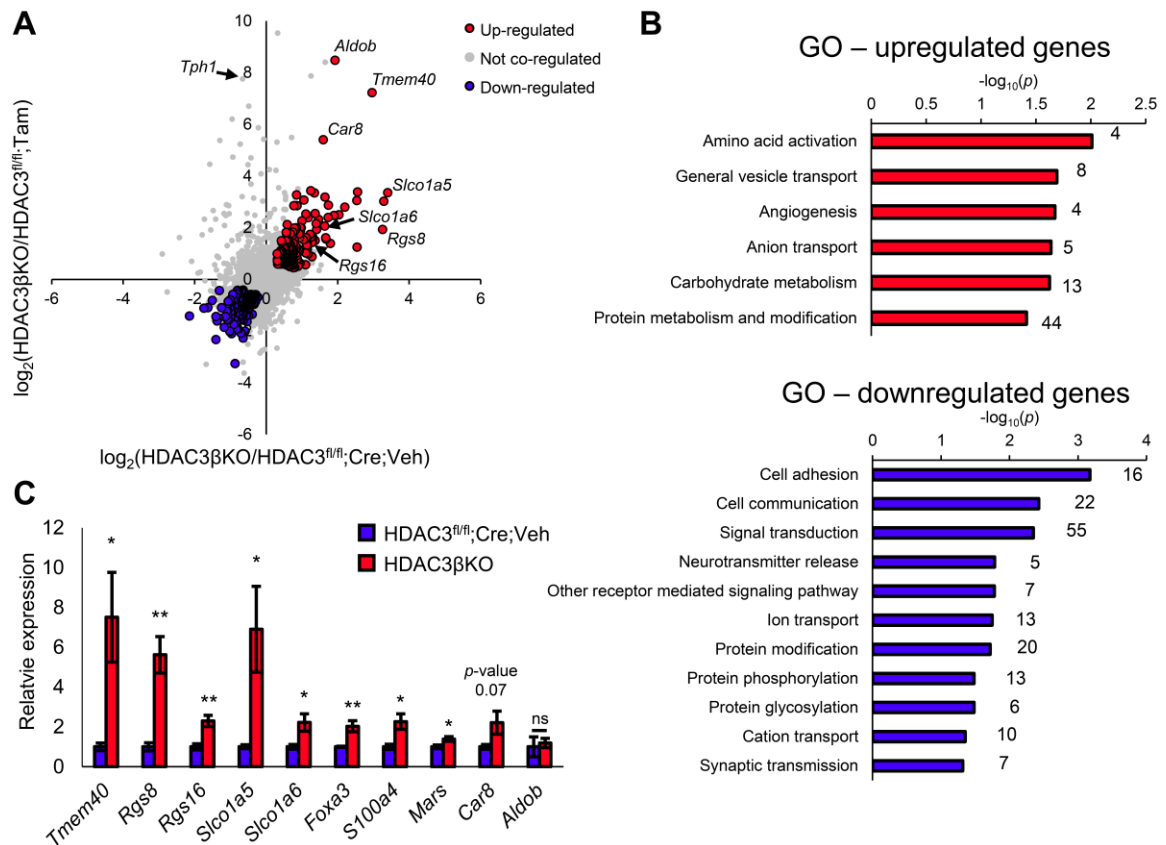


Figure 2.6 RNA-seq analysis of HDAC3 β KO compared to HDAC3^{fl/fl};Cre;Veh and HDAC3^{fl/fl};Tam mice. (A) Scatter plot of log₂ fold change from two separate RNA-seq experiments. Red dots are significant (FDR<0.1) in both experiments and up-regulated 1.5 fold or greater in either HDAC3 β KO. Blue dots are significant (FDR<0.1) in both experiments and down-regulated 1.5 fold or greater in either HDAC3 β KO. (B) Gene ontology (GO) biological process enrichment results using 264 upregulated genes and 222 downregulated genes. Only significantly enriched ($p < 0.05$) terms are shown. For each terms, the numbers of the genes that contribute to the enrichment is labeled. (C) Quantitative RT-PCR confirming significant upregulation of transcripts from RNA-seq in the HDAC3 β KO (n=5) (All error bars, s.e.m., t-test, * $p < 0.05$, ** $p < 0.01$).

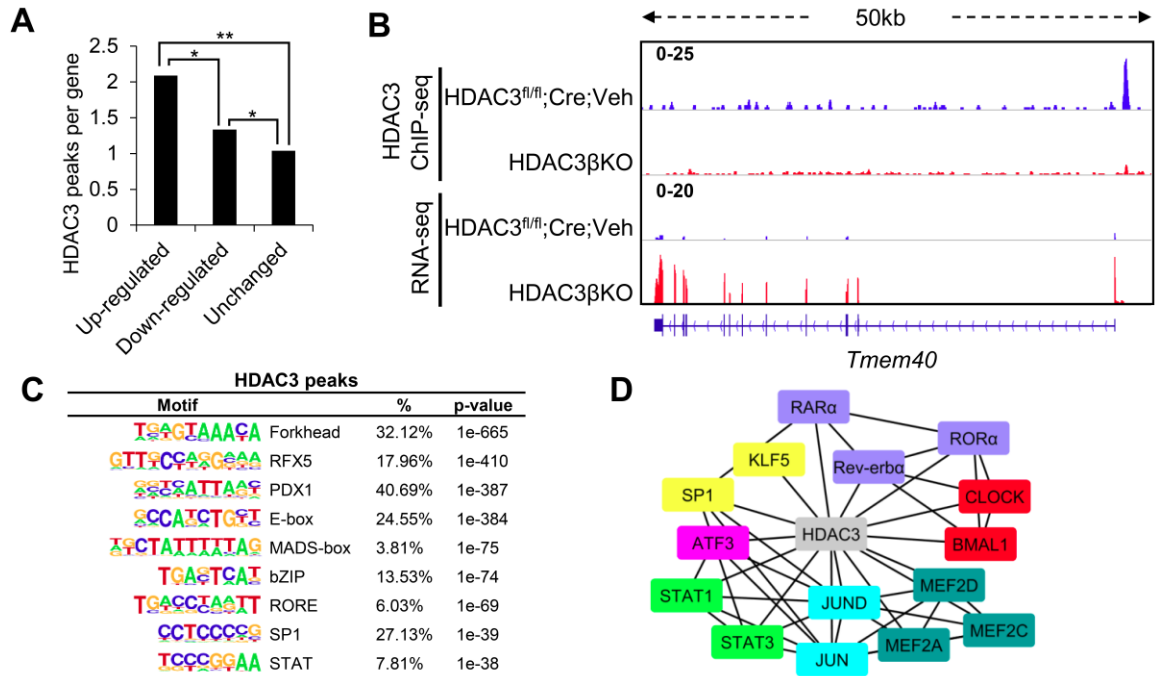


Figure 2.7 HDAC3 cistromic analysis suggests multiple β -cell lineage factors utilize the NCoR complex. (A) HDAC3 peak frequency within 100kb of gene TSS from RNA-seq analysis (Mann-Whitney-Wilcoxon test, $*p < 0.05$, $**p < 0.0001$). **(B)** Genome-browser view of ChIP-seq and RNA-seq tracks of the *Tmem40* gene. **(C)** *De novo* motif analysis at HDAC3 binding sites genome-wide using HOMER. Motifs with p -value $< 1e-150$ or known interactions are shown. **(D)** STRING analysis of transcription factors identified by *de novo* motif analysis of HDAC3 peaks. Transcription factor families are denoted by different colors.

Table 2.1 List of primers for quantitative RT-PCR gene expression.

Gene	Forward Primer	Reverse Primer
<i>Hdac3</i>	TTGGTATCCTGGAGCTGCTT	GACCCGGTCAGTGAGGTAGA
<i>Tmem40</i>	ACAGGGAAACGGAAGATCAC	AGGAGGAAGAGGAGGAAGAAG
<i>Rgs8</i>	AGGTCAACTGCAAAGCTAGTC	CAAAACAAGTCAGGGATGGC
<i>Rgs16</i>	ATCTTTGACGAGTACATCCGC	TCCTTCTCCATCAATGTGCG
<i>Slco1a5</i>	CTGAGGTGTATCAAGTCTGAAGAG	AGAGTTCCCAATGTAAGCAG
<i>Slco1a6</i>	TTGTGCAGTTATGGGCCTAG	GGCTTTAAGGTCTGGGATCTG
<i>Foxa3</i>	CAGTGAAGATGGAGGCTCATG	GAGTGGGTTCAAGGTCATGTAG
<i>S100a4</i>	CAGCAACAGGGACAATGAAG	ACTACACCCCAACACTTCATC
<i>Mars</i>	TGGTCTTTCCGTGTTTCAGTC	GTCTCAAACACTCCTATGCC
<i>Car8</i>	TTGAAGGCTGTGACTGAGATC	CTGCAAGGTGGGATAGTAAGAG
<i>Aldob</i>	CACCGATTTCCAGCCCTC	GTTCTCCACCTTTATCCTTTGC
<i>Actb</i>	ACCGTGAAAAGATGACCCAG	GAGCATAGCCCTCGTAGATG

**CHAPTER 3: An HDAC3-PROX1 Corepressor Module Acts on HNF4 α to Control
Hepatic Triglycerides**

The text, figures, and legends in this chapter were the work of Jarrett Renn Remsberg with the following exceptions. Sean Armour contributed equally to the manuscript and generated ChIP-qPCR and ChIP-seq libraries. Manashree Damle and Zhenghui Li performed ChIP-seq and RNA-seq bioinformatics analyses respectively. The Molecular Pathology and Imagine Core performed histology. Wesley Ho provided mouse husbandry and technical assistance. Simone Sidoli provided mass spectrometry technical assistance.

3.1 ABSTRACT

The histone deacetylase HDAC3 is a critical mediator of hepatic lipid metabolism, and liver-specific deletion of HDAC3 leads to fatty liver. To elucidate the underlying mechanism we developed a method of cross-linking followed by mass spectrometry to define a high-confidence HDAC3 interactome *in vivo* that includes the canonical NCoR-HDAC3 complex as well as Prospero-related homeobox 1 protein (PROX1). HDAC3 and PROX1 co-localize extensively on the mouse liver genome, and are co-recruited by Hepatocyte Nuclear Factor 4 α (HNF4 α). The HDAC3-PROX1 module controls the expression of a gene program regulating lipid homeostasis, and hepatic-specific ablation of either component increases triglyceride content in liver. These findings underscore the importance of specific combinations of transcription factors and coregulators in the fine tuning of organismal metabolism.

3.2 INTRODUCTION

Hepatic lipid homeostasis is critical for the maintenance of normal liver physiology and organismal metabolism. Lipid composition and accumulation in the liver is controlled by a complex network of interconnected metabolic pathways such as lipid synthesis, lipolysis, β -oxidation, secretion, and storage, and the dysregulation of even one of these pathways can lead to lipid accumulation in liver, or hepatic steatosis (Browning and Horton, 2004; Tilg et al., 2016). Non-alcoholic fatty liver disease (NAFLD), defined by excess fat in the liver, is of growing clinical relevance in industrialized countries and is a major risk factor for the development of non-alcoholic steatohepatitis, liver fibrosis and cirrhosis (Cohen et al., 2011). In addition, NAFLD has been linked to cardiovascular disease, metabolic syndrome, insulin resistance and hepatocellular carcinoma (Tilg et al., 2016). Thus, the mechanisms governing liver lipid homeostasis are of broad importance to understanding the development of NAFLD and to identify targets for therapeutic intervention.

These pathways of lipid homeostasis are regulated in liver by a host of transcription factors including the nuclear receptors HNF4 α (Hayhurst et al., 2001; Sladek et al., 1990), Rev-erb α (Feng et al., 2011), LXRs (Calkin and Tontonoz, 2012), PPARs (Gross et al., 2016), and the E-box binding proteins SREBP and ChREBP (Xu et al., 2013) amongst others. In addition to these sequence-specific DNA binding factors, numerous cofactors and coregulators have been shown to influence the expression of genes controlling lipid metabolism (Wang et al., 2015). Previous work has demonstrated histone deacetylase 3 (HDAC3) to be an important epigenomic coregulator in liver (Feng et al., 2011; Knutson et al., 2008), and deletion of HDAC3 in adult liver results in remarkable hepatic steatosis (Sun et al., 2012). However, the fundamental mechanisms of how HDAC3 controls metabolic gene transcription in liver are not completely understood.

HDAC3 is unique among the class I histone deacetylases as it requires binding to the nuclear receptor corepressor (NCOR1) (Hörlein et al., 1995) or the silencing mediator for retinoic acid and thyroid hormone receptors (SMRT or NCOR2) (Chen and Evans, 1995) for its enzymatic activity (Guenther et al., 2001; Wen et al., 2000; You et al., 2013). Together with transducing β -like 1X-linked and receptor 1 (TBL1X and TBL1XR1) (Guenther et al., 2000) and the G-protein suppressor 2 (GPS2) (Zhang et al., 2002), these proteins form the core of the NCoR transcriptional repressor complex (Lazar, 2003). The NCoR complex has been shown to be a major corepressor complex for the nuclear receptor family of transcription factors (Chen and Evans, 1995; Hörlein et al., 1995; Ishizuka and Lazar, 2003; Lazar, 2003). Deletion of individual components of the NCoR complex results in an increase in liver triglycerides (Kulozik et al., 2011; Shimizu et al., 2015; Sun et al., 2012), highlighting the importance of these proteins acting together as a functional complex to regulate liver metabolic gene transcription.

The vast number of transcriptionally relevant complexes highlights the important roles protein-protein interactions play in the control of gene expression. For HDAC3, there are important questions about which transcription factors recruit it to the genome, and which HDAC3-associated

proteins act as downstream effectors to impact lipid gene regulation and hepatic steatosis. Here we describe NEAT ChIP-MS (Nuclear Extraction Affinity Tag), an improved chromatin cross-linking method followed by nano liquid chromatography-tandem mass spectrometry (nLC-MS/MS) analysis to identify *in vivo* interactions in liver and define a high-confidence interactome for HDAC3. We find a strong association between HDAC3 and the Prospero-related homeobox 1 protein (PROX1), which co-localize at the genome and at some sites are completely dependent on the nuclear receptor HNF4 α for their co-recruitment. Interestingly, depletion of PROX1 in liver results in increased hepatic triglycerides similar to loss of HDAC3. Our results suggest an important role for an HDAC3-PROX1 corepression module in regulating the transcription of a gene program important for the maintenance of lipid homeostasis.

3.3 METHODS

3.3a Animal studies

Male wild-type C57BL/6 mice were purchased from Jackson labs. *Hdac3^{fl/fl}* mice generated in-house were described previously (Sun et al., 2012). *Hnf4 α ^{fl/fl}* animals were a kind gift of Dr. Klaus Kaestner (Parviz et al., 2002). Mice were housed in a temperature-controlled specific-pathogen-free facility under 12 hour light/dark cycles (lights on at 7:00, off at 19:00). Adult male mice between the ages of 10-16 weeks old were used in all experiments unless otherwise indicated. AAV8 TBG Cre was intravenously injected at 1.5×10^{11} GC per mouse to induce hepatocyte-specific gene knockout, using AAV8 TBG GFP as a negative control. For MS experiments AAV8 TBG HDAC3-HA or control AAV8 TBG HA-EGFP vectors were injected at 5×10^{10} GC per mouse in combination with either AAV8 TBG Cre or AAV TBG GFP respectively. All mice in an experiment received equal total dosages of AAV vectors by supplementing with AAV8 TBG empty or AAV8 TBG GFP vectors where appropriate. All mice were euthanized by CO₂ inhalation followed by tissue harvest at 2 weeks after viral injection at ZT10 except indicated otherwise. All animal procedures followed the guidelines of the Institutional Animal Care and Use Committee of the University of Pennsylvania.

3.3b Constructs and viral vectors

AAV8 TBG viral constructs for the expression of HA-EGFP and HDAC3-HA were generated by PCR cloning and Gibson Assembly. All constructs were sequence verified by Sanger sequencing at the Penn Genomic Analysis Core. Adeno-associated viruses were produced and purified by the University of Pennsylvania Vector Core. AAV-based knockdown vectors were generated through Gibson cloning of *Egfp* and the UltramiR mir-30 scaffold (Knott et al., 2014) into a modified AAV8 TBG vector containing a downstream Woodchuck Hepatitis Virus Posttranscriptional Regulatory Element (WPRE). Two target sequences used for *Prox1* knockdown, determined using the shERWOOD algorithm (Knott et al., 2014), were: (TTCAGAGCAGGATGTTGAATA) and (GAGAAGGCAGCAACAAAGAAA). The control shRNA sequence targeting Luciferase was (CGCTGAGTACTTCGAAATGTC). For *in vivo* knockdown experiments mice received 1×10^{12} GC per mouse of each *Prox1* targeting virus or 2×10^{12} GC per mouse of the control shLuciferase virus. For enhancer luciferase reporter vectors, enhancers for *G0s2* were selected by comparing H3K27Ac and GRO-seq tracks (GEO Accession number GSM1437738) (Fang et al., 2014) with binding sites for HDAC3, PROX1, and HNF4 α . Enhancer regions of 200 bp were cloned into the MCS of the pGL4 luciferase reporter system (Promega). pRL-SV40 renilla was used as a control for firefly luciferase expression. Primers used in this study can be found in Table 3.2.

3.3c Liver triglyceride measurement and Oil Red O staining

For measuring triglyceride, livers were lysed in lysis buffer (140 mM NaCl, 50 mM Tris and 1% Triton X-100, pH 8.0) followed by triglyceride assay using LiquiColor kit (Stanbio). Oil Red O staining was performed by the University of Pennsylvania Center for Molecular Studies in Digestive and Liver Disease Molecular Pathology & Imaging Core.

3.3d Cell culture and Luciferase Assay

HEK 293T cells purchased from ATCC were maintained in DMEM medium containing 10% FBS and 100 ug/ml Penicillin/Streptomycin at 5% CO₂ and 37°C. Transfections of plasmids for the

expression of proteins and luciferase reporter constructs were performed using Fugene 6 (Roche). For luciferase assays, after 18-24 hours of transfection, cells were washed once with PBS followed by lysis in passive lysis buffer (Promega). Lysates were analyzed for firefly and control renilla luciferase activity using the Dual-Luciferase Reporter Assay System (Promega) according to the manufacturer's instructions and read on a microplate reader equipped with a dual-injection system (BioTek).

3.3e Immunoprecipitation and western blotting

For western blot analysis of total lysates, samples were lysed in a TissueLyser (Qiagen) in radioimmunoprecipitation assay buffer (RIPA buffer) supplemented with Complete EDTA-free protease inhibitor (Roche) and 1 mM PMSF. Samples were resolved by Tris-glycine SDS-PAGE (Biorad), transferred to nitrocellulose membrane (Biorad), and blotted with the indicated antibodies. Antibodies for western blotting were anti-PROX1 (Millipore, 07-537), anti-HDAC3 (GeneTex, GTX113303), anti-HNF4 α (Santa Cruz, sc-8987), anti-HA 3F10 High Affinity (Roche, 12013819001), anti-FLAG M2 (Sigma, A8592), anti-Actin (Santa Cruz, sc-1616) and anti-HSP90 (Cell Signaling, 4874). For immunoprecipitation followed by western blot livers were cross-linked with 2 mM dithiobis(succinimidyl propionate), DSP (Pierce) in PBS at room temperature for 30 mins, quenched with glycine, washed with ice cold PBS, and subsequently lysed in RIPA buffer containing protease inhibitors and PMSF. Samples were pre-cleared with protein A sepharose CL-4B (GE Healthcare), and incubated with either anti-HA agarose (Sigma, A2095) or with anti-HDAC3 (GeneTex, GTX113303) or anti-PROX1 (Millipore, 07-537) antibodies and captured with TrueBlot anti-Rabbit IgG agarose (Rockland). Immunoprecipitates were washed 5 times with RIPA and eluted with SDS loading dye. For *in vitro* coimmunoprecipitation analysis, HEK 293T cells were transfected with pcDNA FLAG-NCOR1 or PROX1 vectors with Fugene 6 (Promega). For domain mapping of PROX1 interaction with HDAC3, pcDNA FLAG-tagged PROX1 mutants, HDAC3-HA and EGFP were transfected as indicated. At 72 hours after transfection, cells were washed with PBS and lysed in IP buffer (50 mM Tris 7.4, 150 mM NaCl, and 0.5% NP-40) containing protease

inhibitors and 1mM PMSF. Samples were pre-cleared with protein A sepharose CL-4B (GE Healthcare), and incubated with anti-FLAG M2 resin (Sigma, A2220). Immunoprecipitates were washed 5 times with IPLS and eluted with SDS loading dye for western blot analysis.

3.3f Mass spectrometry

Livers from *Hdac3^{fl/fl}* animals transduced with AAV8 TBG HDAC3-HA and AAV8 TBG Cre or AAV8 TBG HA-EGFP and AAV8 TBG EGFP were harvested after 2 weeks of infection. A 250 mg sample of liver was dissected, dounced 10 strokes with pestle A in 15 ml swelling buffer (10 mM Tris-HCl pH 7.4, 2 mM MgCl₂, 3 mM CaCl₂) supplemented with 1 mM PMSF, and incubated for 20 mins on ice. Swelled cells were dounced 15 strokes with pestle B, an additional 15 ml swelling buffer with PMSF was added, filtered through a 100 µm cell strainer, and spun at 400 x g for 10 mins to collect cells. Cells were resuspended in 5 ml swelling buffer with 10% glycerol and PMSF and an additional 5 ml of swelling buffer supplemented with 10% glycerol, 1% NP-40, and 1 mM PMSF was added slowly while vortexing. Following lysis, nuclei were washed 1 time with PBS and subsequently fixed with 1% formaldehyde diluted in PBS for 15 mins at room temperature. Cross-linked samples were quenched with glycine, washed once with PBS, and resuspended in 1 ml NCB (20 mM Tris-HCl pH 8.0, 100 mM KCl, 5 mM MgCl₂, 10% glycerol, 0.1% NP-40, 1 mM DTT) supplemented with Complete EDTA-free protease inhibitor tablet (Roche) and 1 mM PMSF. Lysis was allowed to proceed for 1 hour followed by sonication with a probe sonifier (Branson). Cross-linked chromatin extracts were cleared by centrifugation and where indicated samples were treated with 1,000 Kunitz units of either micrococcal nuclease (NEB) or Benzonase nuclease (Sigma) for 30 minutes at 30°C. Extracts were immunoprecipitated with anti-HA agarose (Sigma, A2095) overnight, washed 3 times in NCB supplemented with protease inhibitors and 1 mM PMSF, washed 2 times in NCB, washed 2 times in HPLC-grade water, eluted with 10% ammonium hydroxide diluted in HPLC-grade water, and dried to completion in a SpeedVac (Eppendorf).

Samples were prepared for MS as previously described (Armour et al., 2013). After reduction/alkylation, samples were digested with LysC (Wako) for 2 hours followed by Trypsin (Promega) at 37°C overnight. Samples were resuspended in 1% acetic acid, and desalted with C₁₈ stage tips, as previously described (Rappsilber et al., 2003). EASY-nanoLC (Thermo Fisher Scientific) was configured with a 75 µm ID x 17 cm Reprosil-Pur C₁₈-AQ (3 µm; Dr. Maisch GmbH, Germany) nano-column and coupled with an Orbitrap Fusion mass spectrometer (Thermo Fisher Scientific). Full scan MS spectrum (*m/z* 360–1600) was performed in the Orbitrap with a resolution of 120,000 (at 200 *m/z*). Fragmentation was performed with higher-energy collisional dissociation (HCD) and a maximum injection time of 120 msec. MS/MS data were collected in centroid mode in the ion trap mass analyzer. Peptides were identified using MaxQuant (v1.5.3.30) using the Mus Musculus UniProt FASTA database (March 2016) with an FDR<1% at the peptide spectrum match and protein levels. Protein abundance was deconvoluted from peptide intensity using the intensity-based absolute quantification (iBAQ) (Schwanhäusser et al., 2011) algorithm, followed by log₂ transformation, normalization by the median intensity, and missing values imputed (width 0.25, downshift 2.0) using Perseus (v1.5.5.3). Significance was estimated using a two-tailed homoscedastic t-test (p-value<0.05).

3.3g RT-qPCR and RNA-seq

Total RNA was extracted using TRIzol (Invitrogen) and RNeasy mini kit (Qiagen). Contaminating DNA was removed using the RNase-Free DNase Set (Qiagen) on-column digestion protocol per manufacturer's instructions. RT-qPCR was performed with the High Capacity RT kit (Thermo Fisher Scientific), Power SYBR Green PCR Master Mix (Thermo Fisher Scientific), and a QuantStudio™ 6 Flex Real-Time PCR System (Thermo Fisher Scientific) using absolute quantification method with standard curves. *36b4 (Arbp)* was used as housekeeping control. RNA-seq libraries were generated using the Tru-seq kit (Illumina). Raw reads were aligned to the mm9 reference genome using Tophat version 2.1.9 using the parameters recommended by the original author (Trapnell et

al., 2012a). Differential expression analysis was performed using CuffDiff 2 (Trapnell et al., 2012b) using default parameters.

3.3h ChIP-qPCR, ChIP-reChIP, and ChIP-seq

ChIP and ChIP-seq were as described previously (Feng et al., 2011; Lim et al., 2015). Briefly, livers were mildly dissociated by dounce with pestle A for 6 strokes in PBS containing 1% formaldehyde and rocked for 15 min, quenched with glycine, washed with PBS, and sonicated with a probe-type sonifier (Branson) in RIPA supplemented with protease inhibitors and PMSF. Sonicated extracts were immunoprecipitated with antibodies for HDAC3 (Abcam, ab7030), PROX1 (Millipore, 07-537), HNF4 α (Santa Cruz, sc-8987), or H3K27Ac (Abcam, ab4729), and captured with bovine serum albumin blocked CL-4B protein-A sepharose beads (GE). PROX1 ChIP-seq was validated by comparing results of ChIP-seq with two different PROX1 antibodies raised against separate epitopes (Millipore, 07-537 and Proteintech 51043-1-AP), which showed a highly significant Pearson correlation ($R=0.96$). The HNF4 α and HDAC3 antibodies used for ChIP in this study have been validated previously (Odom et al., 2004; Papazyan et al., 2016a).

ChIP-reChIP from 3 biological replicate livers was performed essentially as standard ChIP, except following the first IP chromatin-protein complexes were eluted in 1% SDS with 10 mM DTT for 15 mins at 65°C. Subsequent to elution of the first ChIP, complexes were re-diluted in 10 volumes RIPA supplemented with protease inhibitors (Roche), PMSF (Sigma), 5 mg/ml BSA, and 2 μ g Lambda DNA/HindIII (NEB), followed by a second ChIP with the either anti-rabbit IgG (Cell Signaling Technologies, #2729) or the indicated antibody.

For ChIP-seq, ChIP was performed independently on livers from different mice ($n=3$). The precipitated DNA samples were barcoded and amplified according Illumina guide protocols, followed by deep sequencing on a HiSeq 2000 (Illumina). Sequencing reads of biological replicates for PROX1 and HDAC3 were aligned to the mm9 genome using Bowtie v0.12.7 (Langmead et al.,

2009b). Duplicate reads were removed and replicates were pooled using HOMER v4.7 (Heinz et al., 2010). Genome browser tracks were generated and peaks were called using HOMER with default parameters and IgG as input. Peaks more than 3-fold over input and >2 rpm in PROX1 and >1.5 rpm in HDAC3 were used for further downstream analyses. Venn diagram was generated using bedtools v2.26.0 (Quinlan and Hall, 2010b) and Vennerable R package with peaks overlapping at least 50% and having at least 1 rpm in the other ChIP-seq. Motif analyses were performed with HOMER using 200bp peak windows. Gene ontology was performed using Reactome 2016 (Fabregat et al., 2016). Track visualization was performed using the Integrated Genomics Viewer (Broad Institute) (Thorvaldsdottir et al., 2013).

Sequencing reads of biological replicates for PROX1, HDAC3, and HNF4 α in *Hnf4 α ^{fl/fl}* and *Hnf4 α* conditional liver knockout animals were processed similarly. Previously published C/EBP α ChIP-seq (GEO Accession numbers GSM1816821 and GSM1816822, replicates combined) (Bauer et al., 2015) and C/EBP β ChIP-seq (GEO Accession number GSM1446070) (Lim et al., 2015) were re-processed using the same parameters. Peaks >1 rpm for PROX1 and HDAC3 and >2 rpm for HNF4 α were used for further downstream analyses. Scatter plots and box plots were generated using the HOMER annotatePeaks command and R.

3.3i Data availability

The data discussed in this publication have been deposited in NCBI's Gene Expression Omnibus (Edgar et al., 2002) and are accessible through GEO Series accession number GSE90533 (<https://www.ncbi.nlm.nih.gov/geo/query/acc.cgi?acc=GSE90533>). All mass spectrometry data reported here have been deposited in Chorus under ID number 1251.

3.3j Statistical Methods

Data are presented as mean \pm s.d. unless otherwise stated. Microsoft Excel software, GraphPad Prism 7, MathWorks MATLAB, or R was utilized for all graphing and statistical tests. For comparison between two groups, Two-tailed unpaired Student's t-test were utilized unless otherwise stated, where $p < 0.05$ was considered statistically significant and the significance is marked by * $p < 0.05$, ** $p < 0.01$, and *** $p < 0.001$ unless otherwise noted. Wilcoxon-Mann-Whitney test was performed for statistical comparison between HNF4 α binding and C/EBP α or C/EBP β binding in the HDAC3-PROX1 down peaks in *Hnf4 α* liver KO vs HDAC3-PROX1 unchanged peaks in *Hnf4 α* liver KO (**Figure 3.11D**) and exact p-values were reported. For correlation analysis of HDAC3-PROX1 coregulated genes with HNF4 α -dependent binding sites, a Chi-squared contingency table with Yates correction was used. All other statistical comparisons for two groups of peaks were done using Pearson's Chi-squared contingency table tests and p-values were reported for each pair. All statistical tests are fully described in figure legends. The required sample size was calculated based on similar experiments and analyses carried out previously. The number of animals in each experiment is stated in the respective figure legends.

3.4 RESULTS

3.4a In vivo screen for HDAC3 interactors

To elucidate nuclear interactors of HDAC3 *in vivo*, we developed NEAT ChIP-MS, a cross-linking proteomic interaction method that allowed for the confident identification of HDAC3 interactors in adult liver (**Figure 3.1A**). *Hdac3^{fl/fl}* animals were tail vein-injected with either AAV virus expressing epitope tagged HDAC3 (AAV8 TBG HDAC3-HA) in conjunction with AAV8 TBG Cre to deplete endogenous HDAC3 in hepatocytes as described (Sun et al., 2012), or with control virus expressing epitope tagged green fluorescent protein (AAV8 TBG HA-EGFP). Subsequent to nuclear isolation, samples were cross-linked and EGFP or HDAC3 was immunoprecipitated with anti-HA resin. Associated proteins were analyzed by nLC-MS/MS and the results of the HDAC3 and EGFP

interactomes were compared to remove non-specific interactions. We applied stringent significance ($p < 0.01$) and fold enrichment (10-fold) cutoffs using label-free quantification values estimated by the intensity-based absolute quantification (iBAQ) (Schwanhäusser et al., 2011) algorithm to the resultant interactome to identify a set of high-confidence HDAC3 interacting proteins *in vivo* in mouse liver (**Figure 3.2A** and **Table 3.1**).

As expected, we observed an enrichment of all the components of the previously identified NCoR complex (sequence coverage indicated in parentheses) consisting of NCOR1/2 (11.14%/12.14%), TBL1X (46.62%), TBL1XR1 (42.52%), GPS2 (4.33%), and HDAC3 (42.85%) itself. In addition, our screen confirmed interaction of HDAC3 with a number of transcription factors known to interact with the NCoR complex, including the circadian nuclear receptor Rev-erb α (Feng et al., 2011; Hu et al., 2001). One of the most significantly enriched HDAC3 interactors, but not considered a core component of the NCoR complex, was the Prospero-related homeobox 1 (PROX1). A highly conserved transcription factor in vertebrates, PROX1 was previously shown to be critical for the development of several organs including the lymphatic system (Wigle and Oliver, 1999), lens (Wigle et al., 1999), liver (Burke and Oliver, 2002; Seth et al., 2014; Sosa-Pineda et al., 2000), pancreas (Burke and Oliver, 2002; Wang et al., 2005), heart (Risebro et al., 2009), and skeletal muscle (Kivelä et al., 2016; Roy et al., 2001). Additionally, PROX1 has been implicated in regulating the functions of several nuclear receptors (Charest-Marcotte et al., 2010; Dufour et al., 2011; Qin et al., 2004; Song et al., 2006; Steffensen et al., 2004; Takeda and Jetten, 2013) and has been shown to act as both a transcriptional repressor (Qin et al., 2004; Song et al., 2006; Steffensen et al., 2004) and activator (Lengler et al., 2001; Wigle et al., 1999) in different biological contexts.

To assess whether the proteins discovered in our chromatin bound complexes purified with HDAC3 directly through protein-protein interactions or indirectly through close genomic proximity we treated our lysates with either micrococcal nuclease (MNase), capable of cutting only in nucleosome free regions, or Benzonase nuclease, which can cleave DNA regardless of nucleosome occupancy.

Although micrococcal nuclease had minimal impact, Benzoylase nuclease significantly reduced the intensity of a subset of protein-protein interactions with HDAC3 (**Figure 3.2B**). This suggested that these proteins are not in direct contact with HDAC3, and thus these protein-protein associations are likely facilitated by DNA. Additionally, interactors associated with HDAC3 exhibiting lower enrichments tended to be more susceptible to Benzoylase treatment, implying that proteins displaying greater abundance were, in general, more likely to occur through protein-protein interactions. The group of proteins maintained upon nuclease treatment included PROX1, indicating that this robust HDAC3 interactor was likely more directly bound and not dependent on DNA bridging for its interaction.

The interaction of PROX1 and HDAC3 in liver was confirmed by co-immunoprecipitation experiments using the reversible cross-linker DSP from livers expressing HA-tagged HDAC3 or endogenously from wild-type livers (**Figure 3.2C**). PROX1 and HDAC3 interaction likely occurs in the context of the NCoR complex, as interaction between PROX1 and NCOR1 was observed in cell culture, and also requires multiple surfaces in the N-terminus of PROX1 for binding (**Figure 3.3A and B**). We next sought to better understand the HDAC3 interactome from a more global functional perspective. Classifying the interactors and their biological links and annotating them using information from the STRING database revealed several interesting clusters of proteins associating with HDAC3 (**Figure 3.4A**). In addition to the NCoR complex, HDAC3 was found to associate with several other transcriptionally important complexes including SWI/SNF, Integrator, Cohesin, and components of the NuRD and CoREST repressor complexes. We also observed a number of sequence-specific DNA binding transcription factors of functional relevance to liver physiology such as C/EBPs, FXR, RXR α and HNF4 α . We also utilized cytoHUBBA, a tool to define network topology (Chin et al., 2014), and identified members of the NCoR complex, NuRD/CoREST complex, Integrator complex, and nuclear receptors as important nodes in the liver HDAC3 interactome (**Figure 3.5A**). These results indicate that HDAC3 likely plays an important role in regulating the expression of liver gene programs through interaction with an array of transcription

factors and suggest that PROX1, as a strong interactor in liver, may be of more general importance to the functionality of HDAC3.

3.4b PROX1 and HDAC3 co-localize extensively at the genome

To further investigate the functional interplay between PROX1 and HDAC3 we performed ChIP-seq on PROX1 and HDAC3 in mouse liver. Bioinformatic analysis of the peaks discovered in the two datasets revealed a strong overlap between the binding sites of the HDAC3 and PROX1 cistromes (**Figure 3.6A**). Visual inspection of individual ChIP-seq tracks confirmed a striking correlation (**Figure 3.6B**). We next performed ChIP-reChIP analysis, which demonstrated that both HDAC3 and PROX1 were co-bound to the same DNA fragments (**Figure 3.6C**). Analysis of overlapping peaks by pathway analysis (Reactome) revealed that co-bound sites were enriched at genes involved in a variety of important metabolic pathways, including those that regulate lipid metabolism (**Figure 3.6D**). As expected peaks bound by HDAC3 selectively showed enrichment both for liver metabolic genes and those involved in circadian rhythm, indicating that HDAC3 likely has functions with Rev-erb α independent of its interaction with PROX1 (**Figure 3.7A**). HOMER motif analysis of the overlapping peaks displayed a strong enrichment for the HNF4 and C/EBP motifs, two transcription factors that are known to play important roles in liver development and adult liver function (**Figure 3.8A**). Upon closer examination of overlapping, HDAC3-only, and PROX1-only peaks we observed that the HNF4 α motif was significantly reduced at HDAC3-only peaks, whereas the Rev-erb α (DR2) motif was significantly enriched at these sites (**Figure 3.8B**). The C/EBP motif followed a similar pattern observed for HNF4 α indicating that it may also play a role in coordinating these sites but not those involved in circadian function. These results suggest that HDAC3 is recruited to at least two subsets of sites, ones that contain only HDAC3, which are recruited by Rev-erb α , and those that have both PROX1 and HDAC3, and are recruited by HNF4 α .

3.4c HNF4 α is required for the recruitment of the HDAC3-PROX1 module

Given our observation that the HNF4 α motif was found prominently at co-occupied sites, we hypothesized that this important liver transcription factor may play a role in the recruitment of HDAC3 and PROX1. CHIP-seq analysis of HNF4 α in control liver demonstrated HNF4 α binding at >60% of HDAC3-PROX1 co-bound peaks (**Figure 3.9A**). In stark contrast, HDAC3-only peaks displayed significantly reduced HNF4 α binding (~14%). Motif analysis of the triply bound peaks showed an increased enrichment of the HNF4 motif and a mild de-enrichment of the C/EBP motif when compared to all HDAC3-PROX1 co-bound peaks (**Figure 3.9B**). Co-binding of both PROX1 and HDAC3 with HNF4 α nearby several lipid-related genes were confirmed by CHIP-reCHIP (**Figure 3.9C and D**). To address whether HNF4 α was required for the recruitment of HDAC3-PROX1 at the co-bound sites we injected *Hnf4 α ^{fl/fl}* mice with AAV8 TBG Cre to delete *Hnf4 α* in hepatocytes (**Figure 3.10A**). CHIP-seq analysis of HNF4 α in these mice revealed near complete loss of HNF4 α binding at the genome (**Figure 3.10B-D**). Remarkably, a significant portion of both HDAC3 and PROX1 peaks were strongly reduced upon loss of HNF4 α (**Figure 3.11A**). Moreover, the HDAC3 and PROX1 sites that were affected were almost exclusively the same sites (**Figure 3.11B**).

In addition, we observed a decreased interaction of PROX1 and HDAC3 in the *Hnf4 α* knockout mice by Co-IP western blot, suggesting HNF4 α may be required to stabilize the HDAC3-PROX1 interaction *in vivo* (**Figure 3.11C**). We compared the binding of both HNF4 α and C/EBP β at the co-bound sites that were lost in *Hnf4 α* knockout versus those that were unaffected and observed a positive relationship between the strength of HNF4 α binding and the dependency of HDAC3/PROX1 on HNF4 α (**Figure 3.11D**). C/EBP, serving as a control comparison, did not display a similar correlation. These results strongly suggest that HNF4 α recruits the HDAC3-PROX1 module to a substantial subset of binding sites, while other factors, like C/EBP, may be more important elsewhere in the genome.

3.4d Liver depletion of PROX1 causes increased hepatic triglycerides

To determine the function of PROX1 in liver, *Prox1* was knocked down in adult hepatocytes of wild-type male mice using an AAV-based shRNA delivery vector (AAV8 TBG shProx1), which led to a ~70% depletion in PROX1 protein 3 weeks following injection (**Figure 3.12A**). Hepatic triglycerides (TG) were significantly elevated following 3 weeks of PROX1 knockdown, with a more striking difference in TG levels observed at 6 weeks post infection (**Figure 3.12B**). Oil Red O staining confirmed an increase in neutral lipid in livers of male mice infected with *Prox1* shRNAs (**Figure 3.12C**). Importantly, no significant change in HDAC3 protein levels were observed upon knockdown of PROX1 (**Figure 3.12D**). Thus, similar to HDAC3 knockout, depletion of PROX1 in liver results in increased triglyceride content. Of note, hepatic PROX1 levels were not significantly changed after 12 weeks of high fat diet (**Figure 3.12E**).

3.4e HDAC3 and PROX1 coregulate a lipid gene expression program

To determine if transcriptional mechanisms of coregulation by HDAC3 and PROX1 played a role in regulating this striking liver lipid phenotype, we performed RNA-seq on *Hdac3* knockouts and 3 week *Prox1* shRNA livers. We observed a significant overlap of genes whose expression was altered by loss of either factor, with a striking over-representation of genes whose directionality of change was correlated and a strong preference for upregulated genes, consistent with the function of both HDAC3 and PROX1 as transcriptional repressors (**Figure 3.13A**). Pathway analysis (Reactome) revealed the group of transcripts co-upregulated by HDAC3 and PROX1 loss to be highly enriched for regulation of lipid metabolism, including a number of important mediators of lipid synthesis and lipolysis. Transcriptional coregulation of a number of genes whose expression are critical to maintenance of lipid homeostasis, such as *G0s2* (Wang et al., 2013), *Elov16* (Matsuzaka et al., 2012), *Mfsd2a* (Berger et al., 2012) and *Cidec* (Matsusue et al., 2008) were confirmed by qPCR following *Hdac3* knockout or *Prox1* knockdown (**Figure 3.13B**). Correlation analysis comparing the frequency of HNF4 α -dependent HDAC3-PROX1 binding sites at unchanged and HDAC3-PROX1 coregulated genes revealed a statistically significant relationship (Chi-square with

Yates correction, $p < 0.0001$). This association was consistent at lipid-related genes (**Figure 3.14A**), and point to a strong correlation between co-upregulated lipid-related gene expression and the co-occupancy of HNF4 α -dependent, HDAC3-PROX1 co-bound sites.

Upon examination, a number of these loci exhibited a strong overlap of HDAC3, PROX1, and HNF4 α ChIP-seq signals, consistent with our genome-wide analysis (**Figure 3.15A and Figure 3.16A**). In addition, we observed upstream co-bound regions that exhibited high H3K27 acetylation, suggesting that these sites may be putative enhancers. Indeed, upon loss of HDAC3 or PROX1 we observed an increase in HNF4 α -dependent H3K27 acetylation at these putative enhancer regions. Moreover, analysis of nascent transcription, utilizing an existing global run-on sequencing (GRO-seq) dataset in liver (Fang et al., 2014), revealed bi-directional enhancer RNAs (eRNAs) at a number of co-bound regions. To determine if these binding sites act as enhancers we cloned the *G0s2* -17kb and -1.7kb binding sites into the pGL4 Luciferase reporter. Co-transfection of the enhancer reporter plasmid with an HNF4 α expression vector revealed strong transcriptional induction by HNF4 α at both the -17kb and -1.7kb sites. Interestingly, expression of PROX1 significantly repressed HNF4 α mediated transcriptional activation, while it was unable to repress trans-activation induced by C/EBP α expression (**Figure 3.16B**). While mutation of the HNF4 α binding site severely disrupted activation by HNF4 α (**Figure 3.17A and B**). These data indicate that the -17kb, and to a lesser extent the -1.7kb, binding sites act as HNF4 α -controlled enhancers for the expression of *G0s2* and that HDAC3 and PROX1 act as direct repressors of these enhancers. Overall our results indicate that the interaction between HDAC3 and PROX1 is critical for regulating liver metabolic gene expression and maintenance of hepatic lipid homeostasis (**Figure 3.18**).

3.5 DISCUSSION

In this study we determined *in vivo* protein interactors of the class I histone deacetylase HDAC3 in mouse liver. This interactome revealed a number of novel binding partners in addition to confirming the well-established role of HDAC3 as a component of the NCoR complex (Guenther et al., 2001; Lazar, 2003; You et al., 2013). Amongst these binding partners we explored the functional interaction between HDAC3 and the Prospero-related homeobox protein PROX1. We determined that HDAC3 and PROX1 co-occupy a high number of genomic binding sites and that these binding sites correlate strongly with both the DNA-binding motif and the cisrome of HNF4 α . Moreover, upon loss of HNF4 α , a significant portion of HDAC3 and PROX1 co-occupied sites exhibit a profound loss of genomic binding. Depletion of PROX1 specifically in mature adult liver resulted in a dramatic increase in liver triglyceride content similar to that observed upon loss of HDAC3 (Sun et al., 2012), likely due to the dysregulation of a coregulated gene expression program important for lipid synthesis and lipolysis. Furthermore, we defined a novel liver enhancer responsible for controlling the expression of the lipolysis inhibitor G0S2, and showed that its transcriptional activation by HNF4 α can be specifically repressed by PROX1. Overall, these results strongly suggest HDAC3 and PROX1 function in liver to corepress gene transcription important for maintenance of lipid homeostasis.

Protein-protein interactions are critical for determining biological functionality, including the control of chromatin function and gene expression, and can be strongly influenced when a binding partner is restricted to a specific cell type or tissue. Previous studies defining interacting partners for HDAC3 by mass spectrometry have not provided significant depth or elucidated tissue-specific factors bound with HDAC3 *in vivo* (Bantscheff et al., 2011; Guenther et al., 2000; Joshi et al., 2013; Wen et al., 2000). Our strategy for identifying HDAC3 interactors in liver differs from methods that have been successful in cultured cells (Mohammed et al., 2013) in two important ways. First, through co-expression of fusion-tagged HDAC3 and Cre recombinase in *Hdac3^{fl/fl}* animals via adeno-associated viral vectors (AAV8) under the control of the thyroxine binding globulin promoter

(TBG), we were able to express our bait protein *in vivo* in hepatocytes lacking endogenous HDAC3. Second, we found that cross-linking isolated nuclei rather than whole liver depleted significant cytoplasmic and mitochondrial liver contaminants leading to reduced sample complexity and increased depth and sensitivity of our interacting protein mass spectrometric identifications. Nuclear isolation prior to functional assays, co-IP, and ChIP has been widely utilized in the transcriptional field (Chaya and Zaret, 2003), most recently being employed for techniques such as GRO-seq (Core et al., 2008) and INTACT (Mo et al., 2015). In addition, we have compared the cistromes of HDAC3 from standard ChIP-seq and those produced with our protocol and found them to be highly correlated (Pearson correlation, $R=0.781$), suggesting that the nuclear isolation step is not having a major effect on the biological landscape that we are attempting to elucidate.

Similar to cross-linking methods developed for cultured cells (Mohammed et al., 2013), the present method is improved in its ability to capture more transient interactions, including those at the genome. Of note, although previous work has shown the circadian nuclear receptor Rev-erb α and other nuclear receptors to be interacting partners for the HDAC3-containing NCoR complex (Feng et al., 2011; Ishizuka and Lazar, 2003), these proteins were not found in a previous HDAC3 proteomic screen performed in CEM T cells (Joshi et al., 2013). By contrast, the current study revealed several important HDAC3-bound nuclear receptors in liver including HNF4 α , RXR α , Rev-erb α , and FXR, implicating HDAC3 in their functions. Our screen also revealed several non-nuclear receptor sequence-specific transcription factors such as C/EBP α , ChREBP, CREB1, and ETV6, possibly pointing to a broader role of HDAC3/NCoR in corepressing non-nuclear receptor transcription factors in liver. Alternatively, it is conceivable that our cross-linking based sample preparation is capable of capturing targets of HDAC3 enzymatic activity. Indeed, a number of the interactors elucidated in our screen have been shown to be regulated by lysine acetylation including C/EBP α (Bararia et al., 2016), ChREBP (Bricambert et al., 2010), CREB1 (Lu et al., 2003), and others, and it is therefore interesting to speculate that HDAC3 may regulate their functions through this mechanism.

Interaction of HDAC3 was also observed with several important nuclear complexes such as Integrator (Gardini et al., 2014; Lai et al., 2015), Cohesin (Kulemzina et al., 2016), SWI/SNF (Euskirchen et al., 2011; Shi et al., 2013), and NuRD (Whyte et al., 2012), which have been implicated in the regulation of transcription through binding and functional control of gene-specific enhancers. Previous studies suggested that HDAC3 genomic binding correlates primarily with regions of active transcription (Wang et al., 2009), which our results strongly support and extend to suggest that these components of the transcriptional machinery may be involved. It will be interesting to determine if HDAC3 plays a role as a bona fide member of these complexes or rather regulates their function through enzymatic or non-enzymatic mechanisms. The processes by which transcriptional activators and repressors act together at these enhancers to specifically tune gene expression remains an important unanswered question.

Although PROX1 has been shown to be critical for the development and specification of several tissues (Burke and Oliver, 2002; Dyer et al., 2003; Risebro et al., 2009; Seth et al., 2014; Sosa-Pineda et al., 2000; Wigle and Oliver, 1999; Wigle et al., 1999), its functions in the physiology of adult liver have not been determined. Our study provides evidence that PROX1 in adult liver helps maintain proper lipid homeostasis, as its depletion results in metabolic gene transcriptional changes and a strong upregulation of hepatic triglycerides. A previous study suggested that haploinsufficiency of *Prox1* in mice results in obesity (Harvey et al., 2005), and these animals exhibited an increase in liver lipids which was suggested to be secondary to obesity. Our results suggest that the haploinsufficiency of *Prox1* in hepatocytes might also contribute to the hepatosteatotic phenotype.

Unlike PROX1, which displays significant tissue specificity (Steffensen et al., 2004), HDAC3 expression is relatively ubiquitous. Even so, PROX1 and HDAC3 are implicated in the control of several overlapping tissues such as pancreas, heart, central nervous system, and liver. Thus it is possible that, in these biological contexts, PROX1 provides tissue-specific functionality to HDAC3

through protein-protein interaction. HDAC3 has been implicated in beta cell function and the regulation of glucose homeostasis (Remsberg et al., 2017). Interestingly, genome-wide association studies have revealed a CC variant SNP of *Prox1* (rs340841) that contributes to the control of fasting glucose levels and the development of diabetes (Dupuis et al., 2010; Lecompte et al., 2013). Perhaps in pancreatic beta cells, as in liver, HDAC3 and PROX1 form a complex to regulate gene expression involved in the control of organismal metabolism.

Non-alcoholic fatty liver disease (NAFLD) is a disorder whose prevalence is increasing alongside metabolic syndrome, obesity, and type 2 diabetes and affects as high as 30% of the adult population in developed countries (Browning and Horton, 2004; Tilg et al., 2016). As a major risk factor for liver inflammation (NASH) and scarring/fibrosis (Cohen et al., 2011), understanding the molecular mechanisms of liver function is of critical importance to development of therapies for this unmet medical need. Here we have defined an interaction between HDAC3 and PROX1 that is nucleated at the genome by HNF4 α , and elucidated the role of this repressor module in controlling hepatic triglyceride content by modulating lipid synthesis and lipolytic gene expression. These results highlight the importance tissue-specific corepressor interactions in maintaining liver metabolism and illustrate new pathways for therapeutic intervention.

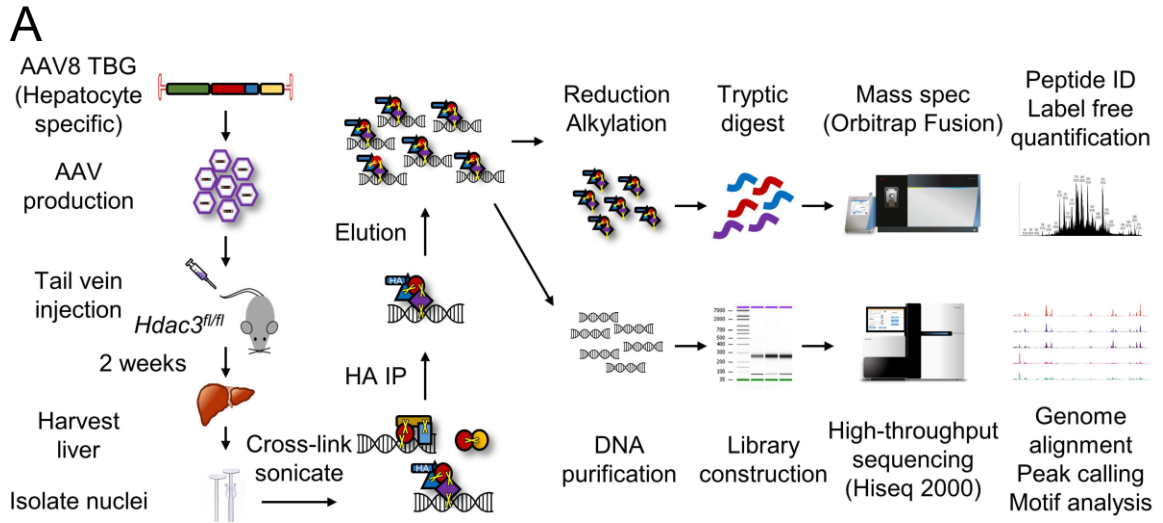


Figure 3.1 NEAT ChIP-MS workflow to interrogate the HDAC3 liver nuclear interactome. (A)

Schematic illustration of the NEAT ChIP-MS protocol. HA-tagged HDAC3 or EGFP was expressed with or without *Cre* in *Hdac3^{fl/fl}* mice specifically in hepatocytes via adeno-associated virus (AAV8 TBG). After isolation of nuclei and cross-linking with formaldehyde, HDAC3 or EGFP control were captured by anti-HA immunoprecipitation. Protein complexes and associated DNA sequences were analyzed by mass spectrometry or high-throughput sequencing respectively.

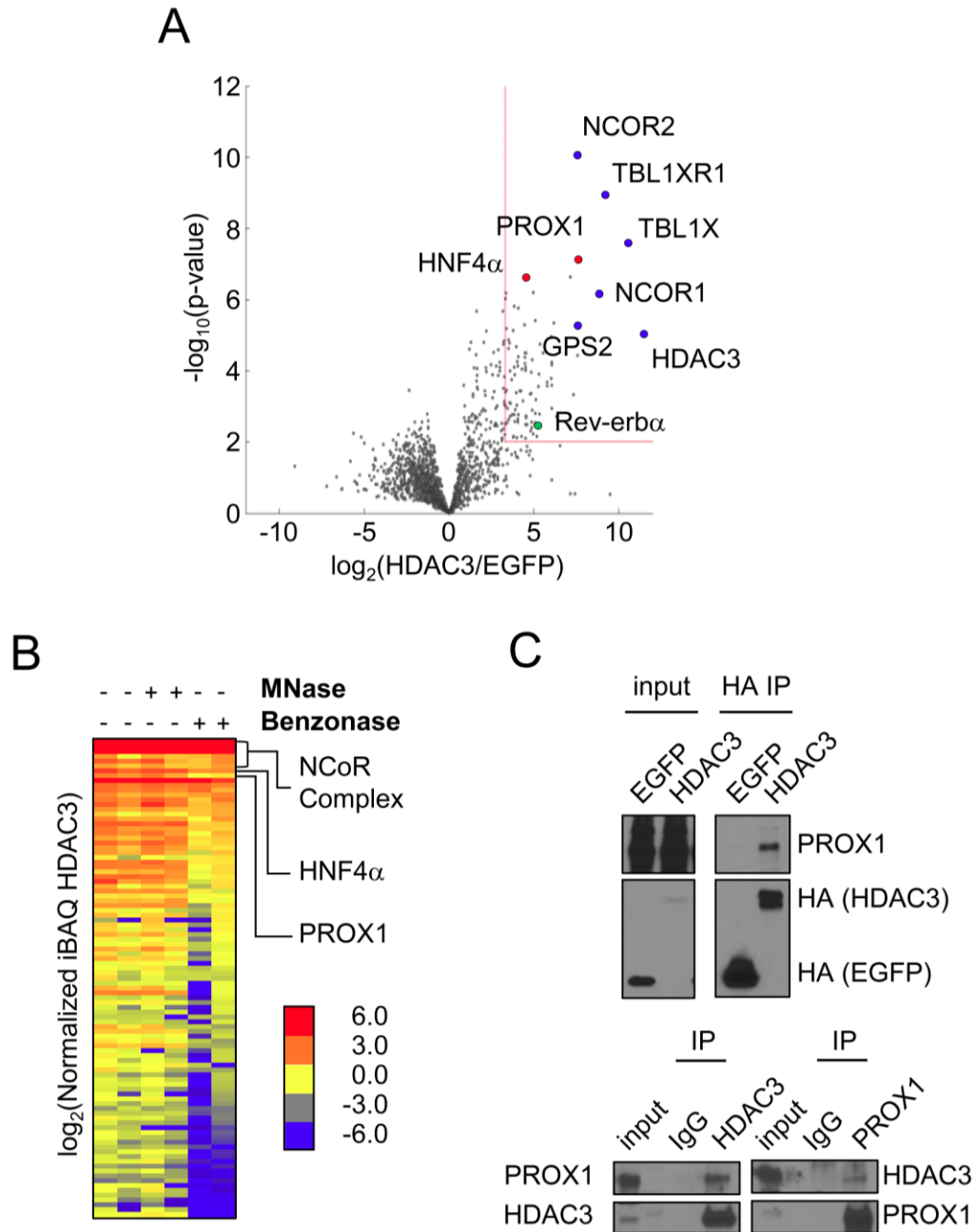
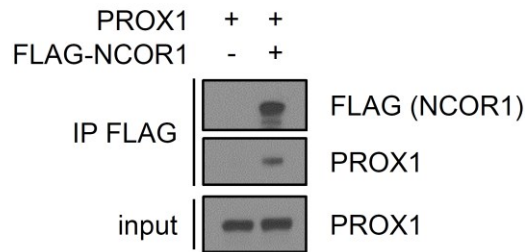


Figure 3.2 HDAC3 liver interactome by NEAT ChIP-MS reveals PROX1 as an abundant interactor. (A) Volcano plot of mass spectrometry analysis of HDAC3 interacting proteins (HDAC3 n=11, EGFP n=13). The x-axis indicates \log_2 ratio of normalized intensity (iBAQ) of proteins discovered in HDAC3 to EGFP control. Red box indicates fold-change (10-fold) and p-value (0.01) cutoffs for interactors. Core NCoR complex components (blue), selected high scoring interactors

(red), and Rev-erb α (green) are indicated. **(B)** Heatmap of normalized intensity (iBAQ) of HDAC3 interactors from **A** in the presence or absence of micrococcal nuclease (MNase) or Benzonase nuclease. Each lane represents an independent experiment. **(C)** Co-IP experiments confirming interaction of HDAC3 with PROX1 from liver expressing tagged HDAC3 (top) or endogenous IPs (bottom).

A



B

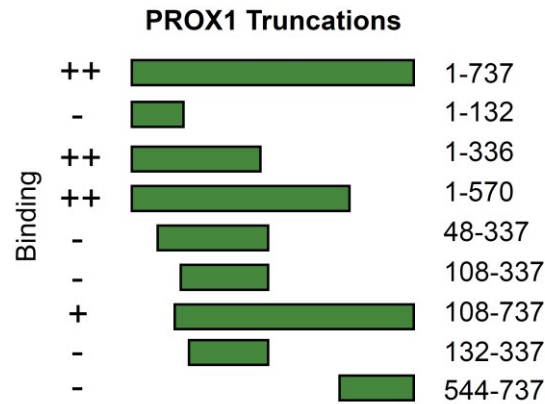
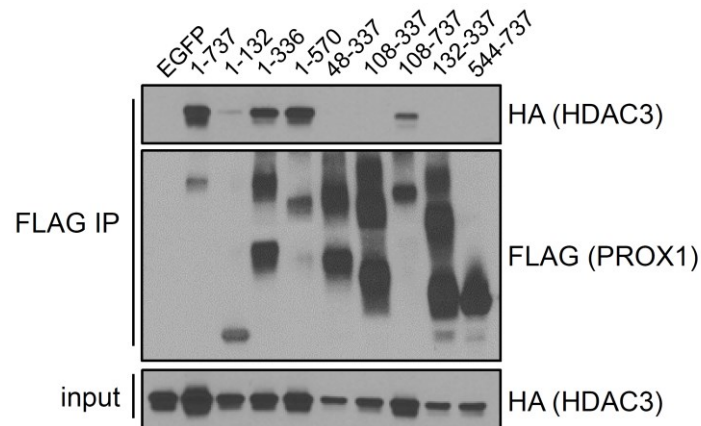


Figure 3.3 Interrogation of PROX1 interaction with HDAC3-NCOR. (A) Co-immunoprecipitation western blot analysis of FLAG-NCOR1 co-expressed with PROX1 in HEK 293T cells. (B) Domain mapping to identify regions of PROX1 required for interaction with HDAC3. FLAG-tagged PROX1 truncations were co-expressed with HDAC3-HA in HEK 293T cells and subjected to FLAG immunoprecipitation followed by western blotting.

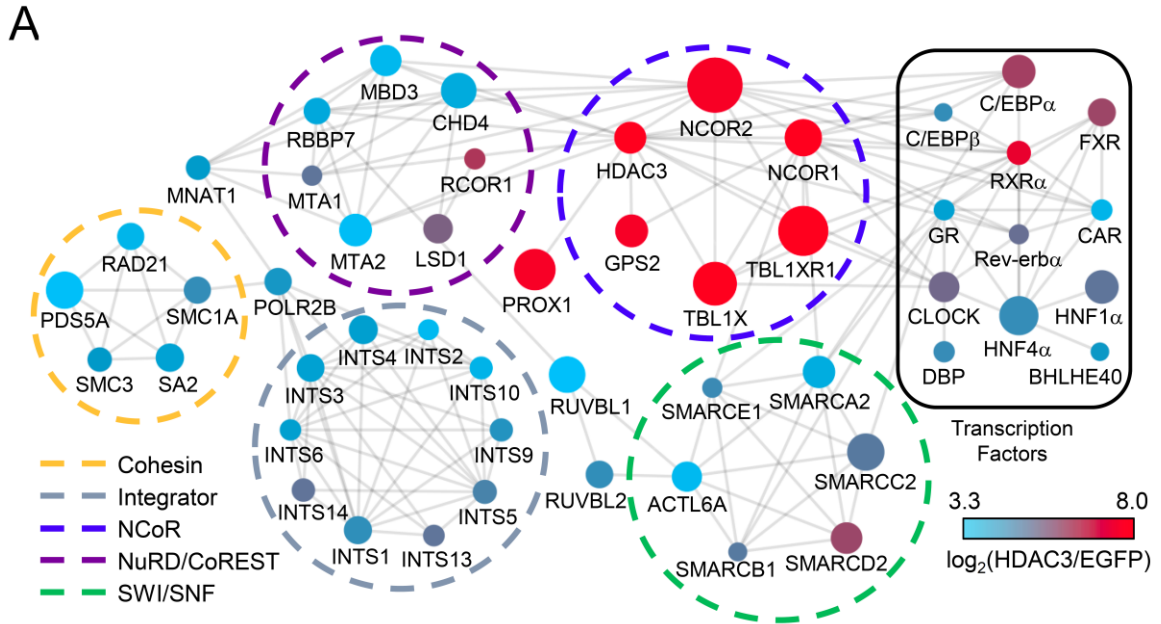


Figure 3.4 HDAC3 interactome network. (A) Protein-protein interaction network analysis. Circle color represents enrichment over control and the size of the circle represents $-\log_{10}(\text{p-value})$. Nodes displayed met 8-fold enrichment cutoff after Benzonase treatment and lines indicate validated interactions (STRING, active interaction sources include experiments and databases, minimum interaction score 0.6). Interactors are grouped by known type and circles indicate known functional complexes.

A

cytoHUBBA analysis

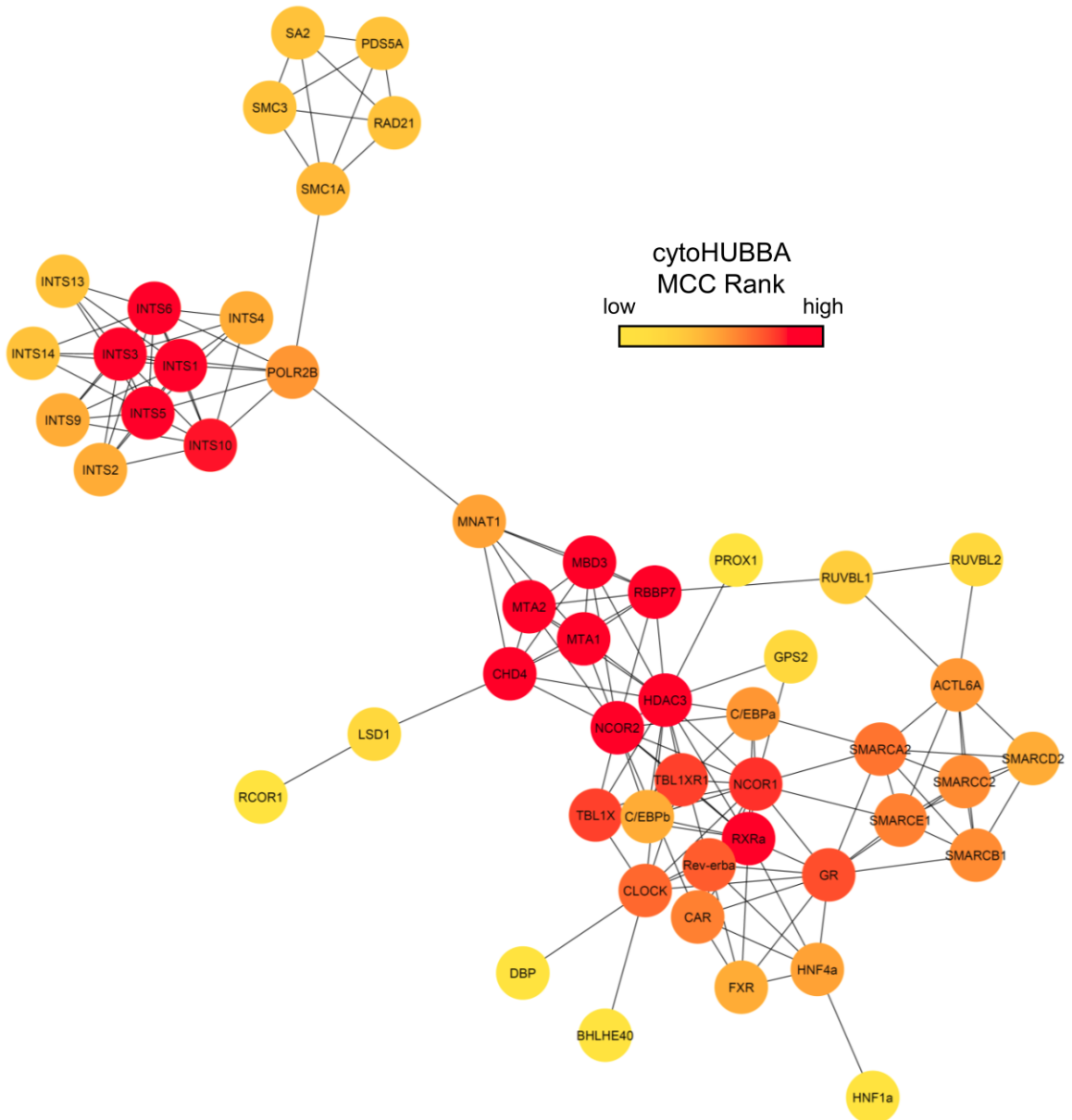


Figure 3.5 HDAC3 interactome topology analysis. (A) cytoHUBBA analysis using the maximal clique centrality (MCC) of HDAC3 interactors annotated from STRING. Active interaction sources include experiments and databases with a minimum interaction score of 0.6. Nodes are colored by rank order.

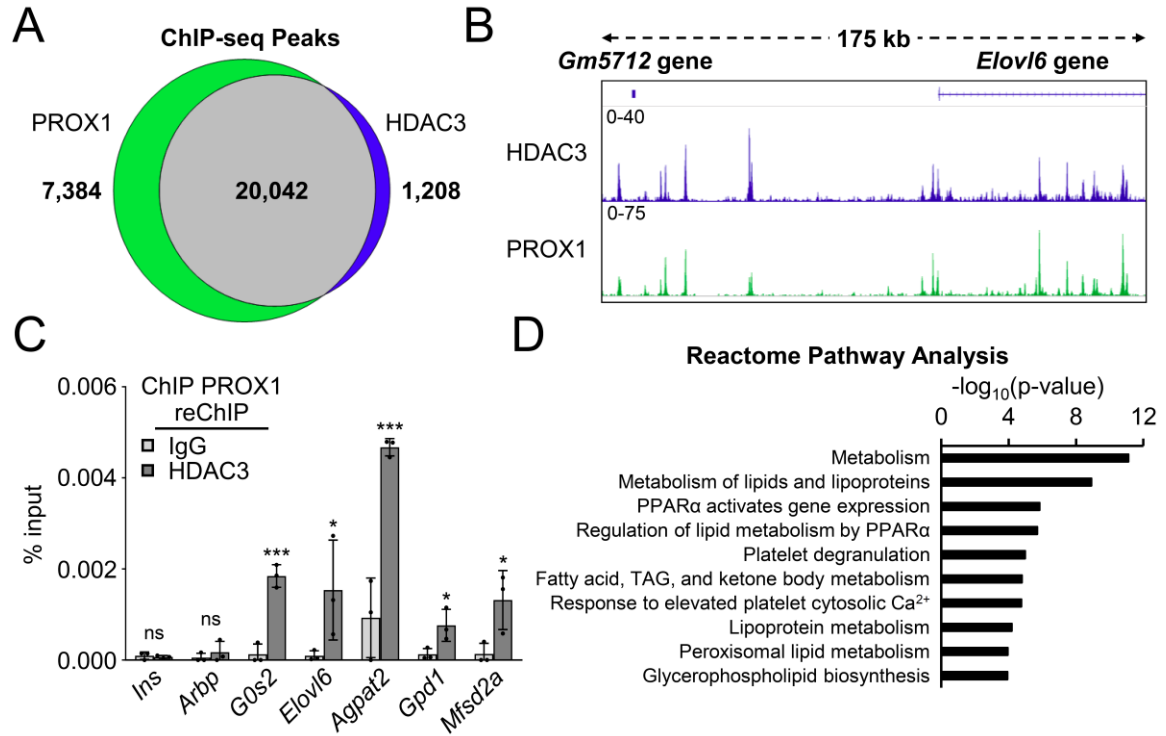


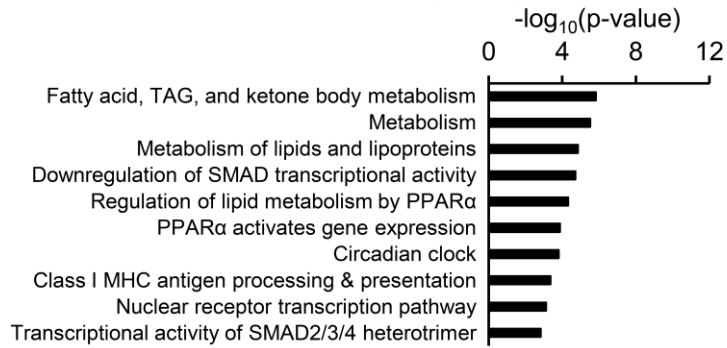
Figure 3.6 HDAC3 and PROX1 exhibit extensive co-binding and reveal a metabolic signature.

(A) Venn diagram displaying overlap of peaks identified in PROX1 (2 rpm cutoff) and HDAC3 (1.5 rpm cutoff) ChIP-seq. Peaks required 50% overlap and have a minimum 1 rpm signal for the other factor. (B) Representative browser tracks of HDAC3 and PROX1 ChIP-seq. Scale is reads per ten million (RPTM). (C) Co-occupancy of PROX1 and HDAC3 as indicated by ChIP-reChIP (n=3) from liver. Legend indicates reChIP antibody following primary PROX1 ChIP elution. Data are presented as mean±s.d., one-tailed unpaired Student's t-test, *p<0.05, **p<0.01, ***p<0.001, ns not significant. (D) Reactome analysis of the nearest genes within 100kb from the top 1000 overlapping HDAC3 and PROX1 peaks.

A

HDAC3-specific binding sites

Reactome Pathway Analysis



PROX1-specific binding sites

Reactome Pathway Analysis

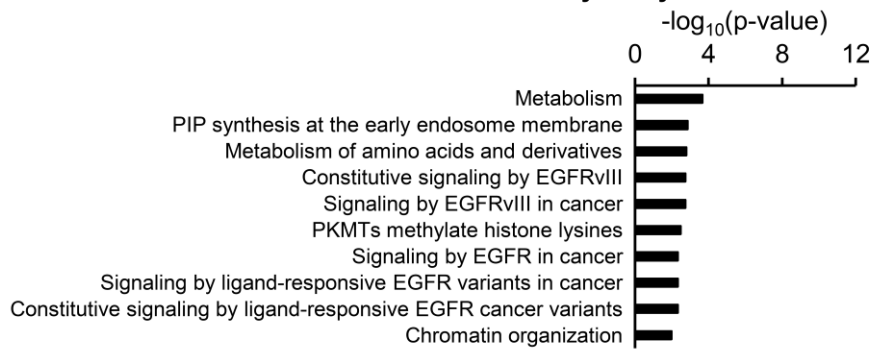


Figure 3.7 HDAC3 and PROX1 specific cistromic analysis. (A) Reactome analysis of the nearest genes within 100kb from the top 1000 HDAC3-specific and PROX1-specific peaks.

A

HDAC3-PROX1 co-bound peaks		
Motif	%	p-value
	HNF4 52.12%	1e-784
	C/EBP 45.74%	1e-987

B

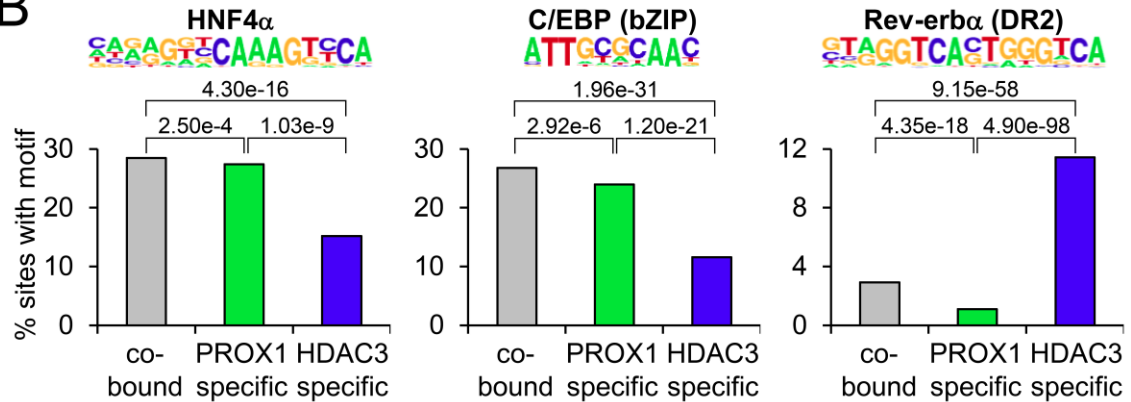


Figure 3.8 Interrogation of cistrome data suggests distinct HDAC3 containing chromatin complexes. (A) HOMER motif analysis of co-bound peaks displaying over-represented sequences. (B) HOMER motif enrichment analysis of the indicated motifs (HNF4 α , CEBP bZIP, and Rev-erb α DR2) at overlapping and non-overlapping peaks determined in **Figure 3.6A**. Numbers above brackets indicate p-values, Chi-squared test.

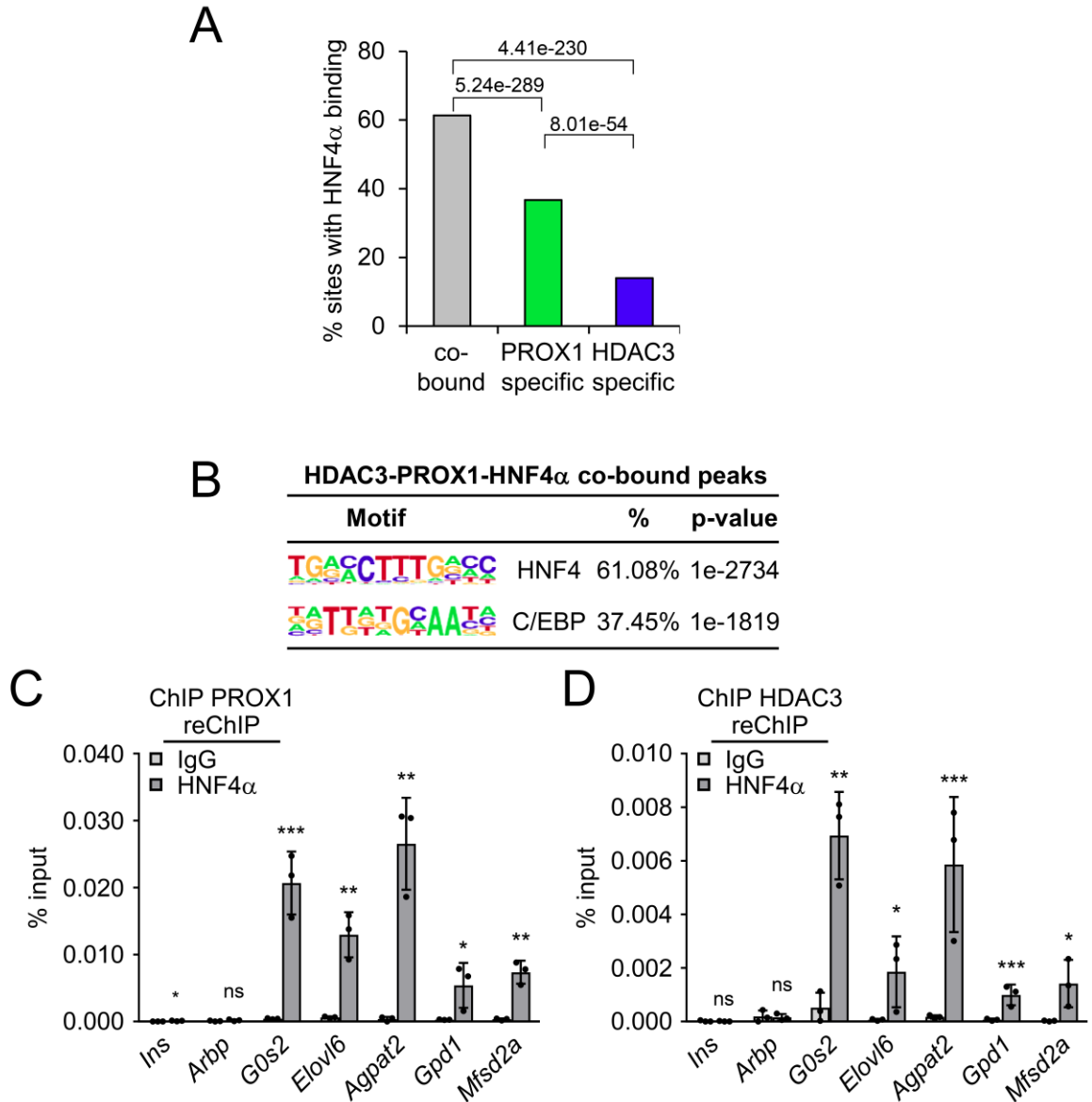


Figure 3.9 The HDAC3-PROX1 module is recruited by HNF4 α in liver. (A) Comparison of HNF4 α binding (> 2 rpm, filtered on the HNF4 α KO, 50% minimum overlap) at overlapping and non-overlapping peaks in the HDAC3 and PROX1 cistromes from **Figure 3.6A**. Numbers above brackets indicate p-values, Chi-squared test. **(B)** HOMER motif analysis of peaks co-bound by HDAC3, PROX1, and HNF4 α displaying over-represented sequences. **(C, D)** Co-occupancy of HDAC3-PROX1 and HNF4 α as indicated by ChIP-reChIP (n=3) from liver. Legend indicates reChIP

antibody following primary HDAC3 or PROX1 ChIP elution. Data are presented as mean±s.d, one-tailed unpaired Student's t-test, *p<0.05, **p<0.01, ***p<0.001, ns not significant.

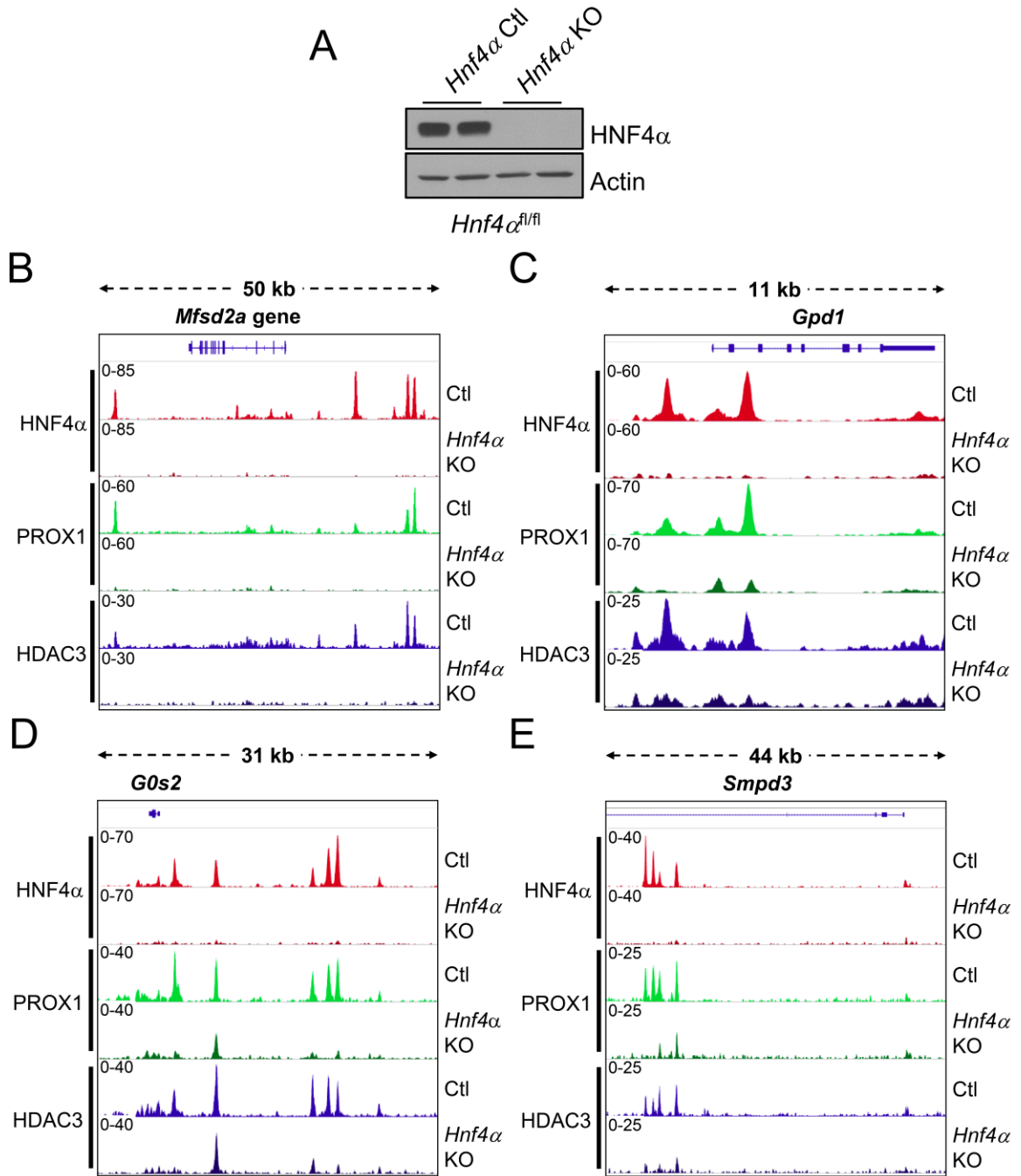
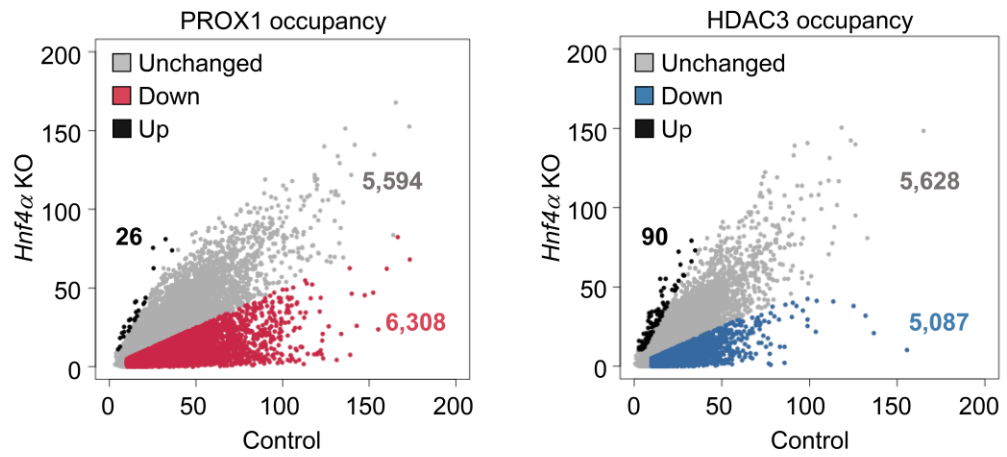
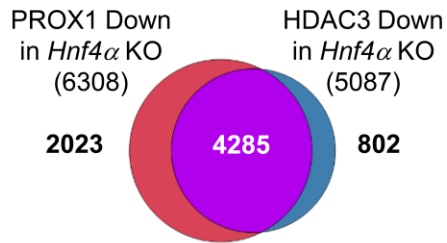


Figure 3.10 HDAC3, PROX1, and HNF4 α genomic binding in control and *Hnf4 α* knockout liver. **(A)** Western blot confirming HNF4 α knockout. **(B-E)** Representative browser tracks at lipid-related genes of HNF4 α , PROX1, and HDAC3 ChIP-seq in *Hnf4 α ^{fl/fl}* livers infected with AAV8 TBG *Egfp* (Ctl) or *Cre* (*Hnf4 α* KO). Indicated scales are in RPTM.

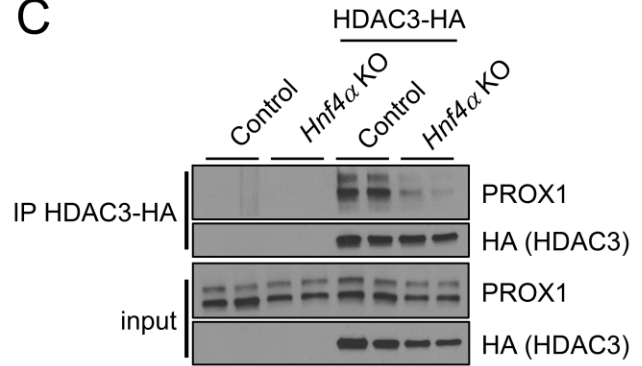
A



B



C



D

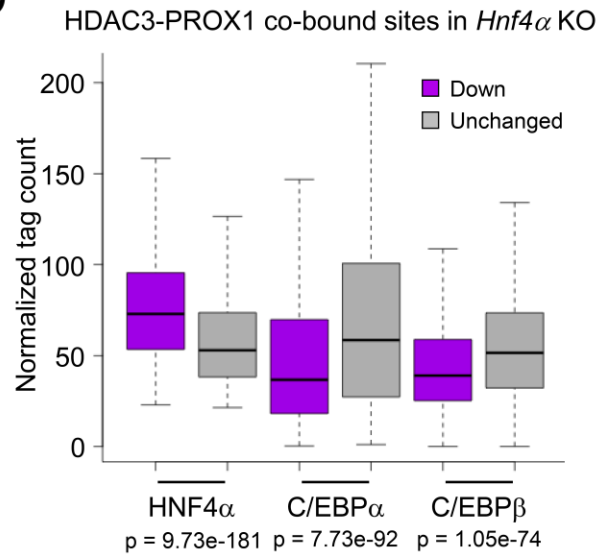


Figure 3.11 The HDAC3-PROX1 module requires HNF4 α for a majority of binding sites in liver. (A) Scatter plots of PROX1 (left) and HDAC3 (right) ChIP-seq in control versus *Hnf4 α* KO. Red and blue shaded regions indicate a 2-fold decrease in peak intensity upon loss of HNF4 α . (B) Venn diagram displaying overlap (at least 50% and 1 rpm) of red and blue regions from A. (C) Co-immunoprecipitation western blot of HDAC3-HA in control and HNF4 α KO liver. (D) Box and whisker plot indicating the ChIP-seq binding strength of HNF4 α , C/EBP α , and C/EBP β at HDAC3-PROX1 sites that are either down upon loss of HNF4 α (purple) or unchanged (gray) (Wilcoxon-Mann-Whitney test).

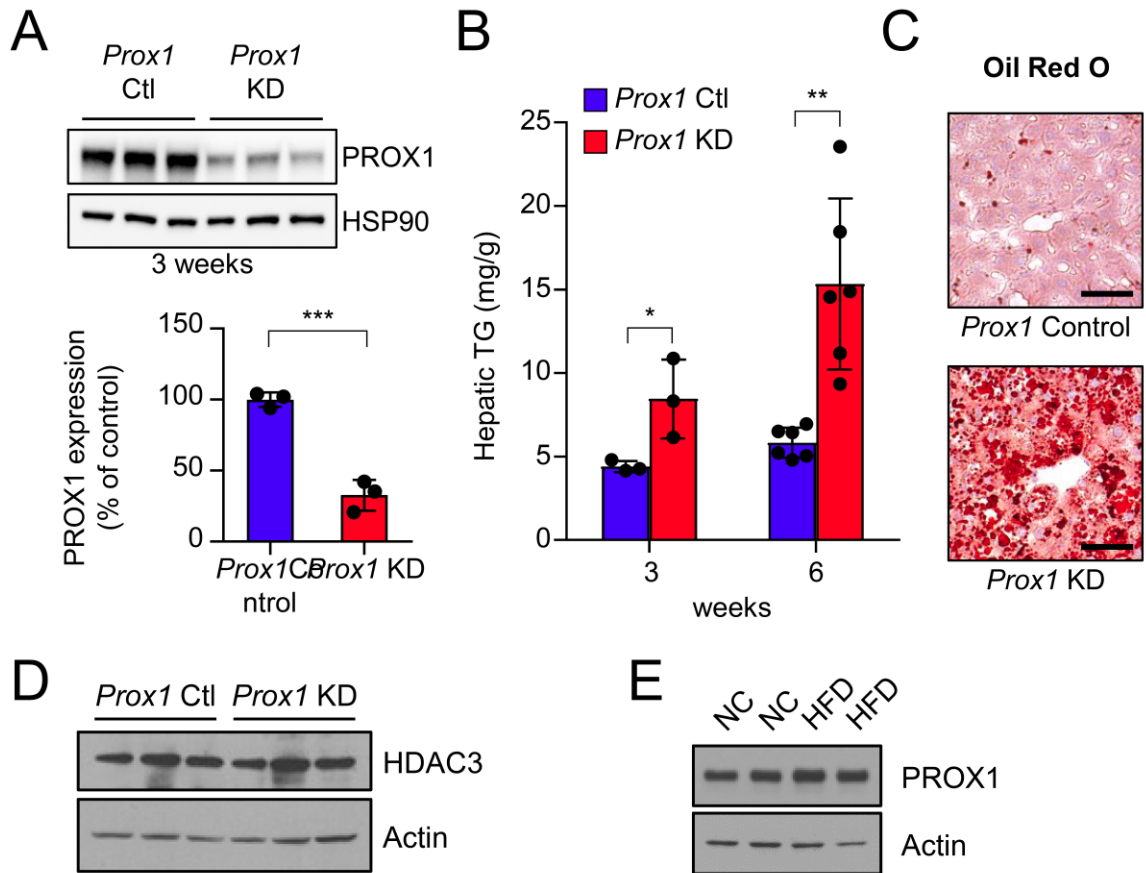


Figure 3.12 PROX1 knockdown causes an increase in hepatic triglyceride content. (A) Western blot of liver samples from mice treated for 3 weeks with AAV8 TBG shLuciferase (*Prox1* Ctl) or shPROX1 (*Prox1* KD). Densitometry of the western blot shown above (n=3). Data are presented as mean±s.d. (B) Hepatic triglyceride assay of livers infected for 3 weeks (n=3) or 6 weeks (n=6) with indicated virus. Data are presented as mean±s.d. (C) Oil red O staining of livers infected for 6 weeks as in B. Scale bar is 50µm. (D) Western blot of HDAC3 in control and PROX1 KD liver. (E) Western blot showing PROX1 levels in male mice at 18 weeks of age fed for 12 weeks with normal chow diet (NC) or high fat diet (HFD).

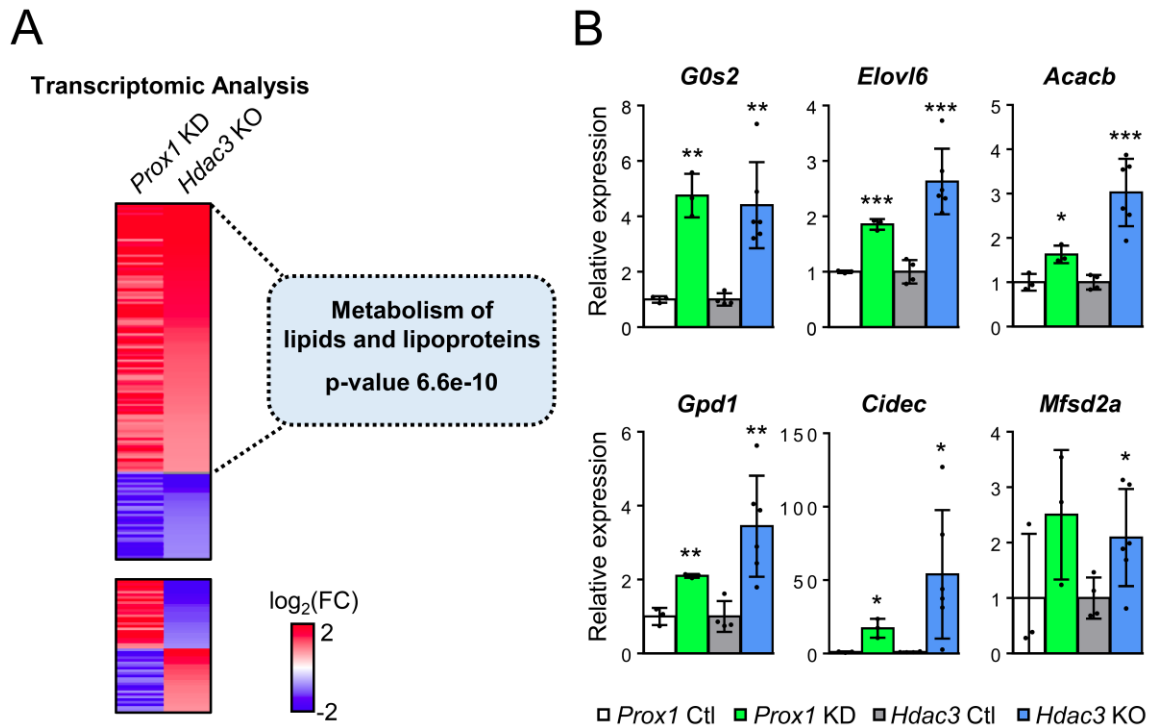


Figure 3.13 Transcriptomic analysis reveals the HDAC3-PROX1 module suppresses steatosis by controlling a hepatic lipid metabolism gene program. (A) RNA-seq analysis of *Hdac3^{fl/fl}* mice infected for 2 weeks with AAV8 TBG *Egfp* (n=2) or *Cre* (*Hdac3* KO, n=3) vs. wild-type mice infected with AAV8 TBG shLuciferase (n=3) or shPROX1 (*Prox1* KD, n=3) for 3 weeks. Heatmap displays coregulated genes (1.7-fold change, p<0.05) grouped by expression correlation (135 genes) or anti-correlation (50 genes) upon ablation of HDAC3 or PROX1. Inset shows the p-value and corresponding gene list for the highest ranking Reactome pathway in the co-upregulated cluster. **(B)** Confirmation of up-regulated lipid-related genes upon loss of HDAC3 (Ctl n=4, KO n=6) or PROX1 (Ctl n=3, KD n=3) by qPCR. Data are presented as mean±s.d. Two-tailed unpaired Student's t-test, *p<0.05, **p<0.01, ***p<0.001.

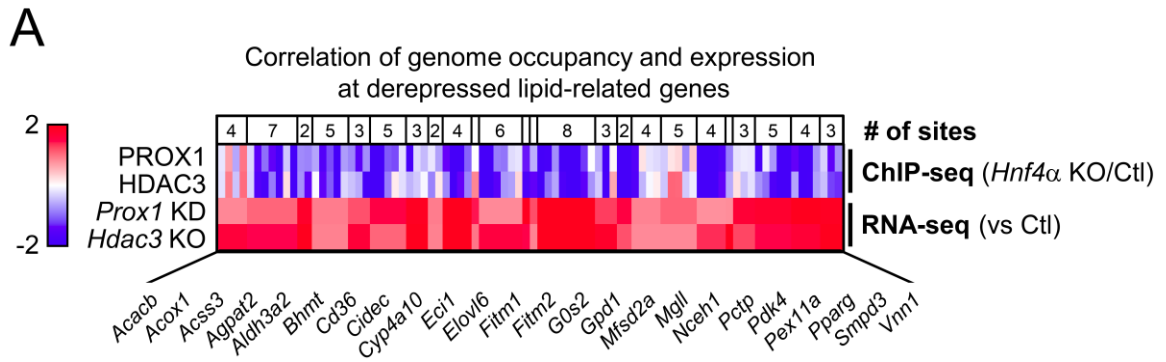


Figure 3.14 RNA-seq and ChIP-seq correlation analysis of HDAC3-PROX1 module recruited by HNF4 α . (A) Heatmap displays co-upregulated lipid-related genes upon ablation of HDAC3 or PROX1 and the corresponding binding strength of adjacent HDAC3-PROX1 co-bound peaks (-50kb upstream of the transcription start site, TSS through +2kb from the transcription end site, TES) in the HNF4 α KO liver relative to control. Scale bar represents $\log_2(\text{fold change})$ for RNA-seq and fold-change for ChIP-seq.

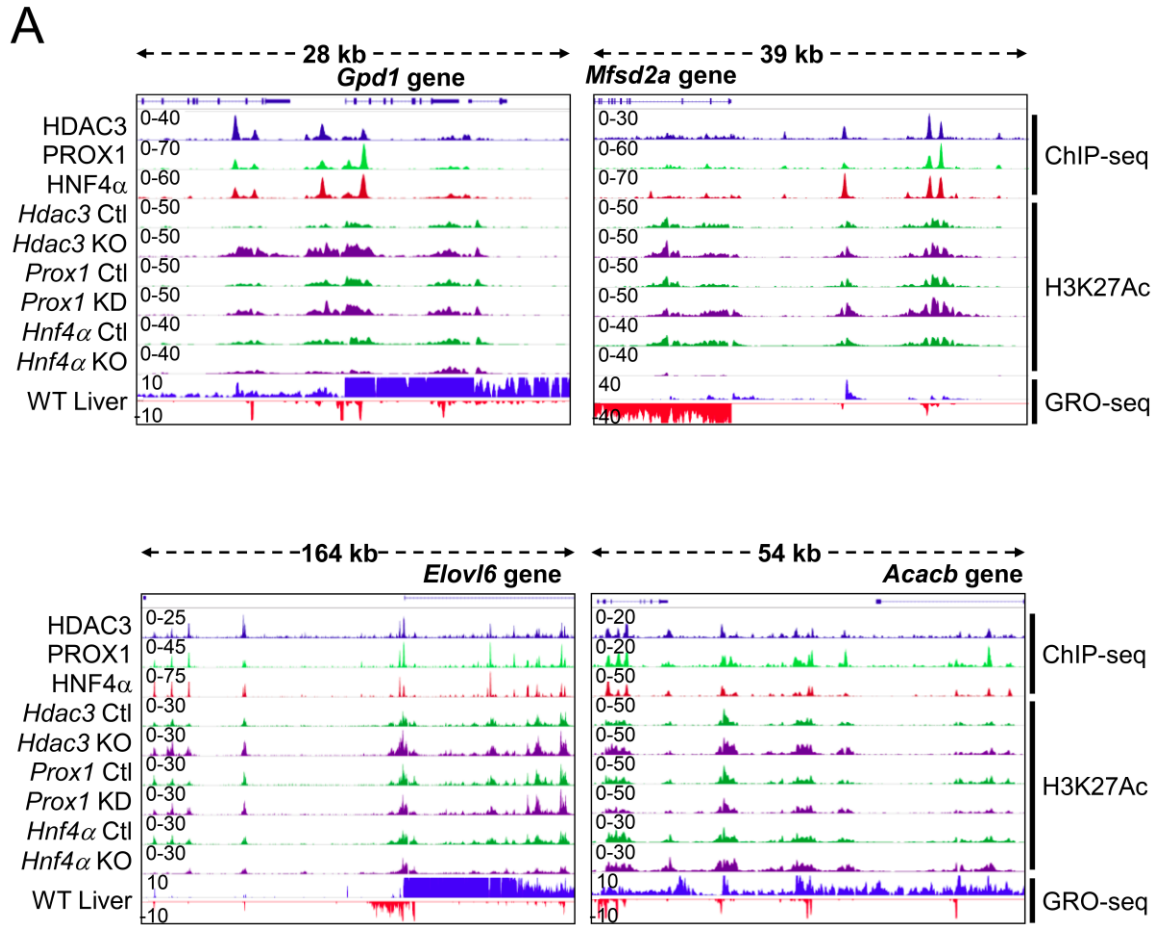


Figure 3.15 Genomic binding and nascent transcription near lipid-related genes coregulated by HDAC3-PROX1. (A) Example ChIP-seq and GRO-seq browser tracks at lipid-related gene loci. Indicated scales are in RPTM.

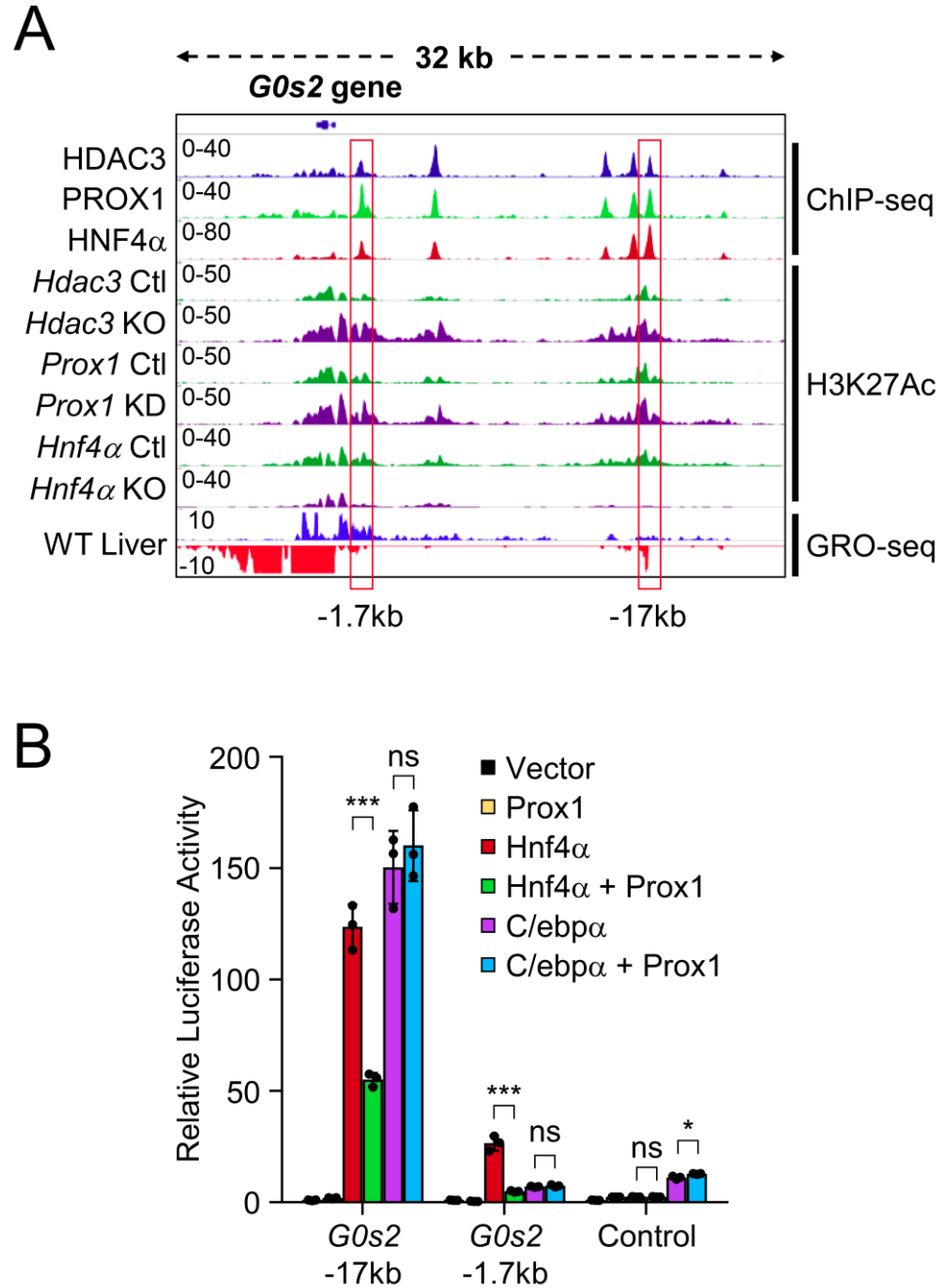


Figure 3.16 HDAC3-PROX1 repress putative *G0s2* enhancers. (A) Example ChIP-seq and GRO-seq browser tracks at the *G0s2* locus. Red boxes indicate location of putative *G0s2* enhancers. (A) Luciferase assay (n=3) indicating transcriptional response to co-expression of HNF4 α , PROX1 and C/EBP α at *G0s2* enhancers as identified in A. Data are presented as mean \pm s.d. Two-tailed unpaired Student's t-test, *p<0.05, **p<0.01, ***p<0.001, ns not significant.

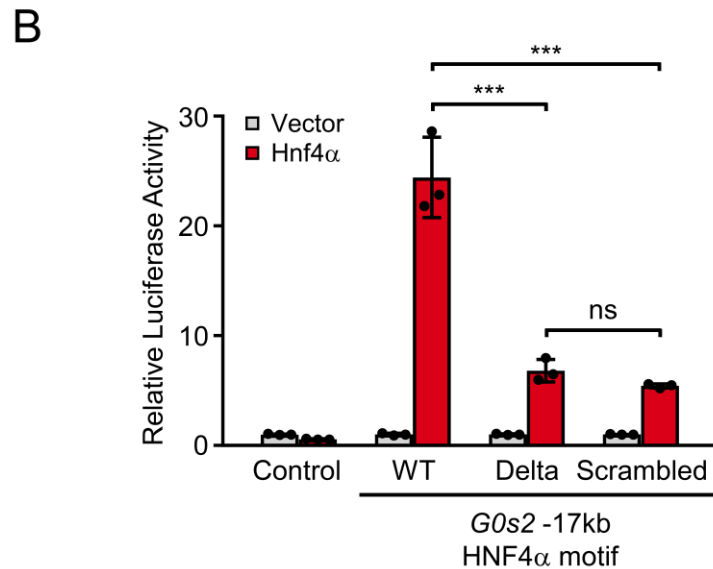
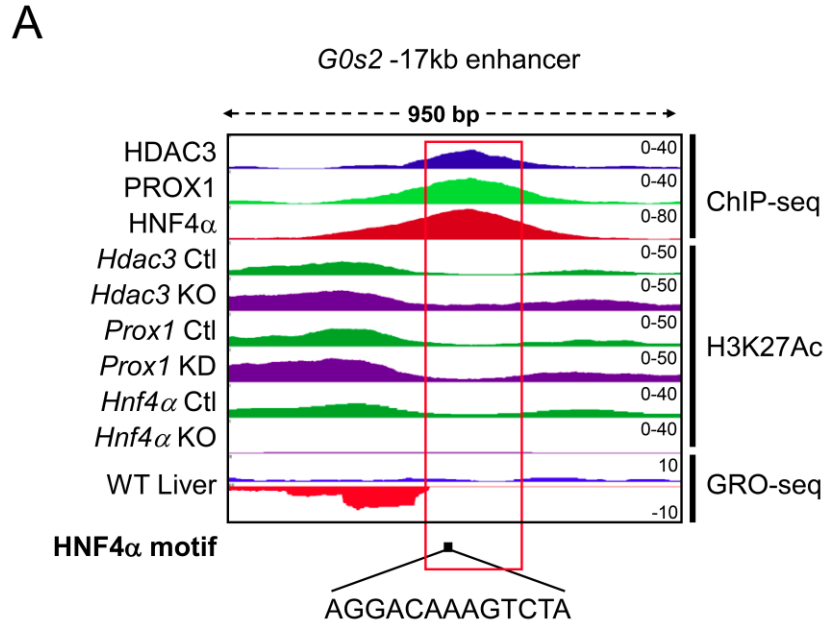


Figure 3.17 HNF4 α -induced enhancer function is dependent on an intact HNF4 α DNA binding motif. (A) Track of *G0s2* locus with identified HNF4 α motif. Indicated scales are in RPTM. (B) Luciferase assay (n=3) indicating transcriptional response to expression of HNF4 α at wild-type and HNF4 α DR1 mutant *G0s2* enhancer as indicated. Data are presented as mean \pm s.d, two-tailed unpaired Student's t-test, *p<0.05, **p<0.01, *p<0.001, ns not significant.**

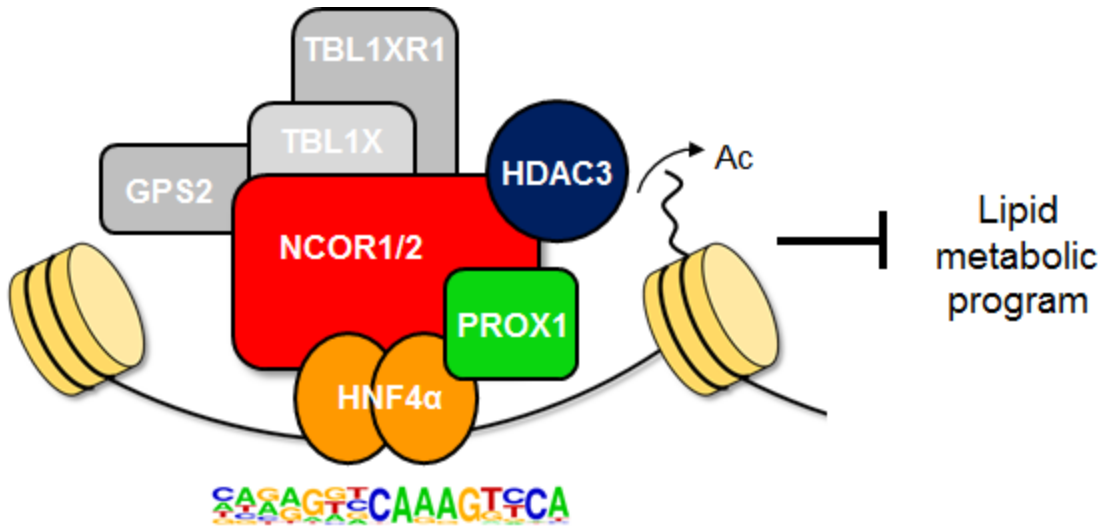


Figure 3.18 Schematic model of HNF4 α recruitment of PROX1 and the NCoR complex to regulate a lipid-related metabolic gene program.

Table 3.1 nLC-MS/MS analysis of HDAC3 high-confidence interacting proteins. Proteins listed met 10-fold enrichment versus EGFP and $p < 0.01$.

Protein names	$\log_2(\text{HDAC3/EGFP})$	negative $\log_{10}(\text{p-value})$	Classification
Hdac3	11.50137525	5.021516227	NCoR Complex
Tbl1x	10.54659342	7.587663608	NCoR Complex
Tbl1xr1	9.24165353	8.95026059	NCoR Complex
Ncor1	8.825403468	6.17251732	NCoR Complex
Ncor2	7.603407958	10.08949853	NCoR Complex
Prox1	7.595525418	7.097347584	Transcription/Chromatin
Mlf2	7.574741457	4.436019601	
Gps2	7.571426065	5.232233167	NCoR Complex
Rxra	7.341950491	3.327213956	Nuclear Receptor
Nfix	7.148035567	6.644835182	Transcription Factor
Rcor1	6.345118027	2.712611201	NuRD/CoREST
Cebpa	6.183333282	5.339815886	Transcription Factor
Nr1h4	6.072994963	4.176496378	Nuclear Receptor
Bag5	6.070137242	4.234131552	
Dnajb4	6.061957981	3.589209458	
Etv6	6.048757593	2.938893161	Transcription Factor
Smarcd2	6.037286742	4.958741634	SWI/SNF
Znf281	6.032345368	3.792904085	Transcription Factor
Zhx2	5.794752614	3.679940103	Transcription/Chromatin
Mlxipl	5.773455481	3.568588182	Transcription Factor
Kdm1a	5.53567459	4.508312652	NuRD/CoREST
Clock	5.366657793	4.746470225	Transcription Factor
Wrnip1	5.319348837	2.782480267	Transcription/Chromatin
Dpf2	5.306182493	3.913796445	Transcription/Chromatin
Nosip	5.285065555	3.559607131	
Nr1d1	5.234286657	2.47193724	Nuclear Receptor
Pias1	5.167487939	2.166612423	Transcription/Chromatin
Vwa9	5.116103328	3.191066711	Integrator
Asun	5.092654541	2.81531689	
Hnf1a	5.078858612	5.410401383	Transcription Factor
Mta1	5.078814908	2.541132063	NuRD/CoREST
Ppara	5.058586349	2.476820827	Nuclear Receptor
Smarcc2	4.978585848	6.199303917	SWI/SNF
Smarcb1	4.964746211	2.228178493	SWI/SNF
Nfib	4.908651202	4.305886841	Transcription Factor

Stat5b	4.892492597	2.889276943	Transcription Factor
Mau2	4.874084295	2.567924363	Cohesin
Arntl	4.865380227	2.406360822	Transcription Factor
Brd4	4.858912757	3.375470207	Transcription/Chromatin
Zhx3	4.847763471	3.957113425	Transcription/Chromatin
Sult1a1	4.82836982	2.321889843	
Ints5	4.778638786	3.342287612	Integrator
Smarca1	4.604676132	2.485552012	SWI/SNF
Gatad2b	4.555632328	4.500371592	Transcription/Chromatin
Zbtb7b	4.547599544	2.682269053	Transcription/Chromatin
Dbp	4.547080983	2.735498485	Transcription Factor
Hnf4a	4.525649856	6.605898044	Nuclear Receptor
Cebpb	4.520503791	2.100955859	Transcription Factor
Smc1a	4.517900637	4.010252604	Cohesin
Arid5b	4.498504251	2.497245671	Transcription/Chromatin
Ruvbl2	4.496709142	4.099500642	Transcription/Chromatin
Ints1	4.477111894	4.212996556	Integrator
Smarca5	4.475990697	4.381754785	SWI/SNF
Arid1a	4.46676445	4.512961942	SWI/SNF
Nab1	4.462064744	5.296508944	Transcription/Chromatin
Ints9	4.370964709	3.150054586	Integrator
Polr2b	4.289036511	4.049194873	Transcription/Chromatin
Bhlhe40	4.256751257	2.152211759	Transcription Factor
Smc3	4.228886734	3.439928347	Cohesin
Mnat1	4.18744312	3.441859023	Transcription/Chromatin
Ints6	4.09958548	2.771826393	Integrator
Ints4	4.099168822	4.407380393	Integrator
Nfic	4.082154089	5.771828847	Transcription Factor
Zhx1	4.066760579	2.562358274	Transcription/Chromatin
Nr3c1	4.046922931	2.645929979	Nuclear Receptor
Ints3	4.04490837	4.1286784	Integrator
Stag2	4.020063973	4.266083132	Cohesin
Esrra	4.00522078	2.123791729	Nuclear Receptor
Paf1	3.995728504	3.041862816	Transcription/Chromatin
Hspa1b;Hspa1a	3.970119408	3.388227113	
Nfia	3.965017835	4.687516874	Transcription Factor
Esrp2	3.914764469	2.908276725	
Gstm6	3.866886589	2.572367699	
Rbbp7	3.86528679	3.890890089	NuRD/CoREST
Ctr9	3.855895003	4.104064485	Transcription/Chromatin

Chd4	3.831952941	5.822887135	NuRD/CoREST
Creb1;Atf1	3.829080483	2.774269322	Transcription Factor
Usf2	3.798018588	2.156114993	Transcription Factor
Smarca2	3.781494617	5.13107819	SWI/SNF
Dnajb1	3.774240199	2.140052457	
Smarca4	3.717048017	2.776681779	SWI/SNF
Gtf2i	3.695064425	3.745739952	Transcription/Chromatin
Ints10	3.643650335	3.093098781	Integrator
Nr1i3	3.613074152	2.71697009	Nuclear Receptor
Rad21	3.595937009	3.99888251	Cohesin
Taf5	3.572662628	3.097665381	Transcription/Chromatin
Zbtb20	3.566321733	4.777392769	Transcription/Chromatin
Mbd3	3.516054008	4.872701732	NuRD/CoREST
Ints2	3.495483998	2.627051313	Integrator
Actl6a	3.494413181	4.633919172	SWI/SNF
Adnp	3.440742452	2.941966284	Transcription/Chromatin
Rprd1b	3.427474467	2.537990764	Transcription/Chromatin
Mta2	3.398119667	5.186276503	NuRD
Wapal	3.38941112	3.458735088	Cohesin
Pds5a	3.343777681	6.188849929	Cohesin
Nmnat1	3.340365082	2.510994062	
Supt16h	3.334988721	3.01811442	Transcription/Chromatin
Srbd1	3.329650536	3.39736468	
Ruvbl1	3.329049763	6.021428559	

Table 3.2 List of primers used for quantitative RT-PCR, ChIP-reChIP-qPCR, and luciferase experiments.

Target	Type	5' Primer	3' Primer
<i>Arbp</i>	qPCR	TCATCCAGCAGGTGTTTGACA	GGCACCGAGGCAACAGTT
<i>G0s2</i>	qPCR	AAGCCAGTCTGACGCAAG	CACACTGCCCAGAACGTATAG
<i>Elovl6</i>	qPCR	CAAGCGAGCCAAGTTTGAAC	AGCATGTAAGCACCAAGTTCG
<i>Acacb</i>	qPCR	GATGGAGCGCATACACTTGA	CCGAGTTTGTCACTCGGTTT
<i>Gpd1</i>	qPCR	CACAGCATTCTCCAACACAAG	TTCCGCTTGTCTCCGTTG
<i>Cidec</i>	qPCR	CCAACACAATCCAACGACAAG	TTGCGAACCTTCCGATCTG
<i>Mfsd2a</i>	qPCR	ATTGGATGTGGCTAAGGTGG	AGGCACAAACCAGATGAGG
<i>Ins</i>	reChIP	CTTCAGCCCAGTTGACCAAT	AGGGAGGAGGAAAGCAGAAC
<i>Arbp</i>	reChIP	CTGGGACGATGAATGAGGAT	AGCAGCTGGCACCTAAACAG
<i>G0s2</i>	reChIP	GGACAAAGTCTACAACCAATCC A	CACGCACAGACACAGACCTT
<i>Elovl6</i>	reChIP	GGCGTTCAAGGACTGACCTA	TGATGAAATTGCCTGACAGC
<i>Agpat2</i>	reChIP	ACTCTGCGGGCCTGTACTAA	CTGCTTCTCAACTGCCTTGG
<i>Gpd1</i>	reChIP	CATTGGTGACACTCCCCTCT	TCCAGTGCTGCACCTTGAC
<i>Mfsd2a</i>	reChIP	GGCAGAATGGACTGGTCACT	CCTGTAATATGTCTGGGGAGGA
pGL4 <i>G0s2</i> enhancer (-17kb)	Gibson Cloning	CGGTACCTGAGCTCGCTAGCCT CGAGGGGGATTTTGTGGACTT GAA	TTATATACCCTCTAGTGTCTAAG CTT ACCAAGGTGGGTTACACC AT
pGL4 <i>G0s2</i> enhancer (-1.7kb)	Gibson Cloning	CGGTACCTGAGCTCGCTAGCCT CGAG AAAGAGGTAGGCCAAAG GGC	TTATATACCCTCTAGTGTCTAAG CTT GTGATCAGCACCTTCTGAG TCT
<i>G0s2</i> (- 17kb) HNF4 α DR1 Delta	gBlock for Gibson Cloning	GGGGATTTTGTGGACTTGAACCTAGGGATGACGGAGTATGCAACC AATCCAACCTACTAATGGGGCACCAGCCAAAATCAACAACCTTGCAA CAGGGGAGAGGCAAAGGTCTGTGTCTGTGCGTGATCTGTATTCA CGTGTTTTAAGAACAGTGCACGTTCAAGATGGTGTAAACCCACCTTG GT	
<i>G0s2</i> (- 17kb) HNF4 α DR1 Scramble	gBlock for Gibson Cloning	GGGGATTTTGTGGACTTGAACCTAGGGATGACGGAGTATG ATAGC GTTCAAGTTGCC AACCAATCCAACCTACTAATGGGGCACCAGCCAA AATCAACAACCTTGCAACAGGGGAGAGGCAAAGGTCTGTGTCTGTG CGTGCATCTGTATTACGTTGTTTAAGAACAGTGCACGTTCAAGAT GGTGTAAACCCACCTTGGT	

CHAPTER 4: Generating epitope tagged mouse models using CRISPR-Cas9

The text, figures, and legends in this chapter were the work of Jarrett Renn Remsberg with the following exceptions. Microinjections were performed by the Transgenic and Chimeric Mouse Facility. Daniel Cohen assisted in Cas9 synthesis. Jorge Henao-Mejia provided reagents and technical assistance. Wesley Ho and Marine Adlanmerini provided mouse husbandry and technical assistance.

4.1 ABSTRACT

Recent advances in high throughput sequencing and –omic technologies have greatly advanced our understanding of biological processes and their molecular mechanisms. However, we are still limited by the constraints of consistent, useful, and available reagents such as antibodies and viruses. To overcome these constraints, we have employed genome editing techniques to generate mouse models encoding epitope tag sequences into the endogenous loci for proteins of interest. Preliminary investigations include the generation of nuclear receptor and corepressor epitope tagged lines thyroid hormone receptor β 1, Rev-erb α , and the nuclear receptor corepressor 1 (NCOR1). These mouse models provide an opportunity to interrogate protein-protein interactions *in vivo* and will be a significant resource of understanding target protein function in a larger context of organismal metabolism.

4.2 INTRODUCTION

Genome editing has traditionally been a challenging process, but recent advances have led to a revolution. The advent of CRISPR-Cas9 technology has given scientists new opportunities in molecular biology not seen since the wave of siRNA technology in decades previous. As part of the bacterial innate immune system, CRISPR (clustered regularly interspaced short palindromic repeats) are part of the bacterial innate immune system, a mechanism by which bacteria store genetic information to fight against viral infections in the future (Barrangou et al., 2007). This process has been repurposed as an RNA directed DNA editing platform. The RNA direction comes in the form of a 20 nucleotide ‘guide’ RNA followed by a scaffold that binds the nuclease, Cas9. This binding and recognition of a protospacer adjacent motif (PAM) sequence allow Cas9 to perform its nuclease catalytic activity and thusly generate a double stranded break in the DNA. One contributing factor to the success of this technique is the simplicity and limited experimental bench work required to prepare all components necessary for genome editing. Furthermore, this technology can be applied to a variety of goals in mind, including but not limited to error-prone

nonhomologous end joining, gene targeting with dCas9 effector mutants, and homology directed repair for specific genome editing (Jiang and Doudna, 2017).

Using the CRISPR-Cas9 platform to generate a small knockin, such as an epitope tag coding sequence, only three reagents are required: Cas9 mRNA, sgRNA, and ssDNA homology donor. This process has been demonstrated to be successful for generation of mice with conditional alleles (Yang et al., 2013, 2014). Several studies have worked to determine the molecular basis and mechanism of Cas9 genomic editing at the atomic resolution (Anders et al., 2014; Jinek et al., 2014; Nishimasu et al., 2014). CRISPR-Cas9 although relatively new in its application to genomic editing has been well characterized (Jiang and Doudna, 2017; Sander and Joung, 2014). In the execution of targeted homology directed repair, two design parameters are required. The first is selection of the 20 nucleotide 'guide' sequence used to target Cas9 to the genomic loci, and the second is the ssDNA homology donor for integration.

4.2a Targeting proteins of interest

Epitope tagged proteins allow for consistency of reagents and overcome antibody limitations that may exist for proteins of interest. A major advantage of knocking in an epitope tag in the coding sequence of a gene is that expression is under endogenous regulatory elements. Therefore we employed CRISPR-Cas9 to generate several epitope tagged mouse models of interest, including thyroid hormone receptor $\beta 1$ (TR $\beta 1$), Rev-erb α , and NCOR1 to study their functions across a variety of tissues.

The thyroid hormone receptor $\beta 1$ is critically important nuclear receptors, with significant importance in human health, serving as its namesake suggests the receptor for thyroid hormone (Yen, 2001). It also has a rich history interacting with the retinoid X receptor (RXR) nuclear receptor and recruiting coregulatory complexes to chromatin (Astapova, 2016). There may be distinct roles for SMRT and NCOR1 in TR mediated repression (Shimizu et al., 2015). Also T3 binding has

recently been shown to regulate DNA binding of TR β 1 (Grøntved et al., 2015; Ramadoss et al., 2014). A novel epitope tagged TR β 1 mouse model would allow targeted investigation of the nuclear receptor paradigm of coregulatory exchange *in vivo*, in part due to the ability to control the availability of the endogenous ligand, thyroid hormone.

To compliment the investigation of TR β 1 *in vivo*, we generated an NCOR1 tagged mouse model. Whereas the perspective of tagged TR β 1 will inform exchange of coregulator complex recruitment, a handle on NCOR1 will determine all factors that utilize the corepressor complex. Analogous to the work already conducted in liver using an epitope tagged HDAC3, an endogenously tagged NCOR1 will provide a setting to continue interaction studies beyond liver. Furthermore, questions remain regarding the contributions of NCOR1 vs SMRT *in vivo* and this reagent aims to address these differences (Shimizu et al., 2015; Sun et al., 2013).

Finally, Rev-erb α expression is a highly regulated at both on the mRNA and protein levels. As a member of the core molecular clock machinery, it oscillates in expression with a period of approximately 24 hours (Papazyan et al., 2016b). Expression is greatest at approximately ZT10 (Zeitgeber time, ZT; where ZT0 is 'lights on' and ZT12 is 'lights off') and troughs at ZT22. Such dynamic regulation suggests possible post-translational modifications, and indeed phosphorylation plays an important role in its stability (Yin et al., 2006). Interestingly, it has also been shown to regulate gene transcription through indirect binding of DNA, but the precise mechanism and interactors are yet to be understood (Zhang et al., 2015). Also, an epitope tag at the endogenous locus presents a rare opportunity to address the protein-protein interactions in a circadian manner for Rev-erb α , as the tagged protein will be under the same endogenous regulatory elements and ideally controlled in the same manner.

4.3 METHODS

4.3a Design guidelines

The online tool, crispr.mit.edu was used to determine potential guide sequences for targeting. The DNA sequence surrounding the locus of interest (+/- 100bp) was used, and guide sequences with their off target sites were compared. In all cases, the sgRNA would target the double stranded cut within approximately 15 bases of the desired insertion site. If multiple guides were available, the one with the least off target hits and highest score was chosen.

4.3b Cas9 mRNA and sgRNA production

To generate Cas9 mRNA, plasmid containing Cas9-HA-2NLS was linearized with XbaI. Approximately 1µg of linearized plasmid was incubated with HiScribe™ T7 Quick High Yield RNA Synthesis kit (NEB #E2050S). RNA was purified using RNeasy mini columns (Qiagen #74106). Capping reaction used Vaccinia Capping System (NEB #M2080S). RNA was purified using RNeasy Micro clean up column (Qiagen #74004). Capped Cas9 mRNA was then subject to polyadenylation (NEB #M0276S) and purified over RNeasy Micro clean up column and eluted in RNase-free water. Cas9 mRNA integrity was validated using RNA BioAnalyzer. T7 promoter was added onto gRNA template by PCR amplification using specific primers. The T7-sgRNA product was purified using a PCR purification kit (Qiagen) and used as the template for *in vitro* transcription using the MegaShortScript kit (Life Technologies) following the manufacturer's instructions. Subsequent sgRNA was purified using the MegaClear Kit (Life Technologies) and verified by RNA BioAnalyzer before dilution for microinjection.

4.3c Microinjection of zygotes

Microinjection was performed by the transgenic mouse facility at UPenn. Microinjection buffer consisted of 1mM Tris pH 8.0, 0.1mM EDTA, 100ng/uL Cas9 mRNA, 50ng/uL sgRNA, and 100ng/uL of ssDNA homology donor.

4.3d PCR genotyping and sequencing

PCR primers flanking the site of insertion were designed using primer3. Edited mice were genotyped by PCR amplification products. Bands of the approximate correct size were gel extracted and sequenced using the same PCR primers (**Table 4.1**).

4.3e Immunoprecipitation and western blotting

For western blot analysis of total lysates, samples were lysed in a TissueLyser (Qiagen) in radioimmunoprecipitation assay buffer (RIPA buffer) supplemented with Complete EDTA-free protease inhibitor (Roche) and 1 mM PMSF. Proteins were precipitated in 2.5 volumes ice cold acetone and washed with 1mL ice cold acetone before being resuspended in RIPA buffer and subject to Bradford assay. Samples were resolved by Tris-glycine SDS-PAGE (Biorad), transferred to nitrocellulose membrane (Biorad), and blotted with the indicated antibodies. Antibodies for western blotting were anti-HA 3F10 High Affinity (Roche, 12013819001) and anti-Actin (Santa Cruz, sc-1616). For immunoprecipitation followed by western blot livers were lysed in RIPA buffer containing protease inhibitors and PMSF. Samples were pre-cleared with protein A sepharose CL-4B (GE Healthcare), and incubated with anti-HA agarose (Sigma, A2095). Immunoprecipitates were washed 5 times with RIPA and eluted with SDS loading dye.

4.3f ChIP-qPCR

ChIP-qPCR were as described previously (Feng et al., 2011; Lim et al., 2015). Briefly, livers were mildly dissociated by dounce with pestle A for 6 strokes in PBS containing 1% formaldehyde and rocked for 15 min, quenched with glycine, washed with PBS, and sonicated with a probe-type sonifier (Branson) in RIPA supplemented with protease inhibitors and PMSF. Sonicated extracts were immunoprecipitated with anti-HA agarose (Sigma, A2095) and isolated DNA was subject to RT-qPCR (**Table 4.1**).

4.3g Mass spectrometry

Livers were dounced in 1mL of RIPA buffer for 10 strokes and sonicated at 10 and 15W for 10 seconds. Extracts were cleared by centrifugation and were immunoprecipitated with anti-HA agarose (Sigma, A2095) overnight, washed 3 times in RIPA supplemented with protease inhibitors and 1 mM PMSF, washed 2 times in RIPA, washed 2 times in HPLC-grade water, eluted with 10% ammonium hydroxide diluted in HPLC-grade water, and dried to completion in a SpeedVac (Eppendorf).

Samples were prepared for MS as previously described (Armour et al., 2013). After reduction/alkylation, samples were digested with LysC (Wako) for 2 hours followed by Trypsin (Promega) at 37°C overnight. Samples were resuspended in 1% acetic acid, and desalted with C18 stage tips, as previously described (Rappsilber et al., 2003). EASY-nanoLC (Thermo Fisher Scientific) was configured with a 75 µm ID x 17 cm Reprosil-Pur C18-AQ (3 µm; Dr. Maisch GmbH, Germany) nano-column and coupled with an Orbitrap Fusion mass spectrometer (Thermo Fisher Scientific). Full scan MS spectrum (m/z 360–1600) was performed in the Orbitrap with a resolution of 120,000 (at 200 m/z). Fragmentation was performed with higher-energy collisional dissociation (HCD) and a maximum injection time of 120 msec. MS/MS data were collected in centroid mode in the ion trap mass analyzer. Peptides were identified using MaxQuant (v1.5.3.30) using the Mus Musculus UniProt FASTA database (March 2016) with an FDR<1% at the peptide spectrum match and protein levels.

4.4 RESULTS

4.4a Designing targeting sequence for CRISPR/Cas9 targeted knockin

The CRISPR-Cas9 system is an elegant means to generate site specific double stranded breaks (DSBs) since the targeting is accomplished by the guide RNA (sgRNA). The sgRNA, Cas9 protein, and target DNA form a ternary complex, and recognition of the PAM sequence allows Cas9 to perform catalysis (**Figure 4.1A**). There are two guiding principles in the design and selection of

sgRNA sequences to generate a successful knockin, minimizing potential off target editing and proximity to insertion site for efficient homology directed repair. We used the publically available crispr.mit.edu to identify potential guide sequences and subsequent off target sites for a given locus. Epitope tags are traditionally placed on the amino (N-) or carboxy (C-) terminus of the protein as to minimize interference with folding and function. A key feature of N-terminally tagged insertions is to place the epitope immediately after the start codon, methionine. Placing the tag prior to the endogenous methionine and creating Met-tag-Met-CDS could result in translation skips and thus protein products that lack the tag. For consideration of the cut site, the sgRNA-Cas9 complexed with DNA generates the DSB 3 bases prior to the end of the target guide sequence. With these principles in mind, a guide sequence meeting all the criteria was chosen (**Figure 4.1B**). For example, the guide chosen for the insertion of a tag at the N-terminus of Rev-erb α generates a DSB closest to the start codon and has the highest score from the algorithm. This score takes into account possible off target editing events based on mismatches in the guide sequence elsewhere in the genome. In the case for Rev-erb α , this highest scoring guide had 141 possible off target sites, 16 of which are in genes and 15 of those are exonic, all with at least 2 mismatches.

4.4b Confirming genome editing by PCR and Sanger sequencing

To determine if successful genome editing occurred, we PCR amplified the target locus with primers flanking the region. If a successful insertion occurred we observed a corresponding increase in the amplicon after PCR, 57 bases for the 6-His-HA tag, and 93 bases for the 3xHA tag. Products with increased size were subject to extraction and Sanger sequencing to confirm if the insertion produced the desired editing and no mutations arose (**Figure 4.2A-C**). Sequencing is crucial to determine those editing events where homologous recombination correctly integrated the ssDNA homology donor versus those that did not. In addition, it is valuable to sequence verify offspring from the founder to ensure the desired editing incorporated into the germ line as founders can be mosaic (data not shown for 3xHA-Rev-erb α).

4.4c Validating epitope tagged proteins *in vivo*

With successful genome editing and introduction of the epitope tag sequence, we next determined if proteins of interest were translated with the epitope tag and if this epitope was functional as a molecular handle. Immunoprecipitation followed by western blot analysis from whole cell liver lysates addressed two questions, first if the tagged protein was expressed, and second if the epitope was able to pull the target protein down. We detected 6His-HA-TR β 1 and enriched for the protein using anti-HA agarose (**Figure 4.3A**). Another feature of multiple proteins with the same epitope tag allows for valid comparisons using the same antibody, previously unachievable with antibodies against endogenous proteins that have varying binding affinity. Western blot analysis of whole cell lysates liver from 6His-HA-TR β 1 and 6His-HA-NCOR1 mice demonstrates that TR β 1 is expressed vastly less than NCOR1 (data not shown).

Additionally, as with TR β 1, we successfully immunoprecipitate tagged NCOR1 (**Figure 4.4A**). However, in addition to full length NCOR1, we observe a number of bands clearly evident in input and after immunoprecipitation. Full length NCOR1 is a very large protein (2454 amino acids), but it can have a variety of splice variants and isoforms. As a result of this epitope tag being inserted at the beginning of the coding sequence for NCOR1, we are likely observing the various splice variants of NCOR1, or possible degradation products. To confirm full length and functional NCOR1 is generated, liver from 6His-HA-NCOR1 mice was subjected to immunoprecipitation followed by nano-liquid chromatography coupled to mass spectrometry. We identified unique peptides spanning the full length of NCOR1, suggesting transcripts containing the epitope tag are successfully translated into the full length construct (**Figure 4.4B**). Additionally, we identified several NCoR complex members including HDAC3, TBL1X, and TBL1XR1 (**Figure 4.4C**). Further research is warranted to determine the role these lower molecular weight variants of NCOR1.

With the success of knocking in 57 base pairs of DNA to include a 6-His and HA tag, we sought to determine if we can achieve proper homologous recombination of a larger tag. Therefore we aimed

to insert a 3xHA tag, totaling 93 bases into the N-terminus of Rev-erb α . To tag Rev-erb α , we are limited to its N-terminus, as the C-terminus overlaps with the thyroid hormone receptor α (Lazar et al., 1989). Moreover, this is an excellent protein example to study since it is highly regulated, both at the transcriptional and protein levels. To ensure that the tag did not disrupt protein stability or regulation, 3xHA-Rev-erb α mice were harvested across circadian time points. Similar to the unmodified Rev-erb α , the 3xHA version at 75kDa was expressed highest at ZT10, and was not detectable at ZT22 (**Figure 4.5A**). It is unclear if the lower band observed at approximately 55kDa in ZT10 is a degradation product or truncation and further investigations are warranted. In addition to the proper regulation of Rev-erb α protein abundance, its circadian mRNA expression displayed a similar pattern and amplitude, as well as *Bmal1*, a known target gene and circadian clock component (**Figure 4.5B**). Further validation of the 3xHA-Rev-erb α was conducted by ChIP-qPCR at known clock target genes (**Figure 4.6A**).

A significant driver for whole mouse models containing epitope tags in the genome is the ability to compare across multiple tissues. We previously understood that Rev-erb α plays an important role in multiple metabolic organs beyond liver and this new tool can be applied to address these functions. Tissue from mice expressing the 3xHA-Rev-erb α on both allele were harvested and subsequently lysed and proteins precipitated. Relatively equivalent total protein was loaded onto an SDS-PAGE gel (**Figure 4.7A**). We observed a significant difference in the abundance of 3xHA-Rev-erb α across liver, fat depots, and muscle (**Figure 4.7B**). The detection of 3xHA-Rev-erb α also serves as a launching pad to employ cross-linking immunoprecipitation mass spectrometry techniques in tissues beyond liver to compare tissue specific interactomes.

4.5 DISCUSSION

We have demonstrated that CRISPR-Cas9 is a simple and effective means for genome editing and generating novel mouse models. The single cell zygote injection can significantly reduce the time

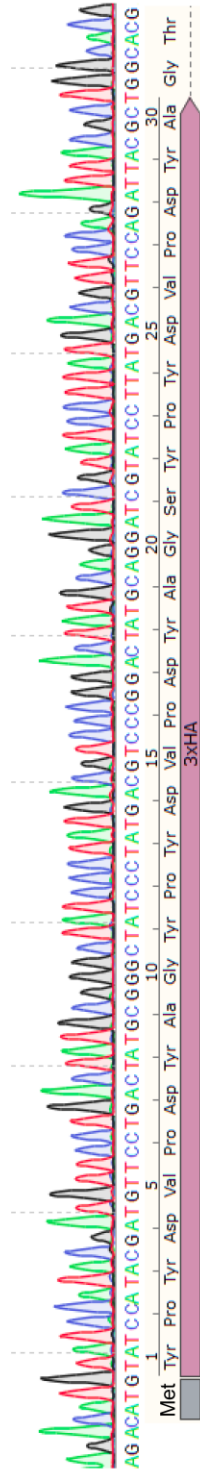
to generate these models. It is important to note however, that offspring from the founder mice should be sequence verified, as the germ line can have variable editing. Also single stranded DNA homology donor limits the insertion size to approximately 100bp, leaving 50bp of homology on either arm. We did not explore the effectiveness of larger insertions, such as fluorescent proteins or regulatory DNA elements such as eRNAs. In the design and execution of genome editing, there is a constant worry of off target events that could occur. Thankfully, these mouse models are back-crossing to ensure the removal of any deleterious editing in their generation, and therefore the most efficient guide with the highest likelihood to succeed can be utilized.

We have demonstrated that knocking in epitope tags allows for the detection of the protein of interest across tissues. Importantly, this can serve to compare relative abundance and expression levels in those tissues. Approximately equivalent total protein in each lane resulted in dramatically different levels of 3xHA-Rev-erb α as observed by western blot. Interestingly, unlike originally observed using northern blotting, protein levels of 3xHA-Rev-erb α in the soleus muscle are less than liver (Lazar et al., 1989). Furthermore, a recent study using mass spectrometry aimed to determine the best loading control across multiple tissues and found DJ-1 to be ideal for brain, liver, and muscle among others (Wiśniewski, 2017; Wiśniewski and Mann, 2016). It should be noted that fat depots were not included in their analyses. Indeed both white, but more prominently the brown fat depot differed greatly in DJ-1 detection compared to liver and muscle where the same total protein abundance was loaded. Future mass spectrometry proteomic studies would be necessary to validate these findings and for comparison of protein abundance across tissues using recent techniques and replicates (Wiśniewski, 2017).

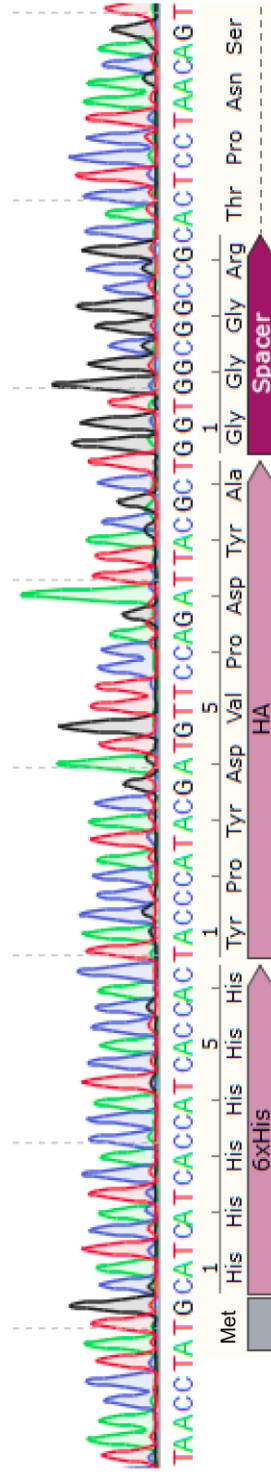
Addition of HA epitope tag has proven useful for detection and immunoprecipitation of target proteins, as well as comparisons across various tissues. A major driving force for the generation of these novel mouse models is for applications in tissues other than liver, an organ that can be easily be manipulated by AAV infection. Also the expression of these tagged proteins is entirely under the

endogenous regulatory elements, as evident by 3xHA-Rev-erb α . Each of the models described serve a distinct purpose to address unanswered questions in their respective areas of research. In regard to TR β 1, a protein that is antibody challenged, we plan to investigate one of the major paradigms in nuclear receptor research. TR β 1 is unique among nuclear receptors due to the ability to control the presence of its endogenous ligand, T3. Future work will assay the genomic occupancy and interactors of TR β 1 in the absence (via propylthiouracil) and presence (T3 injections) *in vivo*, directly testing the nuclear repressor to coactivator switch by ligand binding. The tagged NCOR1 mouse model will be paramount to continue our work from the HDAC3 liver interactome. We hypothesize that nuclear receptors and DNA binding factors, expressed in a tissue specific manner utilize the NCoR complex to repress their target gene program. This will be investigated by comparing the liver interactome to other tissues such as white and brown fat depots, where other work in the lab has demonstrated NCoR complex members are critical. Finally, the 3xHA-Rev-erb α mouse model presents unique opportunities to study, in part to determine interactome as a function of time, sampling across circadian time points.

A 3xHA-
Rev-erb α



B 6His-HA-
TR β 1



C 6His-HA-
NCOR1

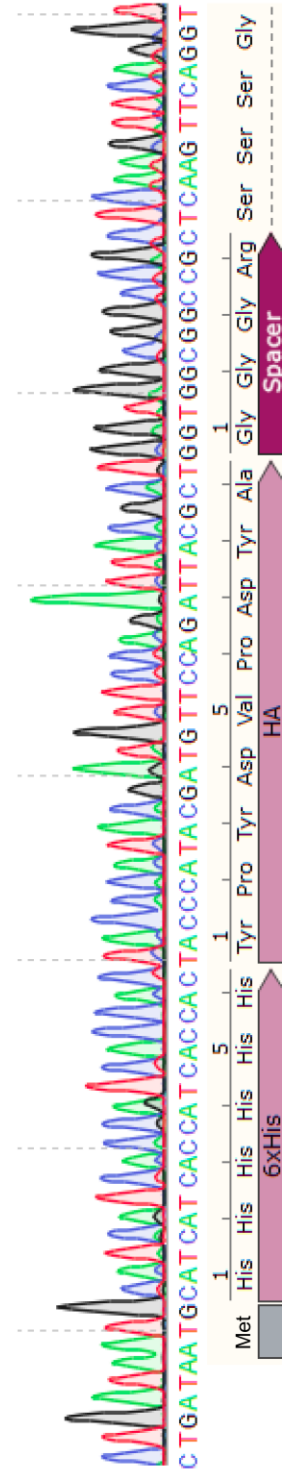


Figure 4.2 Sanger sequencing confirmation of targeted genome editing. (A) 3xHA sequence knocked into the Rev-erb α CDS locus. (B) 6-His-HA sequence knocked into the TR β 1 CDS locus. (C) 6-His-HA sequence knocked into the NCOR1 CDS locus.

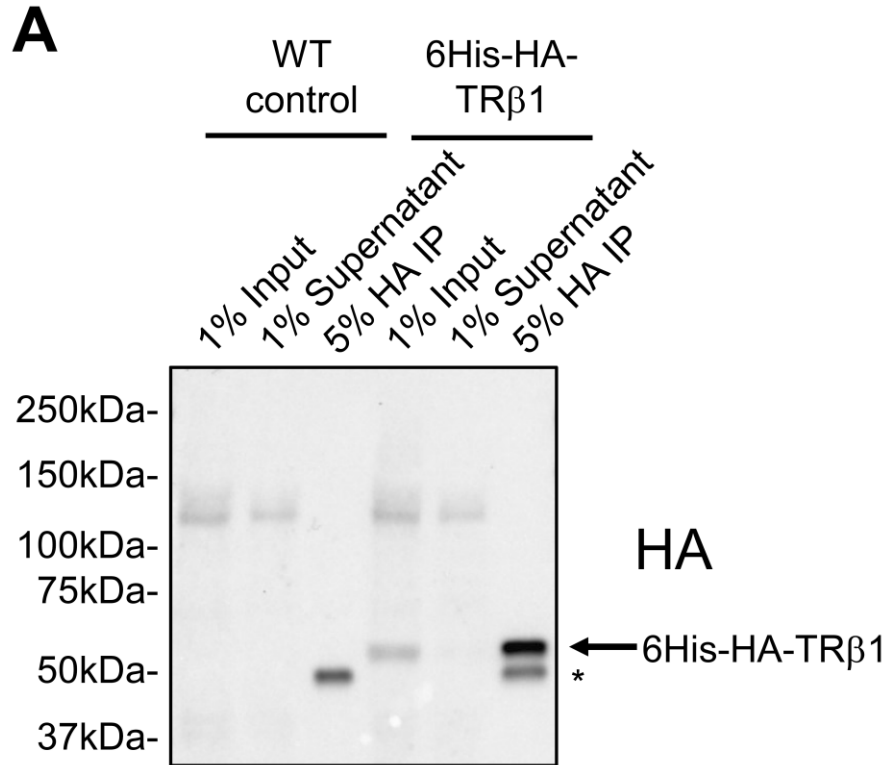


Figure 4.3 Validation and immunoprecipitation western blot of 6-His-HA-TR β 1. (A) Liver from wild-type (WT) control or mice expressing 6-His-HA-TR β 1 on both alleles were lysed and subject to IP-WB using anti-HA agarose and anti-HA-HRP. Non-specific band is denoted by *.

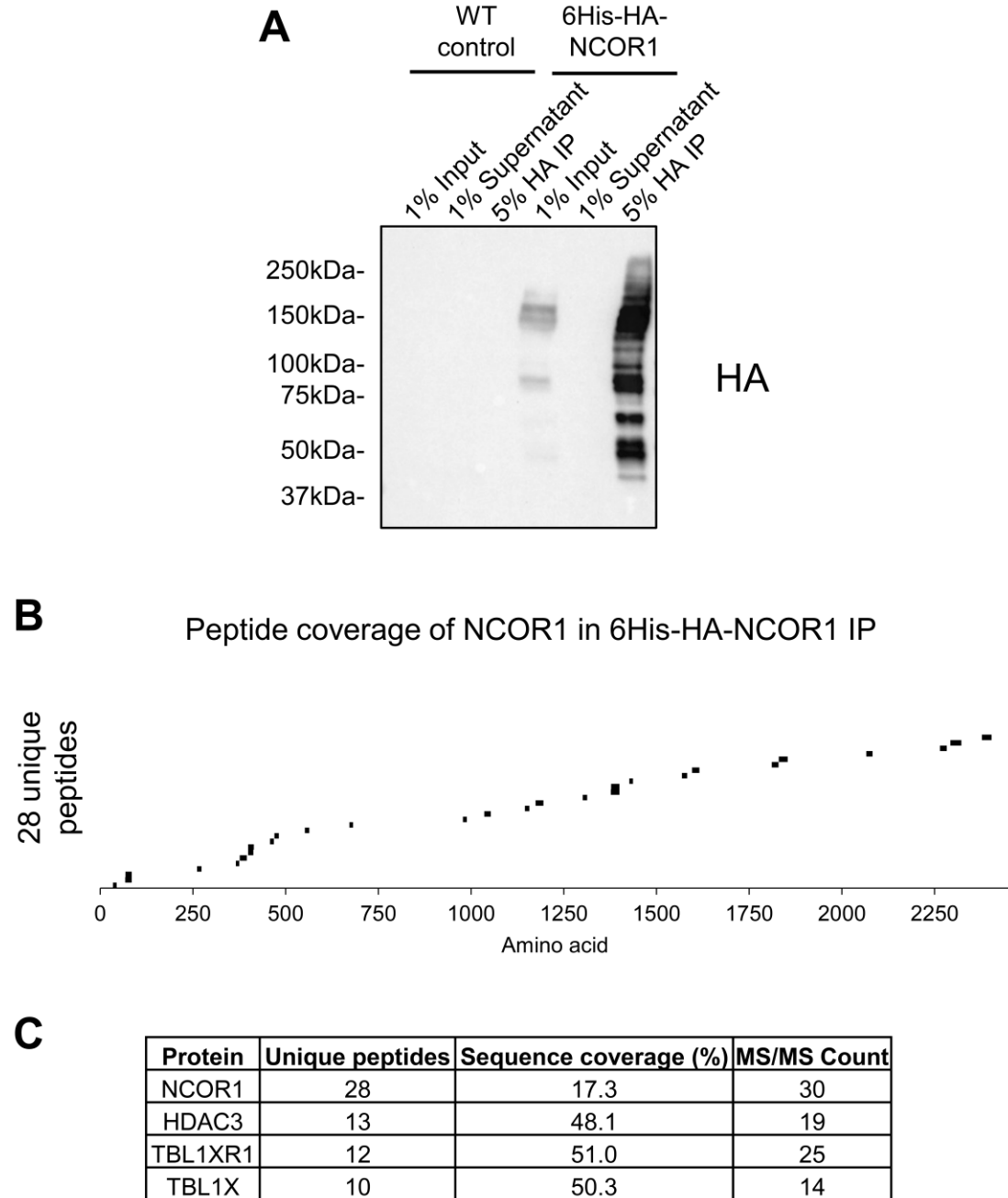
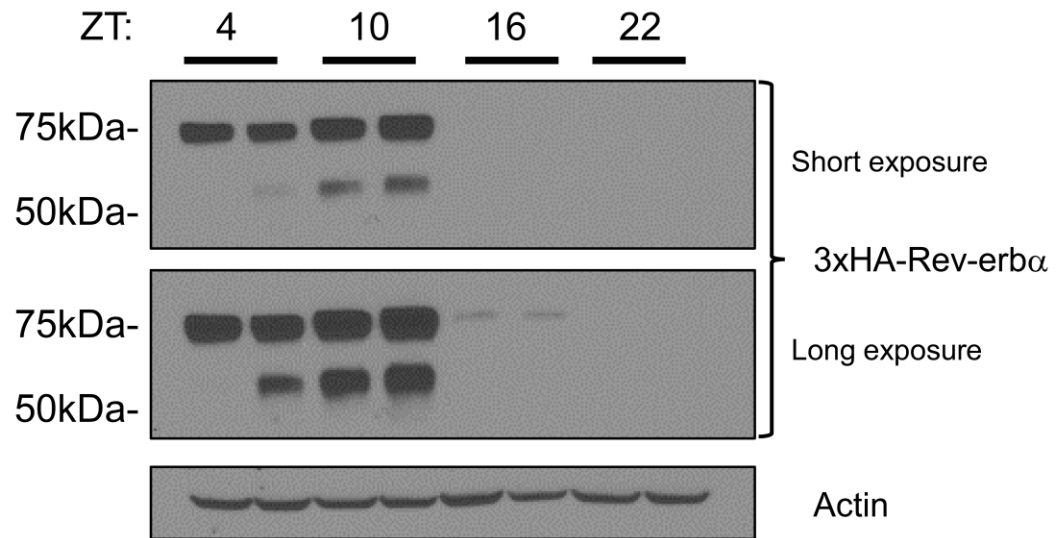


Figure 4.4 Validation of 6-His-HA-NCOR1 by immunoprecipitation western blot and mass spectrometry. (A) Liver from wild-type (WT) control or mice expressing 6-His-HA-NCOR1 on both alleles were lysed and subject to IP-WB using anti-HA agarose and anti-HA-HRP. (B) Graph denoting the unique peptides identified from IP-MS of 6-His-HA-NCOR1. (C) Identification and coverage of NcoR complex members from IP-MS of 6-His-HA-NCOR1.

A



B

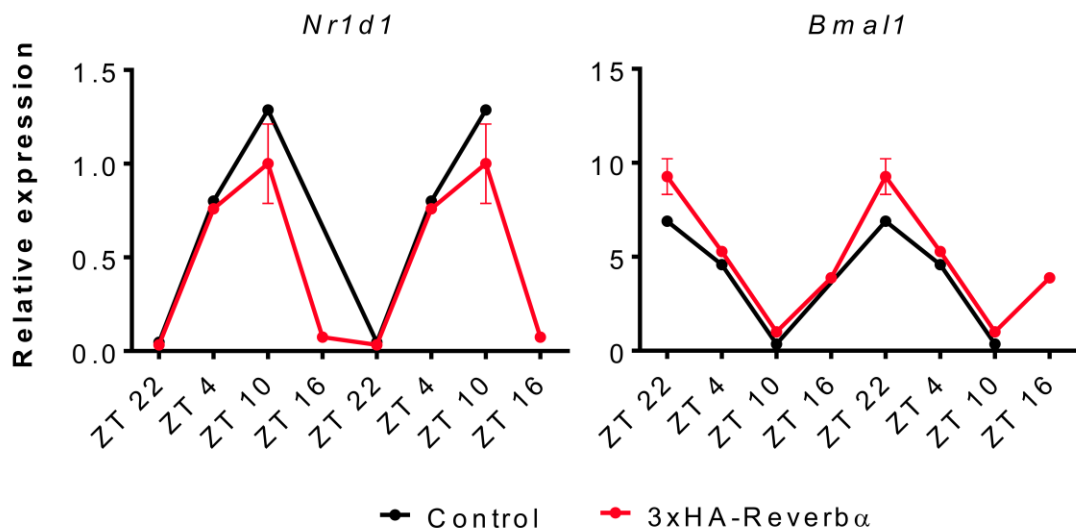


Figure 4.5 Circadian expression of 3xHA-Rev-erb α . (A) Western blot of mice expressing 3xHA-Rev-erb α (band at 75kD) on both alleles across 24 hour cycle in liver. Actin protein levels are shown as loading control. (B) Quantitative RT-PCR in liver of homozygous 3xHA-Rev-erb α and wild-type mice (n=1-3, ZT time points are repeated).

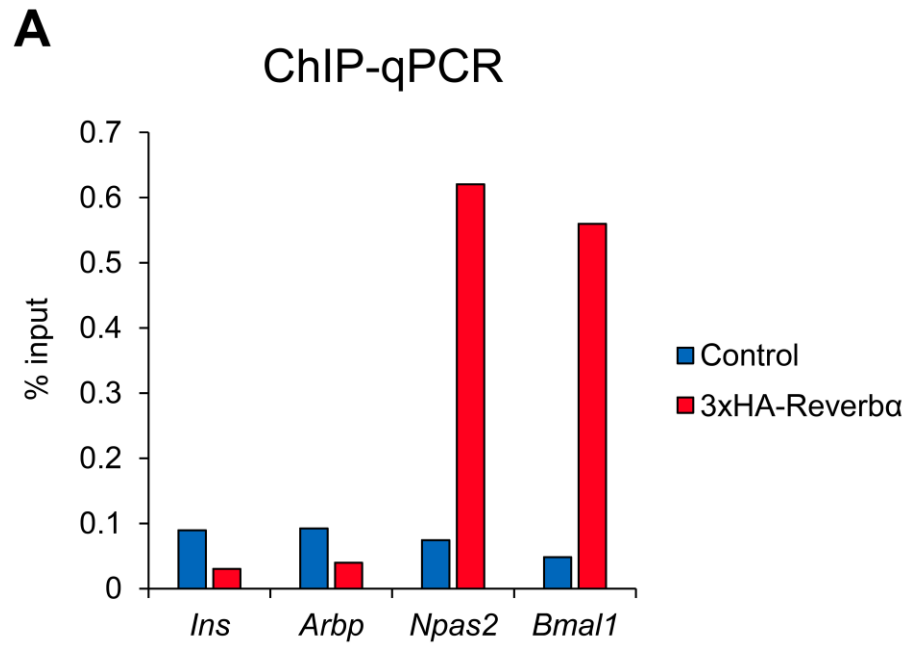


Figure 4.6 Validation of 3xHA-Rev-erb α binding to known target genes. (A) ChIP-qPCR of heterozygous 3xHA-Rev-erb α at known clock target genes (n=1).

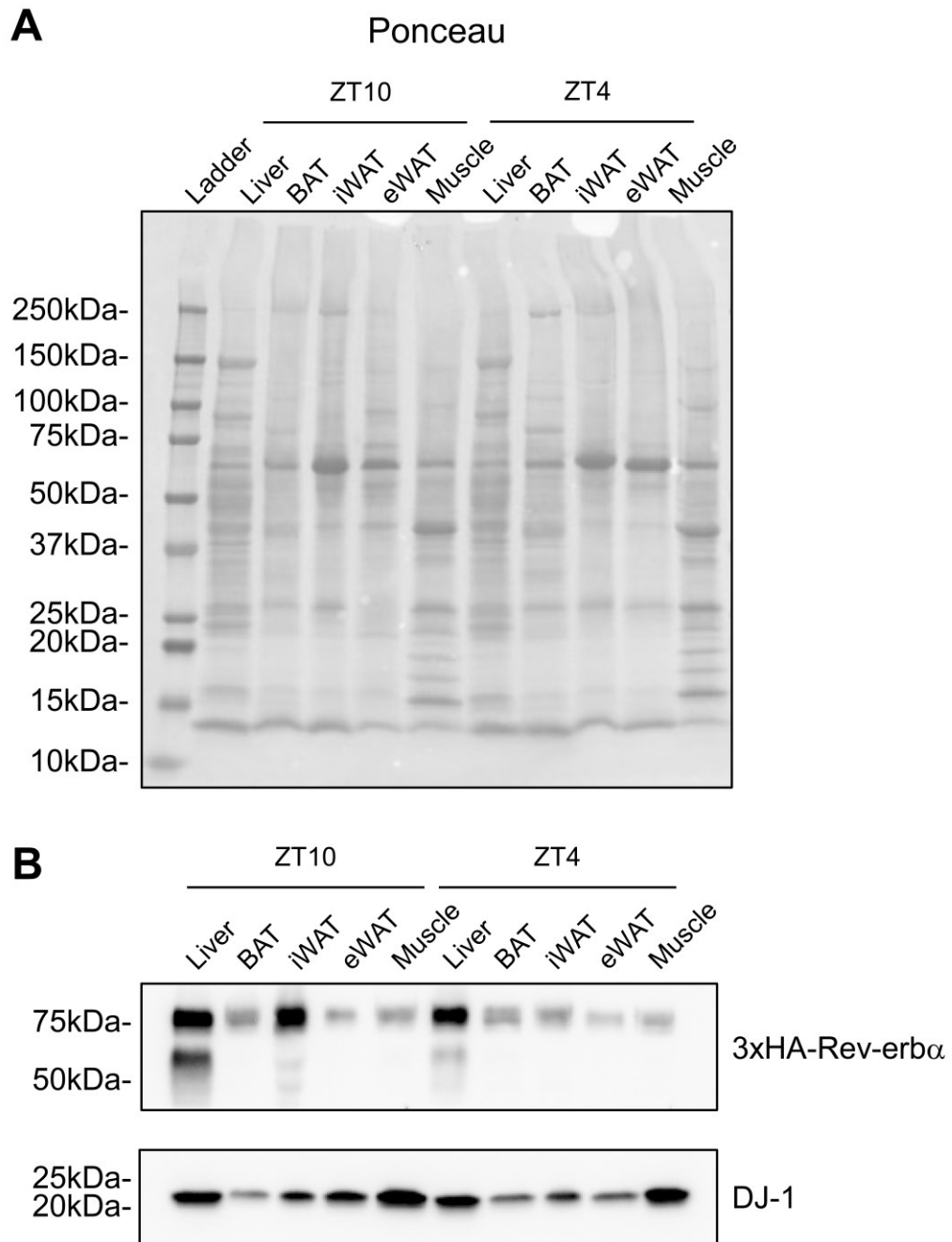


Figure 4.7 Comparison of Rev-erb α protein abundance across tissues. (A) Ponceau staining of western blot. Each lane was loaded with 25 μ g of total protein. (B) Western blot against 3xHA-Rev-erb α at ZT10 and ZT4 in metabolic tissues. DJ-1 is shown as a potential loading control.

Table 4.1 List of primers used for quantitative RT-PCR, ChIP-qPCR, and genotyping.

Target	Type	5' Primer	3' Primer
<i>Arbp</i>	qPCR	TCATCCAGCAGGTGTTTGACA	GGCACCGAGGCAACAGTT
<i>Nr1d1</i>	qPCR	GTCTCTCCGTTGGCATGTCT	CCAAGTTCATGGCGCTCT
<i>Bmal1</i>	qPCR	TAGGATGTGACCGAGGGAAG	TCAAACAAGCTCTGGCCAAT
<i>Ins</i>	ChIP	CTTCAGCCCAGTTGACCAAT	AGGGAGGAGGAAAGCAGAAC
<i>Arbp</i>	ChIP	CTGGGACGATGAATGAGGAT	AGCAGCTGGCACCTAACAG
<i>Npas2</i>	ChIP	TTGCAGAAGCTTGGGAAAAG	TTTCCTGTGGGAGGAGACAG
<i>Bmal1</i>	ChIP	AGCGGATTGGTCGGAAAGT	ACCTCCGTCCCTGACCTACT
<i>Ncor1</i>	Genotyping	ACACACACACACACACATCTTG	GCTTTGCCTGGAAATTGTGGT
<i>Rev-erbα</i>	Genotyping	TAAGCCTTGGATGGAAATGG	AGCCACCCCAAGACCTTACT
<i>TRβ1</i>	Genotyping	CTCTGTGAGTTTGAAGAAAGC	TCAGGTTGGCTTTAGAACCCC
<i>Ncor1</i>	Guide sequence	TTACTGATAATGTCAAGTTC	
<i>Rev-erbα</i>	Guide sequence	TGGTGAAGACATGACGACCC	
<i>TRβ1</i>	Guide sequence	GTCATACTGTTAGGAGTCAT	

CHAPTER 5: Summary and Future Directions

5.1 SUMMARY

This work encompasses significant advances in our understanding of HDAC3 function in mammalian physiology and gene regulation. Utilizing mouse genetic models, we determined this epigenomic regulator plays a critical role in adult mouse β -cells. Interestingly, these findings suggest that ablation of HDAC3 in the β -cells could be beneficial for diet induced obesity as the body struggles to maintain glucose homeostasis. Indeed, another recent study suggests pharmacologic inhibition of HDAC3 has beneficial effects on glucose homeostasis in a diabetic rat model (Lundh et al., 2015). Physiologic measurements showcase HDAC3's important role in glucose-stimulated insulin secretion, whereas transcriptome and cistromic analysis hinted at possible molecular mechanisms. The potentiation of glucose-stimulated insulin secretion as a result of dysregulation of HDAC3 target genes remains to be more clearly understood, but we can speculate from the altered transcriptome. One hypothesis that emerges is that increased bile acid transport potentiates glucose-stimulated insulin secretion in the HDAC3 β KO mice. Two organic anion transporters are significantly upregulated with ablation of HDAC3. To test this hypothesis and better understand the kinetics of insulin secretion in the β -cell knockout of HDAC3, perfusion experiments would be highly informative. These allow the direct measurements of β -cell function over time while controlling the system, modulating the buffer the isolated islets are exposed to, and measuring the resulting output.

Furthermore, we dove into the molecular underpinnings of HDAC3 mediated repression in mammalian liver by combining mass spectrometry and cistromic analyses. This work identified a variety of nuclear receptors and DNA binding proteins that associate with the NcoR complex in liver. Indeed, this workflow could be adapted to other proteins of interest that are within the size limitation of the AAV8 vector or epitope tagged mouse model. Importantly, we identified a previously unknown complex involved in the regulation of lipid-related genes in liver, where HNF4 α recruits both the NCoR complex and PROX1 to repress target genes. Integration of cistromic data proved extremely valuable to segregate potential interactors as well. This is highlighted in the comparison

of PROX1 specific, HDAC3 specific, and co-bound peaks, which suggests that HDAC3 and PROX1 are recruited in conjunction by HNF4 α , however only HDAC3 is recruited to Rev-erb α sites. Dissecting the data in this fashion is important because when we observe interactomes and mass spectrometry data, they are an ensemble of all HDAC3 interactions and we cannot parse which interactors are present with one another. Although, reciprocal interactomes from other proteins could build a more complete network, those experiments are laborious and may not be informative unless some interactors are uniquely identified. Instead, we gained valuable insight from the cistromic data by understanding where along the genome these distinct complexes bind and their potential target genes.

Two directions that can extend our understanding of these chromatin associated complexes are both related to mass spectrometry technologies, one being cross-linking mass spectrometry for the identification of peptide-peptide cross links. Understanding the organization and competition of co-regulators may inform as to how these proteins control gene expression. Combination of traditional structural studies such as cryo-electron microscopy, crystallography, and cross-linking mass spectrometry allow for a more complete picture of large protein complexes. The other and more challenging would be locus specific interrogation of protein-protein interactions. To determine with confidence the DNA binding factors and coregulators present at a given genomic locus would be extremely valuable (Wierer and Mann, 2016). Unfortunately, there is no PCR for proteins, and mass spectrometry techniques are limited in detection. Advances in technology has significantly decreased the minimum number of molecules for detection, but it is still on the order of fmol, or 1e8 molecules, a major challenge for locus specific interrogation.

5.2 FUTURE DIRECTIONS

5.3a Tissue specific interactomes

Generating novel epitope tagged mouse models presents a unique opportunity. Where before we were limited to liver for expression of epitope tagged constructs, by having this encoded in the genome of the animal itself, we can compare different tissues. This is especially exciting for two of the CRISPR-Cas9 generated mouse models, Rev-erb α and NCOR1. For the case of Rev-erb α , we understand it has important roles in multiple metabolic organs such as liver and brown fat, and in liver in particular research shows that other DNA binding proteins may play a critical part in the tethering of Rev-erb α to chromatin. Using this model we can empirically determine those proteins that interact and recruit Rev-erb α to chromatin in liver, and identify if there are others in brown fat. The epitope tagged NCOR1 presents a very unique opportunity for continued investigation of the NCoR complex *in vivo*, namely to determine the tissue specific nuclear receptors and DNA binding proteins that utilize the NCoR complex to repress their target gene program (**Figure 5.1A**).

Another dimension to investigate protein-protein interactions is across circadian time points, and the best example of this is the 3xHA-Rev-erb α mouse model we developed. This specific protein is especially interesting due to its highly regulated expression levels. Future work will investigate if there are circadian specific interactions or modifications on 3xHA-Rev-erb α that are critical for its function in mammalian liver (**Figure 5.1B**).

5.3b Cross-linking mass spectrometry

The past several years has seen the expansion and widespread use of cross-linking mass spectrometry following two major themes. The first is exploited by our own work, mirroring chromatin immunoprecipitation for the capture and identification of DNA binding proteins and lower affinity/transient interactors by formaldehyde cross-linking. The second, more challenging yet more

informative method is that of using cross-linkers to determine peptide-peptide cross-links of proteins in complex. This technology recently overcame a major hurdle in the form of CID (collision induced dissociation) inducible cross-linkers, such as disuccinimidyl sulfoxide (DSSO) (**Figure 5.2A**). Previously, identification of peptide-peptide cross-links was a monumental challenge due to the complex MS2 spectra and subsequent database searching which increased n^2 . The advent of CID cleavable cross-linkers allows users to simplify the complex spectral searching to standard searches including the cleaved cross-linker, substantially decreasing computation time and allowing for more complex samples (**Figure 5.2B**). However, this requires an MS3 event and benefits from more high resolution mass spectrometers. Multiple studies have proven that cellular complexity is no longer an unsurmountable obstacle for cross-linking mass spectrometry (Chavez et al., 2011, 2016; Schweppe et al., 2017; Wang et al., 2017; Weisbrod et al., 2013; Wu et al., 2016; Zhong et al., 2017). Applying this technique to better understand the organization and direct protein-protein interactions of the NCoR complex on chromatin would be invaluable.

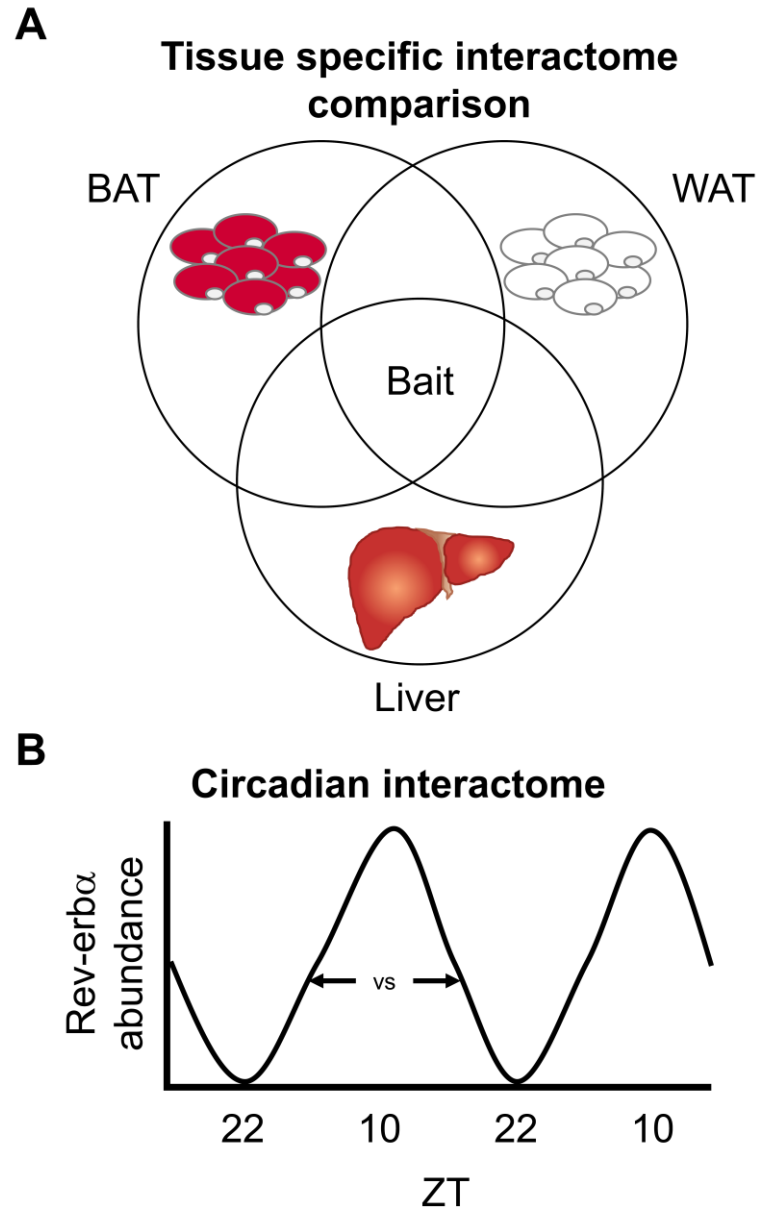


Figure 5.1 Future directions to interrogate interactomes *in vivo*. **(A)** Schematic plan to compare tissue specific interactomes of CRISPR-Cas9 generated epitope tagged mouse models. **(B)** Diagram demonstrating circadian dependent interactome of 3xHA-Rev-erba.

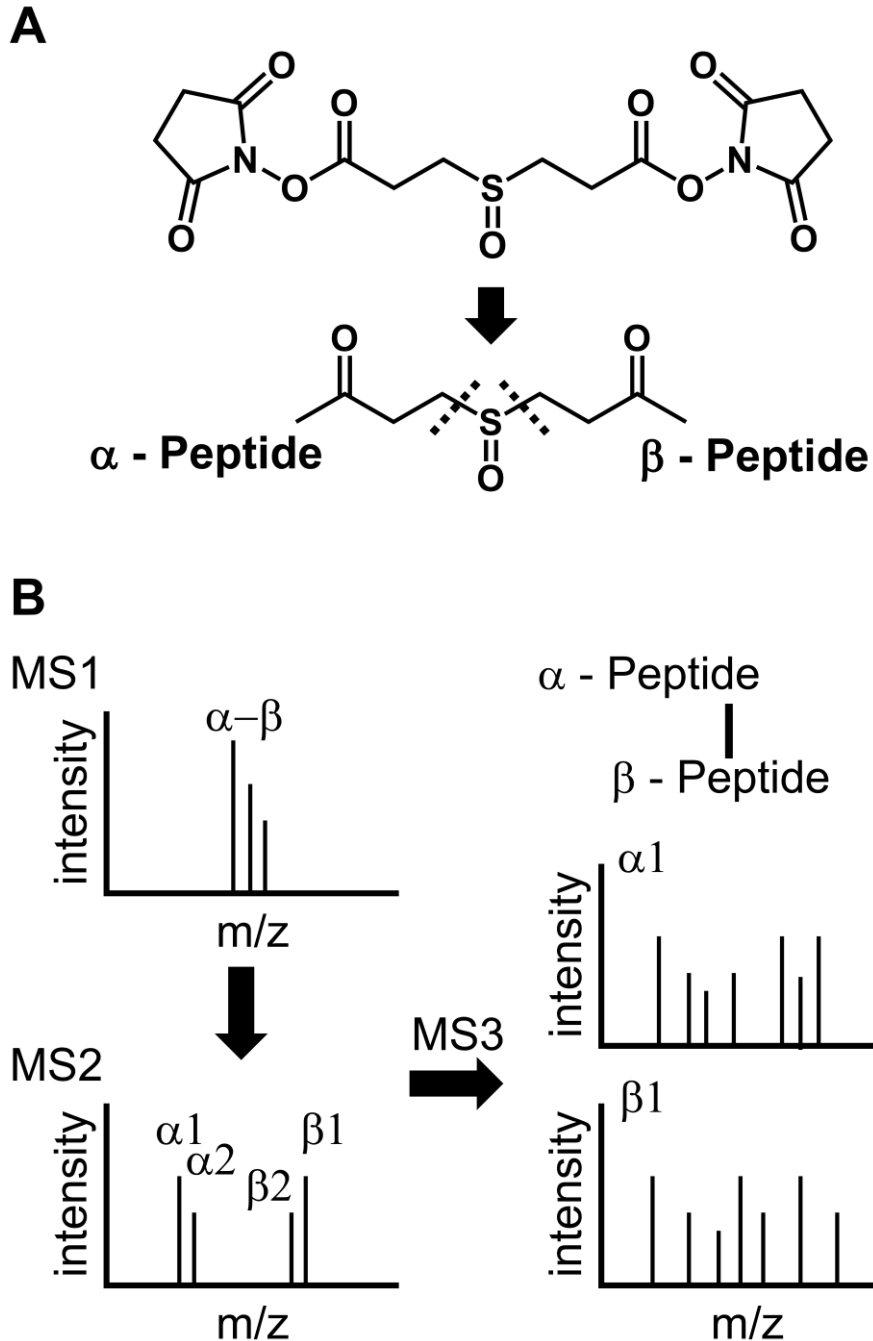


Figure 5.2 CID cleavable cross-linker to identify peptide-peptide cross-links in complex mixtures. (A) Graphic detailing the CID cleavable cross-linker, DSSO reaction with peptides containing lysine primary amines (dashed lines represent bonds that are cleavable). (B) Schematic representation of MSⁿ allowing for traditional analysis of spectra for peptide sequence identification from cross-linked peptides.

BIBLIOGRAPHY

- Abdelkarim, H., Brunsteiner, M., Neelapapu, R., Bai, H., Madriaga, A., van Breemen, R.B., Blond, S.Y., Gaponenko, V., and Petukhov, P. a (2013). Photoreactive “nanorulers” detect a novel conformation of full length HDAC3-SMRT complex in solution. *ACS Chem. Biol.* **8**, 2538–2549.
- Alenghat, T., Meyers, K., Mullican, S.E., Leitner, K., Adeniji-Adele, A., Avila, J., Bućan, M., Ahima, R.S., Kaestner, K.H., and Lazar, M. a (2008). Nuclear receptor corepressor and histone deacetylase 3 govern circadian metabolic physiology. *Nature* **456**, 997–1000.
- Alenghat, T., Osborne, L.C., Saenz, S.A., Kobuley, D., Ziegler, C.G.K., Mullican, S.E., Choi, I., Grunberg, S., Sinha, R., Wynosky-Dolfi, M., et al. (2013). Histone deacetylase 3 coordinates commensal-bacteria-dependent intestinal homeostasis. *Nature* **504**, 153–157.
- Anders, C., Niewoehner, O., Duerst, A., and Jinek, M. (2014). Structural basis of PAM-dependent target DNA recognition by the Cas9 endonuclease. *Nature* **513**, 569–573.
- Anders, S., Pyl, P.T., and Huber, W. (2015). HTSeq-A Python framework to work with high-throughput sequencing data. *Bioinformatics* **31**, 166–169.
- Armour, S.M., Bennett, E.J., Braun, C.R., Zhang, X.-Y., McMahon, S.B., Gygi, S.P., Harper, J.W., and Sinclair, D.A. (2013). A high-confidence interaction map identifies SIRT1 as a mediator of acetylation of USP22 and the SAGA coactivator complex. *Mol. Cell. Biol.* **33**, 1487–1502.
- Astapova, I. (2016). Role of co-regulators in metabolic and transcriptional actions of thyroid hormone. *J. Mol. Endocrinol.* **56**, R73–R97.
- Bantscheff, M., Hopf, C., Savitski, M.M., Dittmann, A., Grandi, P., Michon, A.-M., Schlegl, J., Abraham, Y., Becher, I., Bergamini, G., et al. (2011). Chemoproteomics profiling of HDAC inhibitors reveals selective targeting of HDAC complexes. *Nat. Biotechnol.* **29**, 255–265.
- Bararia, D., Kwok, H.S., Welner, R.S., Numata, A., Sárosi, M.B., Yang, H., Wee, S., Tschuri, S., Ray, D., Weigert, O., et al. (2016). Acetylation of C/EBP α inhibits its granulopoietic function. *Nat. Commun.* **7**, 10968.
- Barrangou, R., Fremaux, C., Deveau, H., Richards, M., Boyaval, P., Moineau, S., Romero, D. a, and Horvath, P. (2007). CRISPR Provides Acquired Resistance Against Viruses in Prokaryotes. *Science* (80-.). **315**, 1709–1712.
- Bauer, R.C., Sasaki, M., Cohen, D.M., Cui, J., Smith, M.A., Yenilmez, B.O., Steger, D.J., and Rader, D.J. (2015). Tribbles-1 regulates hepatic lipogenesis through posttranscriptional regulation of C/EBP α . *J. Clin. Invest.* **125**, 3809–3818.
- Berger, J.H., Charron, M.J., and Silver, D.L. (2012). Major Facilitator Superfamily Domain-Containing Protein 2a (MFSD2A) Has Roles in Body Growth, Motor Function, and Lipid Metabolism. *PLoS One* **7**, e50629.
- Bramswig, N.C., and Kaestner, K.H. (2014). Transcriptional and epigenetic regulation in human islets. *Diabetologia* **57**, 451–454.
- Bricambert, J., Miranda, J., Benhamed, F., Girard, J., Postic, C., and Dentin, R. (2010). Salt-inducible kinase 2 links transcriptional coactivator p300 phosphorylation to the prevention of ChREBP-dependent hepatic steatosis in mice. *J. Clin. Invest.* **120**, 4316–4331.

- Browning, J.D., and Horton, J.D. (2004). Molecular mediators of hepatic steatosis and liver injury. *J. Clin. Invest.* *114*, 147–152.
- Burke, Z., and Oliver, G. (2002). Prox1 is an early specific marker for the developing liver and pancreas in the mammalian foregut endoderm. *Mech. Dev.* *118*, 147–155.
- Calkin, A.C., and Tontonoz, P. (2012). Transcriptional integration of metabolism by the nuclear sterol-activated receptors LXR and FXR. *Nat. Rev. Mol. Cell Biol.* *13*, 213–224.
- Charest-Marcotte, A., Dufour, C.R., Wilson, B.J., Tremblay, A.M., Eichner, L.J., Arlow, D.H., Mootha, V.K., and Giguère, V. (2010). The homeobox protein Prox1 is a negative modulator of ERR α /PGC-1 α bioenergetic functions. *Genes Dev.* *24*, 537–542.
- Chavez, J.D., Liu, N.L., and Bruce, J.E. (2011). Quantification of protein-protein interactions with chemical cross-linking and mass spectrometry. *J. Proteome Res.* *10*, 1528–1537.
- Chavez, J.D., Eng, J.K., Schweppe, D.K., Cilia, M., Rivera, K., Zhong, X., Wu, X., Allen, T., Khurgel, M., Kumar, A., et al. (2016). A general method for targeted quantitative cross-linking mass spectrometry. *PLoS One* *11*, 1–14.
- Chaya, D., and Zaret, K.S. (2003). Sequential Chromatin Immunoprecipitation from Animal Tissues. *Methods Enzymol.* *376*, 361–372.
- Chen, J.D., and Evans, R.M. (1995). A transcriptional co-repressor that interacts with nuclear hormone receptors. *Nature* *377*, 454–457.
- Chen, W., Gao, L., Wang, J., Wang, Y., and Dong, Z. (2016). Conditional ablation of HDAC3 in islet beta cells results in glucose intolerance and enhanced susceptibility to STZ-induced diabetes. *Oncotarget* *7*, 57485–57497.
- Chin, C.-H., Chen, S.-H., Wu, H.-H., Ho, C.-W., Ko, M.-T., and Lin, C.-Y. (2014). cytoHubba: identifying hub objects and sub-networks from complex interactome. *BMC Syst. Biol.* *8*, S11.
- Chou, D.H.C., Holson, E.B., Wagner, F.F., Tang, A.J., Maglathlin, R.L., Lewis, T.A., Schreiber, S.L., and Wagner, B.K. (2012). Inhibition of histone deacetylase 3 protects beta cells from cytokine-induced apoptosis. *Chem. Biol.* *19*, 669–673.
- Cohen, J.C., Horton, J.D., and Hobbs, H.H. (2011). Human fatty liver disease: old questions and new insights. *Science* *332*, 1519–1523.
- Core, L.J., Waterfall, J.J., and Lis, J.T. (2008). Nascent RNA Sequencing Reveals Widespread Pausing and Divergent Initiation at Human Promoters. *Science* (80-.). *322*, 1845–1848.
- Darimont, B.D., Wagner, R.L., Apriletti, J.W., Stallcup, M.R., Kushner, P.J., Baxter, J.D., Fletterick, R.J., and Yamamoto, K.R. (1998). Structure and specificity of nuclear receptor – coactivator interactions. *Genes Dev.* *12*, 3343–3356.
- Doliba, N.M., Liu, Q., Li, C., Chen, J., Chen, P., Liu, C., Frederick, D.W., Baur, J.A., Bennett, M.J., Najj, A., et al. (2015). Accumulation of 3-hydroxytetradecenoic acid: Cause or corollary of glucolipotoxic impairment of pancreatic β -cell bioenergetics? *Mol. Metab.* *4*, 926–939.
- Donath, M.Y., and Shoelson, S.E. (2011). Type 2 diabetes as an inflammatory disease. *Nat. Rev. Immunol.* *11*, 98–107.

- Dowling, D.P., Gantt, S.L., Gattis, S.G., Fierke, C.A., Christianson, D.W., Dowling, D.P., Gantt, S.L., Gattis, S.G., Fierke, C.A., and Christianson, D.W. (2008). Structural Studies of Human Histone Deacetylase 8 and Its Site-Specific Variants Complexed with Substrate and Inhibitors. *Biochemistry* *47*, 13554–13563.
- Düfer, M., Hörth, K., Wagner, R., Schittenhelm, B., Prowald, S., Wagner, T.F.J., Oberwinkler, J., Lukowski, R., Gonzalez, F.J., Krippeit-dreus, P., et al. (2012). Bile Acids Acutely Stimulate Insulin Secretion of Mouse β -Cells via Farnesoid X Receptor Activation and ATP-Sensitive Potassium Channel Inhibition. *Diabetes* *61*, 1–11.
- Dufour, C.R., Levasseur, M.-P., Pham, N.H.H., Eichner, L.J., Wilson, B.J., Charest-Marcotte, A., Duguay, D., Poirier-Héon, J.-F., Cermakian, N., and Giguère, V. (2011). Genomic convergence among ERR α , PROX1, and BMAL1 in the control of metabolic clock outputs. *PLoS Genet.* *7*, e1002143.
- Dupuis, J., Langenberg, C., Prokopenko, I., Saxena, R., Soranzo, N., Jackson, A.U., Wheeler, E., Glazer, N.L., Bouatia-Naji, N., Gloyn, A.L., et al. (2010). New genetic loci implicated in fasting glucose homeostasis and their impact on type 2 diabetes risk. *Nat. Genet.* *42*, 105–116.
- Dyer, M.A., Livesey, F.J., Cepko, C.L., and Oliver, G. (2003). Prox1 function controls progenitor cell proliferation and horizontal cell genesis in the mammalian retina. *Nat. Genet.* *34*, 53–58.
- Edgar, R., Domrachev, M., and Lash, A.E. (2002). Gene Expression Omnibus: NCBI gene expression and hybridization array data repository. *Nucleic Acids Res.* *30*, 207–210.
- Ediger, B.N., Du, A., Liu, J., Hunter, C.S., Walp, E.R., Schug, J., Kaestner, K.H., Stein, R., Stoffers, D.A., and May, C.L. (2014). Islet-1 is essential for pancreatic β -cell function. *Diabetes* *63*, 4206–4217.
- Euskirchen, G.M., Auerbach, R.K., Davidov, E., Gianoulis, T.A., Zhong, G., Rozowsky, J., Bhardwaj, N., Gerstein, M.B., and Snyder, M. (2011). Diverse roles and interactions of the SWI/SNF chromatin remodeling complex revealed using global approaches. *PLoS Genet.* *7*, e1002008.
- Fabregat, A., Sidiropoulos, K., Garapati, P., Gillespie, M., Hausmann, K., Haw, R., Jassal, B., Jupe, S., Korninger, F., McKay, S., et al. (2016). The Reactome pathway Knowledgebase. *Nucleic Acids Res.* *44*, D481-7.
- Fang, B., Everett, L.J., Jager, J., Briggs, E., Armour, S.M., Feng, D., Roy, A., Gerhart-Hines, Z., Sun, Z., and Lazar, M.A. (2014). Circadian enhancers coordinate multiple phases of rhythmic gene transcription in vivo. *Cell* *159*, 1140–1152.
- Feng, W. (1998). Hormone-Dependent Coactivator Binding to a Hydrophobic Cleft on Nuclear Receptors. *Science* (80-). *280*, 1747–1749.
- Feng, D., Liu, T., Sun, Z., Bugge, A., Mullican, S.E., Alenghat, T., Liu, X.S., and Lazar, M. a (2011). A circadian rhythm orchestrated by histone deacetylase 3 controls hepatic lipid metabolism. *Science* *331*, 1315–1319.
- Finnin, M.S., Donigian, J.R., Cohen, a, Richon, V.M., Rifkind, R. a, Marks, P. a, Breslow, R., and Pavletich, N.P. (1999). Structures of a histone deacetylase homologue bound to the TSA and SAHA inhibitors. *Nature* *401*, 188–193.

- Gardini, A., Baillat, D., Cesaroni, M., Hu, D., Marinis, J.M., Wagner, E.J., Lazar, M.A., Shilatifard, A., and Shiekhattar, R. (2014). Integrator regulates transcriptional initiation and pause release following activation. *Mol. Cell* **56**, 128–139.
- Gronemeyer, H., Gustafsson, J.-A., and Laudet, V. (2004). Principles for modulation of the nuclear receptor superfamily. *Nat. Rev. Drug Discov.* **3**, 950–964.
- Grøntved, L., Waterfall, J.J., Kim, D.W., Baek, S., Sung, M.-H., Zhao, L., Park, J.W., Nielsen, R., Walker, R.L., Zhu, Y.J., et al. (2015). Transcriptional activation by the thyroid hormone receptor through ligand-dependent receptor recruitment and chromatin remodelling. *Nat. Commun.* **6**, 7048.
- Gross, B., Pawlak, M., Lefebvre, P., and Staels, B. (2016). PPARs in obesity-induced T2DM, dyslipidaemia and NAFLD. *Nat. Rev. Endocrinol.*
- Guenther, M.G., Lane, W.S., Fischle, W., Verdin, E., Lazar, M.A., and Shiekhattar, R. (2000). A core SMRT corepressor complex containing HDAC3 and TBL1, a WD40-repeat protein linked to deafness. *Genes Dev.* **14**, 1048–1057.
- Guenther, M.G., Barak, O.R.R., and Lazar, M.A. (2001). The SMRT and N-CoR Corepressors Are Activating Cofactors for Histone Deacetylase 3. *Mol. Cell. Biol.* **21**, 6091–6101.
- Guenther, M.G., Yu, J., Kao, G.D., Yen, T.J., and Lazar, M.A. (2002). Assembly of the SMRT – histone deacetylase 3 repression complex requires the TCP-1 ring complex. *Genes Dev.* **16**, 3130–3135.
- Haberland, M., Montgomery, R.L., and Olson, E.N. (2009). The many roles of histone deacetylases in development and physiology: implications for disease and therapy. *Nat. Rev. Genet.* **10**, 32–42.
- Harvey, N.L., Srinivasan, R.S., Dillard, M.E., Johnson, N.C., Witte, M.H., Boyd, K., Sleeman, M.W., and Oliver, G. (2005). Lymphatic vascular defects promoted by Prox1 haploinsufficiency cause adult-onset obesity. *Nat. Genet.* **37**, 1072–1081.
- Hayhurst, G.P., Lee, Y.H., Lambert, G., Ward, J.M., and Gonzalez, F.J. (2001). Hepatocyte nuclear factor 4alpha (nuclear receptor 2A1) is essential for maintenance of hepatic gene expression and lipid homeostasis. *Mol. Cell. Biol.* **21**, 1393–1403.
- Heery, D., Kalkhoven, E., Hoare, S., and Parker, M.G. (1997). A signature motif in transcriptional co-activators mediates binding to nuclear receptors. *Nature* **387**, 733–736.
- Heinz, S., Benner, C., Spann, N., Bertolino, E., Lin, Y.C., Laslo, P., Cheng, J.X., Murre, C., Singh, H., and Glass, C.K. (2010). Simple Combinations of Lineage-Determining Transcription Factors Prime cis-Regulatory Elements Required for Macrophage and B Cell Identities. *Mol. Cell* **38**, 576–589.
- Hong, S., Zhou, W., Fang, B., Lu, W., Loro, E., Damle, M., Ding, G., Jager, J., Zhang, S., Zhang, Y., et al. (2016). Dissociation of muscle insulin sensitivity from exercise endurance in mice by HDAC3 depletion. *Nat. Med.* **23**, 223–234.
- Hörlein, A.J., Näär, A.M., Heinzl, T., Torchia, J., Gloss, B., Kurokawa, R., Ryan, A., Kamei, Y., Söderström, M., Glass, C.K., et al. (1995). Ligand-independent repression by the thyroid hormone receptor mediated by a nuclear receptor co-repressor. *Nature* **377**, 397–404.

- Hu, X., and Lazar, M. a (1999). The CoRNR motif controls the recruitment of corepressors by nuclear hormone receptors. *Nature* 402, 93–96.
- Hu, X., Li, Y., and Lazar, M.A. (2001). Determinants of CoRNR-dependent repression complex assembly on nuclear hormone receptors. *Mol. Cell. Biol.* 21, 1747–1758.
- Huang, P., Chandra, V., and Rastinejad, F. (2010). Structural overview of the nuclear receptor superfamily: insights into physiology and therapeutics. *Annu. Rev. Physiol.* 72, 247–272.
- Inoue, A., and Fujimoto, D. (1969). Enzymatic deacetylation of histone. *Biochem. Biophys. Res. Commun.* 36, 146–150.
- Ishizuka, T., and Lazar, M.A. (2003). The N-CoR/histone deacetylase 3 complex is required for repression by thyroid hormone receptor. *Mol. Cell. Biol.* 23, 5122–5131.
- Ishizuka, T., and Lazar, M. a (2005). The nuclear receptor corepressor deacetylase activating domain is essential for repression by thyroid hormone receptor. *Mol. Endocrinol.* 19, 1443–1451.
- Jiang, F., and Doudna, J.A. (2017). CRISPR – Cas9 Structures and Mechanisms. *Annu. Rev. Biophys.* 46, 505–529.
- Jinek, M., Jiang, F., Taylor, D.W., Sternberg, S.H., Kaya, E., Ma, E., Anders, C., Hauer, M., Zhou, K., Lin, S., et al. (2014). Structures of Cas9 Endonucleases Reveal RNA-Mediated Conformational Activation. *Science* (80-.). 343, 1247997–1247997.
- Joshi, P., Greco, T.M., Guise, A.J., Luo, Y., Yu, F., Nesvizhskii, A.I., and Cristea, I.M. (2013). The functional interactome landscape of the human histone deacetylase family. *Mol. Syst. Biol.* 9, 1–21.
- Kanyo, Z.F., Scolnick, L.R., Ash, D.E., and Christianson, D.W. (1996). Structure of a unique binuclear manganese cluster in arginase. *Nature* 383, 554–557.
- Kim, H., Toyofuku, Y., Lynn, F.C., Chak, E., Uchida, T., Mizukami, H., Fujitani, Y., Kawamori, R., Miyatsuka, T., Kosaka, Y., et al. (2010). Serotonin regulates pancreatic beta cell mass during pregnancy. *Nat. Med.* 16, 804–808.
- Kivelä, R., Salmela, I., Nguyen, Y.H., Petrova, T. V., Koistinen, H.A., Wiener, Z., Alitalo, K., Cheung, T.H., Rando, T.A., Yin, H., et al. (2016). The transcription factor Prox1 is essential for satellite cell differentiation and muscle fibre-type regulation. *Nat. Commun.* 7, 13124.
- Knott, S.R. V, Maceli, A.R., Erard, N., Chang, K., Marran, K., Zhou, X., Gordon, A., El Demerdash, O., Wagenblast, E., Kim, S., et al. (2014). A computational algorithm to predict shRNA potency. *Mol. Cell* 56, 796–807.
- Knutson, S.K., Chyla, B.J., Amann, J.M., Bhaskara, S., Huppert, S.S., and Hiebert, S.W. (2008). Liver-specific deletion of histone deacetylase 3 disrupts metabolic transcriptional networks. *EMBO J.* 27, 1017–1028.
- Kulemzina, I., Ang, K., Zhao, X., Teh, J.-T., Verma, V., Suranthran, S., Chavda, A.P., Huber, R.G., Eisenhaber, B., Eisenhaber, F., et al. (2016). A Reversible Association between Smc Coiled Coils Is Regulated by Lysine Acetylation and Is Required for Cohesin Association with the DNA. *Mol. Cell* 63, 1044–1054.
- Kulozik, P., Jones, A., Mattijssen, F., Rose, A.J., Reimann, A., Strzoda, D., Kleinsorg, S., Raupp, C., Kleinschmidt, J., Müller-Decker, K., et al. (2011). Hepatic deficiency in transcriptional cofactor TBL1 promotes liver steatosis and hypertriglyceridemia. *Cell Metab.* 13, 389–400.

- Lai, F., Gardini, A., Zhang, A., and Shiekhhattar, R. (2015). Integrator mediates the biogenesis of enhancer RNAs. *Nature* 525, 399–403.
- Langmead, B., Trapnell, C., Pop, M., and Salzberg, S. (2009a). 2C- Ultrafast and memory-efficient alignment of short DNA sequences to the human genome. *Genome Biol.* 10, R25.1-10.
- Langmead, B., Trapnell, C., Pop, M., and Salzberg, S.L. (2009b). Ultrafast and memory-efficient alignment of short DNA sequences to the human genome. *Genome Biol.* 10, R25.
- Lazar, M.A. (2003). Nuclear receptor corepressors. *Nucl. Recept. Signal.* 1, e001.
- Lazar, M.A., Hodin, R.A., Darling, D.S., and Chin, W.W. (1989). A novel member of the thyroid/steroid hormone receptor family is encoded by the opposite strand of the rat c-erbA alpha transcriptional unit. *Mol. Cell. Biol.* 9, 1128–1136.
- Lecompte, S., Pasquetti, G., Hermant, X., Grenier-Boley, B., Gonzalez-Gross, M., De Henauw, S., Molnar, D., Stehle, P., Béghin, L., Moreno, L.A., et al. (2013). Genetic and molecular insights into the role of PROX1 in glucose metabolism. *Diabetes* 62, 1738–1745.
- Lee, J., Liu, R., de Jesus, D., Kim, B.S., Ma, K., Moulik, M., and Yechoor, V. (2015). Circadian control of β -cell function and stress responses. *Diabetes. Obes. Metab.* 17, 123–133.
- Lengler, J., Krausz, E., Tomarev, S., Prescott, A., Quinlan, R.A., and Graw, J. (2001). Antagonistic action of Six3 and Prox1 at the gamma-crystallin promoter. *Nucleic Acids Res.* 29, 515–526.
- Li, J., Wang, J., Nawaz, Z., Liu, J.M., Qin, J., and Wong, J. (2000). Both corepressor proteins SMRT and N-CoR exist in large protein complexes containing HDAC3. *EMBO J.* 19, 4342–4350.
- Li, J.Y., Daniels, G., Wang, J., and Zhang, X. (2015). TBL1XR1 in physiological and pathological states. *Am J Clin Exp Urol* 3, 13–23.
- Lim, H.W., Uhlenhaut, N.H., Rauch, A., Weiner, J., Hübner, S., Hübner, N., Won, K.J., Lazar, M.A., Tuckermann, J., and Steger, D.J. (2015). Genomic redistribution of GR monomers and dimers mediates transcriptional response to exogenous glucocorticoid in vivo. *Genome Res.* 25, 836–844.
- Lombardi, P.M., Cole, K.E., Dowling, D.P., and Christianson, D.W. (2011). Structure, mechanism, and inhibition of histone deacetylases and related metalloenzymes. *Curr. Opin. Struct. Biol.* 21, 735–743.
- Love, M.I., Huber, W., and Anders, S. (2014). Moderated estimation of fold change and dispersion for RNA-seq data with DESeq2. *Genome Biol.* 15, 550.
- Lu, Q., Hutchins, A.E., Doyle, C.M., Lundblad, J.R., and Kwok, R.P.S. (2003). Acetylation of cAMP-responsive element-binding protein (CREB) by CREB-binding protein enhances CREB-dependent transcription. *J. Biol. Chem.* 278, 15727–15734.
- Luger, K., Dechassa, M.L., and Tremethick, D.J. (2012). New insights into nucleosome and chromatin structure: an ordered state or a disordered affair? *Nat. Rev. Mol. Cell Biol.* 13, 436–447.

- Lundh, M., Christensen, D.P., Damgaard Nielsen, M., Richardson, S.J., Dahllöf, M.S., Skovgaard, T., Berthelsen, J., Dinarello, C.A., Stevenazzi, A., Mascagni, P., et al. (2012). Histone deacetylases 1 and 3 but not 2 mediate cytokine-induced beta cell apoptosis in INS-1 cells and dispersed primary islets from rats and are differentially regulated in the islets of type 1 diabetic children. *Diabetologia* 55, 2421–2431.
- Lundh, M., Galbo, T., Poulsen, S.S., and Mandrup-Poulsen, T. (2015). Histone deacetylase 3 inhibition improves glycaemia and insulin. *Diabetes, Obes. Metab.* 17, 703–707.
- Magnuson, M.A., and Osipovich, A.B. (2013). Pancreas-specific Cre driver lines and considerations for their prudent use. *Cell Metab.* 18, 9–20.
- Matschinsky, F.M. (2005). Glucokinase, glucose homeostasis, and diabetes mellitus. *Curr. Diab. Rep.* 5, 171–176.
- Matsumura, H., Kusaka, N., Nakamura, T., Tanaka, N., Sagegami, K., Uegaki, K., Inoue, T., and Mukai, Y. (2012). Crystal structure of the N-terminal domain of the yeast general corepressor Tup1p and its functional implications. *J. Biol. Chem.* 287, 26528–26538.
- Matsusue, K., Kusakabe, T., Noguchi, T., Takiguchi, S., Suzuki, T., Yamano, S., and Gonzalez, F.J. (2008). Hepatic Steatosis in Leptin-Deficient Mice Is Promoted by the PPAR γ Target Gene Fsp27. *Cell Metab.* 7, 302–311.
- Matsuzaka, T., Atsumi, A., Matsumori, R., Nie, T., Shinozaki, H., Suzuki-Kemuriyama, N., Kuba, M., Nakagawa, Y., Ishii, K., Shimada, M., et al. (2012). Elovl6 promotes nonalcoholic steatohepatitis. *Hepatology* 56, 2199–2208.
- McGee-Lawrence, M.E., Bradley, E.W., Dudakovic, A., Carlson, S.W., Ryan, Z.C., Kumar, R., Dadsetan, M., Yaszemski, M.J., Chen, Q., An, K.-N., et al. (2013). Histone deacetylase 3 is required for maintenance of bone mass during aging. *Bone* 52, 296–307.
- McInerney, E.M., Rose, D.W., Flynn, S.E., Westin, S., Mullen, T.M., Krones, A., Inostroza, J., Torchia, J., Nolte, R.T., Assa-Munt, N., et al. (1998). Determinants of coactivator LXXLL motif specificity in nuclear receptor transcriptional activation. *Genes Dev.* 12, 3357–3368.
- McLean, C.Y., Bristor, D., Hiller, M., Clarke, S.L., Schaar, B.T., Lowe, C.B., Wenger, A.M., and Bejerano, G. (2010). GREAT improves functional interpretation of cis-regulatory regions. *Nat. Biotechnol.* 28, 495–501.
- McQuown, S.C., Barrett, R.M., Matheos, D.P., Post, R.J., Rogge, G.A., Alenghat, T., Mullican, S.E., Jones, S., Rusche, J.R., Lazar, M.A., et al. (2011). HDAC3 Is a Critical Negative Regulator of Long-Term Memory Formation. *J. Neurosci.* 31, 764–774.
- Millard, C.J., Watson, P.J., Celardo, I., Gordiyenko, Y., Cowley, S.M., Robinson, C. V., Fairall, L., and Schwabe, J.W.R. (2013a). Class I HDACs share a common mechanism of regulation by inositol phosphates. *Mol. Cell* 51, 57–67.
- Millard, C.J., Watson, P.J., Fairall, L., and Schwabe, J.W.R. (2013b). An evolving understanding of nuclear receptor coregulator proteins. *J. Mol. Endocrinol.* 51, 23–36.
- Mo, A., Mukamel, E.A., Davis, F.P., Luo, C., Henry, G.L., Picard, S., Urich, M.A., Nery, J.R., Sejnowski, T.J., Lister, R., et al. (2015). Epigenomic Signatures of Neuronal Diversity in the Mammalian Brain. *Neuron* 86, 1369–1384.

- Mohammed, H., D'Santos, C., Serandour, A. a, Ali, H.R., Brown, G.D., Atkins, A., Rueda, O.M., Holmes, K. a, Theodorou, V., Robinson, J.L.L., et al. (2013). Endogenous purification reveals GREB1 as a key estrogen receptor regulatory factor. *Cell Rep.* 3, 342–349.
- Mosley, A.L., and Özcan, S. (2003). Glucose regulates insulin gene transcription by hyperacetylation of histone H4. *J. Biol. Chem.* 278, 19660–19666.
- Mullican, S.E., Gaddis, C.A., Alenghat, T., Nair, M.G., Giacomini, P.R., Everett, L.J., Feng, D., Steger, D.J., Schug, J., Artis, D., et al. (2011). Histone deacetylase 3 is an epigenomic brake in macrophage alternative activation. *Genes Dev.* 25, 2480–2488.
- Nagy, L., Kao, H.Y., Love, J.D., Li, C., Banayo, E., Gooch, J.T., Krishna, V., Chatterjee, K., Evans, R.M., and Schwabe, J.W.R. (1999). Mechanism of corepressor binding and release from nuclear hormone receptors. *Genes Dev.* 13, 3209–3216.
- Nishimasu, H., Ran, F.A., Hsu, P.D., Konermann, S., Shehata, S.I., Dohmae, N., Ishitani, R., Zhang, F., and Nureki, O. (2014). Crystal structure of Cas9 in complex with guide RNA and target DNA. *Cell* 156, 935–949.
- Nolte, R.T., Wisely, G.B., Westin, S., Cobb, J.E., Lambert, M.H., Kurokawa, R., Rosenfeld, M.G., Willson, T.M., Glass, C.K., and Milburn, M. V (1998). Ligand binding and co-activator assembly of the peroxisome proliferator-activated receptor-gamma. *Nature* 395, 137–143.
- Nott, A., Cheng, J., Gao, F., Lin, Y.-T., Gjoneska, E., Ko, T., Minhas, P., Zamudio, A.V., Meng, J., Zhang, F., et al. (2016). Histone deacetylase 3 associates with MeCP2 to regulate FOXO and social behavior. *Nat. Neurosci.*
- Oberoi, J., Fairall, L., Watson, P.J., Yang, J.-C., Czimmerer, Z., Kampmann, T., Goult, B.T., Greenwood, J. a, Gooch, J.T., Kallenberger, B.C., et al. (2011). Structural basis for the assembly of the SMRT/NCOR core transcriptional repression machinery. *Nat. Struct. Mol. Biol.* 18, 177–184.
- Odom, D.T., Zizlsperger, N., Gordon, D.B., Bell, G.W., Rinaldi, N.J., Murray, H.L., Volkert, T.L., Schreiber, J., Rolfe, P.A., Gifford, D.K., et al. (2004). Control of Pancreas and Liver Gene Expression by HNF Transcription Factors. *Science* (80-.). 303, 1378–1381.
- Okazaki, K., Niki, I., Iino, S., Kobayashi, S., and Hidaka, H. (1994). A Role of Calcyclin, a Ca²⁺-binding Protein, on the Ca²⁺-dependent Insulin Release from the Pancreatic β Cell. *J. Biol. Chem.* 269, 6149–6152.
- Oropeza, D., Jouvett, N., Budry, L., Campbell, J.E., Bouyakdan, K., Lacombe, J., Perron, G., Bergeron, V., C. Neuman, J., Brar, H.K., et al. (2015). Phenotypic characterization of MIP-CreERT1Lphi mice with transgene-driven islet expression of human growth hormone. *Diabetes* 64, 3798–3807.
- Papazyan, R., Sun, Z., Kim, Y.H., Titchenell, P.M., Hill, D.A., Lu, W., Damle, M., Wan, M., Zhang, Y., Briggs, E.R., et al. (2016a). Physiological Suppression of Lipotoxic Liver Damage by Complementary Actions of HDAC3 and SCAP/SREBP. *Cell Metab.* 24, 863–874.
- Papazyan, R., Zhang, Y., and Lazar, M.A. (2016b). Genetic and epigenomic mechanisms of mammalian circadian transcription. *Nat. Struct. Mol. Biol.* 23, 1045–1052.
- Parviz, F., Li, J., Kaestner, K.H., and Duncan, S.A. (2002). Generation of a conditionally null allele of hnf4alpha. *Genesis* 32, 130–133.

- Patterson, C.C., Dahlquist, G.G., Gyürüs, E., Green, A., and Soltész, G. (2009). Incidence trends for childhood type 1 diabetes in Europe during 1989-2003 and predicted new cases 2005-20: a multicentre prospective registration study. *Lancet* *373*, 2027–2033.
- Perelis, M., Marcheva, B., Ramsey, K.M., Schipma, M.J., Hutchison, A.L., Taguchi, A., Peek, C.B., Hong, H., Huang, W., Omura, C., et al. (2015). Pancreatic β cell enhancers regulate rhythmic transcription of genes controlling insulin secretion. *Science* *350*, aac4250-1-9.
- Perissi, V., Staszewski, L.M., Mcinerney, E.M., Kurokawa, R., Krones, A., Rose, D.W., Lambert, M.H., Milburn, M. V, Glass, C.K., and Rosenfeld, M.G. (1999). Molecular determinants of nuclear receptor – corepressor interaction Molecular determinants of nuclear receptor – corepressor interaction. *Genes Dev.* *13*, 3198–3208.
- Perissi, V., Aggarwal, A., Glass, C.K., Rose, D.W., and Rosenfeld, M.G. (2004). A Corepressor/Coactivator Exchange Complex Required for Transcriptional Activation by Nuclear Receptors and Other Regulated Transcription Factors. *Cell* *116*, 511–526.
- Perissi, V., Scafoglio, C., Zhang, J., Ohgi, K.A., Rose, D.W., Glass, C.K., and Rosenfeld, M.G. (2008). TBL1 and TBLR1 Phosphorylation on Regulated Gene Promoters Overcomes Dual CtBP and NCoR/SMRT Transcriptional Repression Checkpoints. *Mol. Cell* *29*, 755–766.
- Perissi, V., Jepsen, K., Glass, C.K., and Rosenfeld, M.G. (2010). Deconstructing repression: evolving models of co-repressor action. *Nat. Rev. Genet.* *11*, 109–123.
- Phillips, D.M.P. (1963). The presence of acetyl groups in histones. *Biochem. J.* *87*, 258–263.
- Plaisance, V., Rolland, L., Gmyr, V., Annicotte, J.-S., Kerr-Conte, J., Pattou, F., and Abderrahmani, A. (2014). The class I histone deacetylase inhibitor MS-275 prevents pancreatic beta cell death induced by palmitate. *J. Diabetes Res.* *2014*, 195739.
- Qin, J., Gao, D.-M., Jiang, Q.-F., Zhou, Q., Kong, Y.-Y., Wang, Y., and Xie, Y.-H. (2004). Prospero-related homeobox (Prox1) is a corepressor of human liver receptor homolog-1 and suppresses the transcription of the cholesterol 7-alpha-hydroxylase gene. *Mol. Endocrinol.* *18*, 2424–2439.
- Quinlan, A.R., and Hall, I.M. (2010a). BEDTools: A flexible suite of utilities for comparing genomic features. *Bioinformatics* *26*, 841–842.
- Quinlan, A.R., and Hall, I.M. (2010b). BEDTools: a flexible suite of utilities for comparing genomic features. *Bioinformatics* *26*, 841–842.
- Ramadoss, P., Abraham, B.J., Tsai, L., Zhou, Y., Costa-e-Sousa, R.H., Ye, F., Bilban, M., Zhao, K., and Hollenberg, A.N. (2014). Novel mechanism of positive versus negative regulation by thyroid hormone receptor β 1 (TR β 1) identified by genome-wide profiling of binding sites in mouse liver. *J. Biol. Chem.* *289*, 1313–1328.
- Rappsilber, J., Ishihama, Y., and Mann, M. (2003). Stop and go extraction tips for matrix-assisted laser desorption/ionization, nanoelectrospray, and LC/MS sample pretreatment in proteomics. *Anal. Chem.* *75*, 663–670.
- Remsberg, J.R., Ediger, B.N., Ho, W.Y., Damle, M., Li, Z., Teng, C., Lanzillotta, C., Stoffers, D.A., and Lazar, M.A. (2017). Deletion of histone deacetylase 3 in adult beta cells improves glucose tolerance via increased insulin secretion. *Mol. Metab.* *6*, 30–37.

Risebro, C.A., Searles, R.G., Melville, A.A.D., Ehler, E., Jina, N., Shah, S., Pallas, J., Hubank, M., Dillard, M., Harvey, N.L., et al. (2009). Prox1 maintains muscle structure and growth in the developing heart. *Development* 136, 495–505.

Rogge, G.A., Singh, H., Dang, R., and Wood, M.A. (2013). HDAC3 Is a Negative Regulator of Cocaine-Context-Associated Memory Formation. *J. Neurosci.* 33, 6623–6632.

Roy, S., Wolff, C., and Ingham, P.W. (2001). The u-boot mutation identifies a Hedgehog-regulated myogenic switch for fiber-type diversification in the zebrafish embryo. *Genes Dev.* 15, 1563–1576.

Sander, J.D., and Joung, J.K. (2014). CRISPR-Cas systems for editing, regulating and targeting genomes. *Nat. Biotechnol.* 32, 347–355.

Schwanhäusser, B., Busse, D., Li, N., Dittmar, G., Schuchhardt, J., Wolf, J., Chen, W., and Selbach, M. (2011). Global quantification of mammalian gene expression control. *Nature* 473, 337–342.

Schweppe, D.K., Chavez, J.D., Lee, C.F., Caudal, A., Kruse, S.E., Stuppard, R., Marcinek, D.J., Shadel, G.S., Tian, R., and Bruce, J.E. (2017). Mitochondrial protein interactome elucidated by chemical cross-linking mass spectrometry. *Proc. Natl. Acad. Sci.* 114, 1732–1737.

Seth, A., Ye, J., Yu, N., Guez, F., Bedford, D.C., Neale, G.A., Cordi, S., Brindle, P.K., Lemaigre, F.P., Kaestner, K.H., et al. (2014). Prox1 ablation in hepatic progenitors causes defective hepatocyte specification and increases biliary cell commitment. *Development* 141, 538–547.

Shi, J., Whyte, W.A., Zepeda-Mendoza, C.J., Milazzo, J.P., Shen, C., Roe, J.-S., Minder, J.L., Mercan, F., Wang, E., Eckersley-Maslin, M.A., et al. (2013). Role of SWI/SNF in acute leukemia maintenance and enhancer-mediated Myc regulation. *Genes Dev.* 27, 2648–2662.

Shimizu, H., Astapova, I., Ye, F., Bilban, M., Cohen, R.N., and Hollenberg, A.N. (2015). NCoR1 and SMRT play unique roles in thyroid hormone action in vivo. *Mol. Cell. Biol.* 35.

Singh, N., Trivedi, C.M., Lu, M., Mullican, S.E., Lazar, M.A., and Epstein, J.A. (2011). Histone deacetylase 3 regulates smooth muscle differentiation in neural crest cells and development of the cardiac outflow tract. *Circ. Res.* 109, 1240–1249.

Sladek, F.M., Zhong, W.M., Lai, E., and Darnell, J.E. (1990). Liver-enriched transcription factor HNF-4 is a novel member of the steroid hormone receptor superfamily. *Genes Dev.* 4, 2353–2365.

Soccio, R.E., Chen, E.R., Rajapurkar, S.R., Civelek, M., Voight, B.F., Lazar, M.A., Soccio, R.E., Chen, E.R., Rajapurkar, S.R., Safabakhsh, P., et al. (2015). Genetic Variation Determines PPAR α Function and Anti-diabetic Drug Response In Vivo. *Cell* 162, 33–44.

Song, K.-H., Li, T., and Chiang, J.Y.L. (2006). A Prospero-related homeodomain protein is a novel co-regulator of hepatocyte nuclear factor 4 α that regulates the cholesterol 7 α -hydroxylase gene. *J. Biol. Chem.* 281, 10081–10088.

Sosa-Pineda, B., Wigle, J.T., and Oliver, G. (2000). Hepatocyte migration during liver development requires Prox1. *Nat. Genet.* 25, 254–255.

Steffensen, K.R., Holter, E., Båvner, A., Nilsson, M., Pelto-Huikko, M., Tomarev, S., and Treuter, E. (2004). Functional conservation of interactions between a homeodomain cofactor and a mammalian FTZ-F1 homologue. *EMBO Rep.* 5, 613–619.

- Struhl, K. (1998). Histone acetylation and transcriptional regulatory mechanisms. *Genes Dev.* *12*, 599–606.
- Sun, Z., Miller, R. a, Patel, R.T., Chen, J., Dhir, R., Wang, H., Zhang, D., Graham, M.J., Unterman, T.G., Shulman, G.I., et al. (2012). Hepatic Hdac3 promotes gluconeogenesis by repressing lipid synthesis and sequestration. *Nat. Med.* *18*, 934–942.
- Sun, Z., Feng, D., Fang, B., Mullican, S.E., You, S.-H., Lim, H.-W., Everett, L.J., Nabel, C.S., Li, Y., Selvakumaran, V., et al. (2013). Deacetylase-Independent Function of HDAC3 in Transcription and Metabolism Requires Nuclear Receptor Corepressor. *Mol. Cell* *52*, 769–782.
- Szklarczyk, D., Franceschini, A., Wyder, S., Forslund, K., Heller, D., Huerta-Cepas, J., Simonovic, M., Roth, A., Santos, A., Tsafou, K.P., et al. (2015). STRING v10: Protein-protein interaction networks, integrated over the tree of life. *Nucleic Acids Res.* *43*, D447–D452.
- Takeda, Y., and Jetten, A.M. (2013). Prospero-related homeobox 1 (Prox1) functions as a novel modulator of retinoic acid-related orphan receptors α - and γ -mediated transactivation. *Nucleic Acids Res.* *41*, 6992–7008.
- Tamarina, N.A., Roe, M.W., and Philipson, L.H. (2014). Characterization of mice expressing Ins1 gene promoter driven CreERT recombinase for conditional gene deletion in pancreatic β -cells. *Islets* *6*.
- Taunton, J., Hassig, C.A., and Schreiber, S.L. (1996). A Mammalian Histone Deacetylase Related to the Yeast Transcriptional Regulator Rpd3p. *Science* (80-.). *272*, 408–411.
- Thorvaldsdottir, H., Robinson, J.T., and Mesirov, J.P. (2013). Integrative Genomics Viewer (IGV): high-performance genomics data visualization and exploration. *Brief. Bioinform.* *14*, 178–192.
- Tian, J., Keller, M.P., Oler, A.T., Rabaglia, M.E., Schueler, K.L., Stapleton, D.S., Broman, A.T., Zhao, W., Kendzioriski, C., Yandell, B.S., et al. (2015). Identification of the bile acid transporter Slco1a6 as a candidate gene that broadly affects gene expression in mouse pancreatic islets. *Genetics* *201*, 1253–1262.
- Tilg, H., Moschen, A.R., and Roden, M. (2016). NAFLD and diabetes mellitus. *Nat. Rev. Gastroenterol. Hepatol.* *14*, 32–42.
- Trapnell, C., Roberts, A., Goff, L., Pertea, G., Kim, D., Kelley, D.R., Pimentel, H., Salzberg, S.L., Rinn, J.L., and Pachter, L. (2012a). Differential gene and transcript expression analysis of RNA-seq experiments with TopHat and Cufflinks. *Nat. Protoc.* *7*, 562–578.
- Trapnell, C., Hendrickson, D.G., Sauvageau, M., Goff, L., Rinn, J.L., and Pachter, L. (2012b). Differential analysis of gene regulation at transcript resolution with RNA-seq. *Nat. Biotechnol.* *31*, 46–53.
- Vannini, A., Volpari, C., Gallinari, P., Jones, P., Mattu, M., Carfí, A., De Francesco, R., Steinkühler, C., and Di Marco, S. (2007). Substrate binding to histone deacetylases as shown by the crystal structure of the HDAC8-substrate complex. *EMBO Rep.* *8*, 879–884.
- Villasenor, A., Wang, Z. V, Rivera, L.B., Ocal, O., Asterholm, I.W., Scherer, P.E., Brekken, R. a, Cleaver, O., and Wilkie, T.M. (2010). Rgs16 and Rgs8 in embryonic endocrine pancreas and mouse models of diabetes. *Dis. Model. Mech.* *3*, 567–580.
- Vivot, K., Moullé, V.S., Zarrouki, B., Tremblay, C., and Mancini, A.D. (2016). The regulator of G-protein signaling RGS16 promotes insulin secretion and β -cell proliferation in rodent and human islets. *Mol. Metab.* 1–9.

- Wagner, F.F., Lundh, M., Kaya, T., McCarren, P., Zhang, Y.L., Chattopadhyay, S., Gale, J.P., Galbo, T., Fisher, S.L., Meier, B.C., et al. (2016). An Isochemogenic Set of Inhibitors to Define the Therapeutic Potential of Histone Deacetylases in β -Cell Protection. *ACS Chem. Biol.* *11*, 363–374.
- Wang, J., Kilic, G., Aydin, M., Burke, Z., Oliver, G., and Sosa-Pineda, B. (2005). Prox1 activity controls pancreas morphogenesis and participates in the production of “secondary transition” pancreatic endocrine cells. *Dev. Biol.* *286*, 182–194.
- Wang, L., Zuercher, W.J., Consler, T.G., Lambert, M.H., Miller, A.B., Orband-Miller, L.A., McKee, D.D., Willson, T.M., and Nolte, R.T. (2006). X-ray crystal structures of the estrogen-related receptor- α ligand binding domain in three functional states reveal the molecular basis of small molecule regulation. *J. Biol. Chem.* *281*, 37773–37781.
- Wang, X., Cimermancic, P., Yu, C., Schweitzer, A., Chopra, N., Engel, J.L., Greenberg, C.H., Huszagh, A.S., Beck, F., Sakata, E., et al. (2017). Molecular Details Underlying Dynamic Structures and Regulation of the Human 26S Proteasome. *Mol. Cell. Proteomics* mcp.M116.065326.
- Wang, Y., Zhang, Y., Qian, H., Lu, J., Zhang, Z., Min, X., Lang, M., Yang, H., Wang, N., and Zhang, P. (2013). The g0/g1 switch gene 2 is an important regulator of hepatic triglyceride metabolism. *PLoS One* *8*, e72315.
- Wang, Y., Viscarra, J., Kim, S.-J., and Sul, H.S. (2015). Transcriptional regulation of hepatic lipogenesis. *Nat. Rev. Mol. Cell Biol.* *16*, 678–689.
- Wang, Z., Zang, C., Cui, K., Schones, D.E., Barski, A., Peng, W., and Zhao, K. (2009). Genome-wide mapping of HATs and HDACs reveals distinct functions in active and inactive genes. *Cell* *138*, 1019–1031.
- Watson, P.J., Fairall, L., and Schwabe, J.W.R. (2012a). Nuclear hormone receptor co-repressors: structure and function. *Mol. Cell. Endocrinol.* *348*, 440–449.
- Watson, P.J., Fairall, L., Santos, G.M., and Schwabe, J.W.R. (2012b). Structure of HDAC3 bound to co-repressor and inositol tetrakisphosphate. *Nature* *481*, 335–340.
- Watson, P.J., Millard, C.J., Riley, A.M., Robertson, N.S., Wright, L.C., Godage, H.Y., Cowley, S.M., Jamieson, A.G., Potter, B.V.L., and Schwabe, J.W.R. (2016). Insights into the activation mechanism of class I HDAC complexes by inositol phosphates. *Nat. Commun.* *7*, 11262.
- Weir, G.C., and Bonner-Weir, S. (2004). Five of stages of evolving β -cell dysfunction during progression to diabetes. *Diabetes* *53*.
- Weisbrod, C.R., Chavez, J.D., Eng, J.K., Yang, L., Zheng, C., and Bruce, J.E. (2013). In Vivo Protein Interaction Network Identified with a Novel Real-Time Cross-Linked Peptide Identification Strategy. *J. Proteome Res.*
- Wen, Y.D., Perissi, V., Staszewski, L.M., Yang, W.M., Krones, A., Glass, C.K., Rosenfeld, M.G., and Seto, E. (2000). The histone deacetylase-3 complex contains nuclear receptor corepressors. *Proc. Natl. Acad. Sci. U. S. A.* *97*, 7202–7207.
- Whyte, W.A., Bilodeau, S., Orlando, D.A., Hoke, H.A., Frampton, G.M., Foster, C.T., Cowley, S.M., and Young, R.A. (2012). Enhancer decommissioning by LSD1 during embryonic stem cell differentiation. *Nature* *482*, 221.

- Wierer, M., and Mann, M. (2016). Proteomics to study DNA-bound and chromatin-associated gene regulatory complexes. *Hum. Mol. Genet.* 25, R106–R114.
- Wigle, J.T., and Oliver, G. (1999). Prox1 function is required for the development of the murine lymphatic system. *Cell* 98, 769–778.
- Wigle, J.T., Chowdhury, K., Gruss, P., and Oliver, G. (1999). Prox1 function is crucial for mouse lens-fibre elongation. *Nat. Genet.* 21, 318–322.
- Wiśniewski, J.R. (2017). Label-Free and Standard-Free Absolute Quantitative Proteomics Using the “Total Protein” and “Proteomic Ruler” Approaches. *Methods Enzymol.* 585, 49–60.
- Wiśniewski, J.R., and Mann, M. (2016). A proteomics approach to the protein normalization problem: Selection of unvarying proteins for MS-based proteomics and western blotting. *J. Proteome Res.* 15, 2321–2326.
- Wu, X., Chavez, J.D., Schweppe, D.K., Zheng, C., Weisbrod, C.R., Eng, J.K., Murali, A., Lee, S.A., Ramage, E., Gallagher, L.A., et al. (2016). In vivo protein interaction network analysis reveals porin-localized antibiotic inactivation in *Acinetobacter baumannii* strain AB5075. *Nat. Commun.* 7, 13414.
- Xu, H.E., Stanley, T.B., Montana, V.G., Lambert, M.H., Shearer, B.G., Cobb, J.E., McKee, D.D., Galardi, C.M., Plunket, K.D., Nolte, R.T., et al. (2002). Structural basis for antagonist-mediated recruitment of nuclear co-repressors by PPAR α . *Nature* 415, 813–817.
- Xu, X., So, J.-S., Park, J.-G., and Lee, A.-H. (2013). Transcriptional control of hepatic lipid metabolism by SREBP and ChREBP. *Semin. Liver Dis.* 33, 301–311.
- Yang, X.J., and Seto, E. (2008). Lysine Acetylation: Codified Crosstalk with Other Posttranslational Modifications. *Mol. Cell* 31, 449–461.
- Yang, H., Wang, H., Shivalila, C.S., Cheng, A.W., Shi, L., and Jaenisch, R. (2013). One-step generation of mice carrying reporter and conditional alleles by CRISPR/Cas-mediated genome engineering. *Cell* 154, 1370–1379.
- Yang, H., Wang, H., and Jaenisch, R. (2014). Generating genetically modified mice using CRISPR/Cas-mediated genome engineering. *Nat. Protoc.* 9, 1956–1968.
- Yen, P.M. (2001). Physiological and molecular basis of thyroid hormone action. *Physiol. Rev.* 81, 1097–1142.
- Yin, L., Wang, J., Klein, P.S., and Lazar, M.A. (2006). Nuclear Receptor Rev-erba Is a Critical Lithium-Sensitive Component of the Circadian Clock. *Science* 311, 1002–1005.
- Yoon, H., Chan, D.W., Huang, Z., Li, J., Fondell, J.D., Qin, J., and Wong, J. (2003). Purification and functional characterization of the human N-CoR complex : the roles of HDAC3 , TBL1 and TBLR1. *EMBO J.* 22, 1336–1346.
- You, S.-H., Lim, H.-W., Sun, Z., Broache, M., Won, K.-J., and Lazar, M. a (2013). Nuclear receptor co-repressors are required for the histone-deacetylase activity of HDAC3 in vivo. *Nat. Struct. Mol. Biol.* 20, 182–187.
- Zhang, J., Kalkum, M., Chait, B.T., and Roeder, R.G. (2002). The N-CoR-HDAC3 nuclear receptor corepressor complex inhibits the JNK pathway through the integral subunit GPS2. *Mol. Cell* 9, 611–623.

Zhang, Y., Fang, B., Emmett, M.J., Damle, M., Sun, Z., Feng, D., Armour, S.M., Remsberg, J.R., Jager, J., Soccio, R.E., et al. (2015). Discrete functions of nuclear receptor Rev-erba couple metabolism to the clock. *Science* (80-). *348*, 1488–1492.

Zhao, Y., and Garcia, B.A. (2015). Comprehensive catalog of currently documented histone modifications. *Cold Spring Harb. Perspect. Biol.* *7*, 1–21.

Zhong, X., Navare, A.T., Chavez, J.D., Eng, J.K., Schweppe, D.K., and Bruce, J.E. (2017). Large-Scale and Targeted Quantitative Cross-Linking MS Using Isotope-Labeled Protein Interaction Reporter (PIR) Cross-Linkers. *J. Proteome Res.* *16*, 720–727.